Sediment Transport and Gravity Flow Routing in Highstand Submarine Canyons: Multiscale Evidence from Sediment Stratigraphy and Water Column Observations

Evan Lahr

A dissertation

submitted in partial fulfillment of the

requirements for the degree of

Doctor of Philosophy

University of Washington

2026

Reading Committee:

Andrea S. Ogston, Chair

Charles A. Nittrouer

Jenna C. Hill

Program Authorized to Offer Degree:

Oceanography

University of Washington

Abstract

Sediment Transport and Gravity Flow Routing in Highstand Submarine Canyons: Multiscale Evidence from Sediment Stratigraphy and Water Column Observations

Evan Lahr

Chair of the Supervisory Committee:

Andrea S. Ogston

Oceanography

Submarine canyons are the sites of the largest individual sediment transport events on Earth—sediment gravity flows—which over time build submarine fans, which are among the largest sedimentary deposits on the planet. While canyons are known to exert globally significant control on sediment transport, modern sediment transport events remain poorly understood due to challenging data collection and unpredictable event timing. Today, most canyons are partially decoupled from the coastal processes that are known to trigger flows, and this has led to the view of a majority of highstand submarine canyons as sedimentologically inactive, with implications for the interpretation of stratigraphy accumulating on continental margins. This thesis presents four complementary studies that integrate sediment stratigraphy and nearbed hydrodynamic observations to investigate event-driven sediment transport in seismically active, highstand-detached submarine canyons.

The first study examines the seasonal processes that initiate sediment transport through a highstand-detached submarine canyon head on the northern Cascadia margin. Using nearbed hydrodynamic observations collected over a three-month deployment, this study evaluates how surface waves and river plume dynamics resuspend and transport sediment under modern oceanographic conditions. Results reveal distinct seasonal transport regimes, with summer transport dominated by persistent canyon-aligned currents and internal waves, and more energetic winter conditions estimated to generate bed stresses sufficient for widespread sediment resuspension. These observations demonstrate that sediment transport remains active within the canyon despite separation from littoral and fluvial processes and that the relative importance of transport mechanisms varies seasonally.

The second study analyzes sediment cores from a canyon head to evaluate whether nonseismic turbidity currents are preserved in modern canyon stratigraphy. Turbidite deposits are confirmed within the canyon, and multiple metrics of geochemical and sedimentological properties reveal modern, nonseismic turbidite deposits. These turbidites are ~15 cm thick, graded, and internally laminated, with low excess ^{210}Pb activity and depositional ages that align with major Columbia River floods. Their organic matter composition is distinctly terrestrial and recent (δ^{13}C = −26‰, C:N = 18, and elevated lignin concentrations), indicating a fluvial source. These results provide the first direct evidence of modern nonseismic turbidite deposition in northern Cascadia and demonstrate that highstand canyon stratigraphy preserves flood-driven event beds. They further show that turbidite composition reflects sediment source and that such deposits contribute significantly to sediment and carbon accumulation within canyon systems.

The third study expands this framework by comparing flood- and earthquake-generated deposits within the same canyon system. Astoria Canyon, which has experienced both major floods and the 1700 CE Cascadia megathrust earthquake, provides a natural laboratory for linking event deposits to independently constrained triggers, with particularly well-preserved stratigraphy in an oxygen minimum zone. Sediment core geochronology, geochemical composition, and density structure reveal two distinct modes of gravity-flow deposition: terrestrial-rich turbidites generated by river floods and heterogeneous, marine-sourced mass transport deposits associated with seismic events. A diagnostic compositional model can distinguish between these origins at multiple core sites along the canyon axis, demonstrating that organic carbon signatures can provide a robust indicator of deposit source, whereas internal density structure varies over short spatial scales and is not consistently diagnostic. These findings revise assumptions of highstand canyon sediment routing by showing that nonseismic sediment gravity flow triggers remain active, coseismic deposits can accumulate on the upper slope, and deposit structure is not reliably correlatable over short distances.

The fourth study addresses the process-based controls on sediment transport through direct observation. Although highstand canyons are often overlooked as active sediment transport systems, their bathymetry strongly modifies ocean circulation and enhances the exchange of water, nutrients, and sediment across continental margins. Using year-long moored observations in two adjacent canyons with contrasting morphology, this study evaluates whether sediment transport is synchronous under similar oceanic forcing and the parameters needed to form sediment gravity flows based on the canyon head dynamics. Results show that bottom boundary layer currents are persistently downslope and that sediment resuspension occurs under a range of conditions, with smaller events during summer and larger events associated with storm waves and increased river discharge. Despite similar regional forcing, sediment transport between the two canyons is largely asynchronous, indicating that canyon morphology exerts a primary control on sediment routing.

Together, these studies demonstrate that highstand submarine canyons are not dormant but instead host complex, episodic sediment transport regimes driven by both seismic and oceanic processes. These findings improve upon the conventional interpretations of highstand dormancy and seismoturbidite records, and more broadly, this dissertation shows that highstand submarine canyon channels remain partially active and the dynamics within canyon heads impose a complex filter on downslope transport.

TABLE OF CONTENTS

LIST OF FIGURES

ACKNOWLEDGEMENTS

This work was funded by National Science Foundation Award Number 2147983, the United States Geological Survey Cascadia Initiative, the University of Washington School of Oceanography, and the University of Washington Quaternary Research Center. The authors thank the crew of the research vessels Thomas G. Thompson, Rachel Carson, Robert Gordon Sproul, and Sikuliaq for supporting ship operations. A number of interdisciplinary labs were also instrumental in this work, including the University of Washington Keil laboratory, the University of Washington Isolab, and the University of Oregon Paleoecology Group. The authors also thank reviewers at Geophysical Research Letters and Marine Geology, and Brian Atwater, Rick Keil, and Jaqui Neibauer for constructive feedback. Finally, this work would not be possible without the guidance and mentorship of Andrea Ogston, Jenna Hill, and Kurt Rosenberger.

GLOSSARY OF KEY TERMS:

Sediment gravity flow (SGF): A density-driven sediment transport process characterized by downslope movement of fluid and sediment. This term encompasses multiple mechanisms that maintain grain suspension. One example is a turbidity current, in which suspension is supported by fluid turbulence.

Turbidity current: One type of sediment gravity flow in which particle suspension is maintained by fluid turbulence.

Turbidite: A seafloor sediment deposit formed by a turbidity current.

Highstand-dormant paradigm: The conceptual model that submarine canyons are largely inactive with respect to sediment gravity flows during sea-level highstand, accumulating fine-grained sediment rather than exporting it downslope.

Hemipelagic sediment: Marine sediment composed of a mixture of fine terrestrial lithogenic particles (silt and clay) and marine biogenic material. This sediment type is common along continental slopes, marking the transition between terrestrial and marine sediment sources; also referred to in this text as *hemipelagite*.

Bottom boundary layer (BBL): The portion of the water column directly influenced by the seabed, typically extending ~1–10 m above the bed.

Chapter 1. INTRODUCTION

1.1 SUBMARINE CANYONS AND HIGHSTAND PROCESSES

Submarine canyons are present along nearly all continental margins and are globally significant sites for ocean mixing, biological productivity, and sediment transport (Allen & Hickey, 2010; Hickey, 1997; Wright and Nittrouer, 1995; Paull et al., 2018; Talling et al., 2024). Canyon sediment transport and morphology are tightly connected to the action of sediment gravity flows (SGFs), a family of density-driven, downslope-moving “sediment avalanches” that are seldom observed in situ yet transport annual sediment volumes comparable to the world’s rivers (Azpiroz-Zabala et al., 2017; Piper et al., 1999; Talling et al., 2024). SGF presence is mostly inferred from the sediment deposits they leave behind, and this stratigraphy informs interpretations of prior climatic, faunal, and tectonic settings (Adams, 1990; Paull et al., 2014; Shanmugam & Moiola, 1982, 1988). Although density-driven flows are recognized as key transport mechanisms throughout the global ocean and canyons are known to be sites of rapid delivery of terrestrial sediment to the deep ocean, the triggering, evolution, and fate of SGFs in canyons today remain difficult to predict, precluding a clear view of how canyon processes operate and build stratigraphy.

The evolution of submarine canyons over geologic time is often simplified to the following paradigm: in times of sea-level lowstand, successive SGFs erode the continental slope, incising canyon channels and displacing shallow-water sediment directly into the abyssal ocean. During sea-level highstand (including at present), SGF activity is diminished, and canyon axes infill with fine-grained sediment. This view has led to a simplified characterization of canyons as "active" or "inactive" depositional environments (Covault & Graham, 2010; Shanmugam & Moiola, 1982). A growing number of studies identify a spectrum of triggering processes that operate in highstand canyons, and in some highstand canyons today SGFs continue to occur, driven by local resuspension processes such as storm waves, floods, or canyon-axis currents (Lamb & Mohrig, 2009; T. Mulder et al., 2001a; Parsons et al., 2007; P. Puig et al., 2004; Puig et al., 2013; St-Onge et al., 2004; Traykovski et al., 2007). While canyon morphology and position relative to the coast may provide a cursory assessment of active canyon processes, recent observational studies document how morphology-based transport assumptions overlook a range of active canyon processes.

1.2 THE CASCADIA MARGIN AND THE SEISMOTURBIDITE CONCEPTUAL MODEL

One setting where improved constraints on highstand canyon sediment transport have clear societal relevance is the Cascadia subduction zone, where canyon stratigraphy informs geohazard assessments of major subduction zone earthquakes (Adams, 1990; Goldfinger et al., 2012, 2017). Along the Cascadia margin, strain accumulates on a locked plate interface and is released episodically in great earthquakes with estimated magnitude M~9 (Satake et al., 2003). The interseismic period is estimated to be approximately 300–500 years (Goldfinger et al., 2012), and the most recent event predates direct observational records (1700 CE, Atwater et al., 2016). As a result, there is a clear societal need to constrain the timing and recurrence of major earthquakes, and current estimates rely primarily on geological evidence, including coastal subsidence, tsunami deposits, and abyssal turbidites. Among these, the turbidite record—the most temporally extensive and spatially consistent proxy for earthquakes—is interpreted under the premise that seismic events trigger widespread slope failure and sediment gravity flow activity across canyon systems along the margin.

Importantly, the seismoturbidite record relies upon assumptions regarding highstand sediment transport in submarine canyons. Briefly, one of the primary assumptions is that (1) large earthquakes generate regionally synchronous sediment gravity flows that propagate downslope from sites of sediment recharge into the abyssal ocean and produce turbidite deposits correlatable across multiple canyon systems (Goldfinger et al., 2012, 2017). This conceptual model further assumes that (2) nonseismic processes such as storm-driven resuspension, river floods, and localized slope failures are too weak, infrequent, or spatially limited to generate widespread event beds within canyon stratigraphy. It also suggests that sediment gravity flows during highstand conditions begin in areas of active sediment recharge, i.e., canyon heads, and this sediment is transmitted to the abyssal plain. Exceptions to these assumptions have been documented in canyon environments globally, raising questions on the potential for oceanic sediment gravity flow initiation (Bailey et al., 2021; Puig et al., 2004), turbidite source locations (Hill et al., 2022, 2026), and the validity of turbidite correlation (Nieminski et al., 2024). More broadly, these uncertainties highlight a consequential gap between the conceptual model for highstand inactive canyons and the few process-based constraints available from studies of highstand canyon systems.

1.3 CENTRAL QUESTIONS AND APPROACH

One central question in submarine canyon dynamics is the degree to which sediment transport and sediment gravity flows (SGFs) remain active under sea-level highstand in response to oceanic and meteorological processes. While this question has global relevance, we investigate it along the Cascadia margin, where processes within canyon heads create uncertainty that may limit the interpretation of canyon stratigraphy in paleoseismic applications that assume turbidite deposits record regional seismic events. More specifically, we structure this topic as three research questions addressed in the following chapters:

1. Do oceanic processes generate sediment gravity flows in highstand submarine canyons?
2. How can the origin of submarine canyon deposits be reliably distinguished between seismic and oceanic events?
3. Do active canyon head processes trigger synchronous sediment transport and gravity flows across multiple canyon systems on the margin?

Each of the chapters outlined below is set along the Washington margin, often within or near Astoria Canyon, a shelf-incised submarine canyon along the Cascadia margin. These questions are addressed using the most robust approach for studying sediment transport and SGF activity: combined observations of sediment stratigraphy and nearbed hydrodynamics. Stratigraphic observations provide a clear record of century-scale deposition, while hydrodynamic observations constrain the processes that trigger and sustain sediment transport. Together, these datasets allow the frequency, origin, and pathways of sediment transport to be resolved more completely than either approach alone.

These questions are addressed through four complementary studies that link stratigraphic observations with hydrodynamic measurements. Chapter 2 demonstrates that highstand canyon heads remain active sediment-transport environments, with summer internal-wave processes promoting sediment retention and winter storms driving resuspension and down-canyon export. Chapter 3 provides a high-resolution, multi-measurement analysis of two turbidite deposits within a single core, demonstrating a well-constrained example of turbidite deposition driven by oceanic processes. Chapter 4 expands this analysis across multiple cores and contrasts oceanic deposits with coseismic mass transport deposits associated with the 1700 earthquake and prior events. Chapter 5 uses year-long observations from two Cascadia submarine canyons to test whether synoptic-scale ocean forcing drives synchronous nearbed sediment transport and sediment gravity flows under modern conditions. Together, these chapters build toward an updated view of highstand inactive canyons that recognizes the full range of Earth surface processes shaping canyon morphology and stratigraphy.

Chapter 2. SUBMARINE CANYON SEDIMENT TRANSPORT AND ACCUMULATION DURING SEA-LEVEL HIGHSTAND: INTERACTIVE SEASONAL REGIMES IN THE HEAD OF ASTORIA CANYON, WA

2.1 Introduction

Submarine canyons are morphological features present along nearly every continental margin on Earth, and they are sites of significant ocean mixing, sediment transport, and nutrient exchange between coastal and abyssal environments (Carter and Gregg, 2002; Puig et al., 2014; Azpiroz-Zabala et al., 2017; Thomsen et al., 2017; Paull et al., 2018). Many of these submarine canyons were initially incised during the Pleistocene, when terrestrial sediment was supplied directly to the shelf break and frequent sediment gravity flows incised canyon thalwegs (Shanmugam et al., 1985; Piper and Normark, 2009). The frequency of these flows dramatically decreased during the Holocene transgression when the coastal sediment supply was displaced landward of the shelf break, and canyon floors began infilling with hemipelagic sediment (Carlson, 1968; Nelson, 1976). However, episodic density-driven sediment transport processes remain active in submarine canyons during the Holocene (Heijnen et al., 2022). Identifying the triggers for both episodic and tidal-to-seasonal transport events is critical for understanding canyon functioning, geochemical fluxes, and continental margin stratigraphy.

Nearbed hydrodynamic observations provide the most detailed evidence for how sediment is transported through the canyon environment, and these types of observations have revealed a wide spectrum of canyon sediment transport processes. Processes that act to incrementally distribute sediment throughout canyons include biogenic pelagic sedimentation, settling from river plumes, internal and surface tides, and subtidal currents (Puig et al., 2014). Punctuated transport events have been initiated by aseismic slope failure (Xu et al., 2013), storm-induced liquefaction (Puig et al., 2004), surface wave shear stresses (Ma et al., 2008; Traykovski et al., 2007), dense shelf-water cascading (Canals et al., 2006), hyperpycnal river plumes (Warrick et al., 2008; Liu et al., 2012), and hypopycnal river plumes (Hage et al., 2019). The cumulative effect of transport within canyon systems dictates the locations and rates of sediment accumulation, in some cases driving deposits toward unstable morphologies that are prone to mass failure. This pre-conditioning of canyon sediment can drive sediment gravity flow triggering, and recent studies have found that major canyon-confined turbidity currents do not require major external triggers if there are unstable deposits (Paull et al., 2018; Bailey et al., 2021). Further, the processes responsible for unstable sediment preconditioning are poorly understood, particularly in canyons which are detached from land under highstand yet actively redistribute sediment.

The regional setting of this study is the northern Cascadia Margin (Fig. 2.1), where morphology is characterized by a 40 km wide continental shelf, steep continental slope, and abyssal trench which has been infilled by Plio-Pleistocene sedimentation. The Cascadia Margin contains eleven major canyon systems which fit the Pleistocene-

Holocene timeframe of incision and infill, evidenced by deep-water fan geochronology (Nelson, 1976; Knudson and Hendy, 2009), seismic profiles, multibeam bathymetry (Hill et al., 2020), and canyon sedimentation (Carlson, 1968; Carson et al., 1986). Turbidites and other sedimentary structures emplaced by sediment transport events punctuate hemipelagic Holocene stratigraphy from submarine canyons and channels throughout the Cascadia Margin (Adams, 1990; Nelson et al., 2000; Paull et al., 2014). Some of these deposits have been attributed to large (7-9 M_w) subduction zone earthquakes, but several coarse and fine layers remain unattributed to triggering events (Carlson, 1968; Goldfinger et al., 2012). Observations of in situ sediment transport are rarely made within canyons on the Cascadia Margin or elsewhere, due to the logistical challenges of data collection. As a result, the balance between event-driven and gradual sedimentation in highstand canyons remains poorly understood.

The aim of this study is to expand our understanding of resuspension and transport processes in highstand submarine canyons and identify the processes that deposit and transport canyon-head sediment. We hypothesize that sediment transport patterns during summer load the canyon head with sediment, preconditioning the seabed in the upper channel for episodic remobilization during winter conditions. To address this hypothesis, we combine hydrodynamic timeseries observations with cores obtained from modern sediment deposits in the head of Astoria Canyon. This combined approach allows for the comparison of canyon hydrodynamic processes and seabed accumulation, connecting modern processes to sediment loading in the canyon head.

We evaluate these in situ data in the context of the Cascadia Margin and contrast this highstand canyon with a range of active and inactive systems.

2.2 Study Site

2.2.1 Astoria Canyon

The study site is focused over a 200 km^2 area encompassing the head of Astoria Canyon, one of north Cascadia's major canyons. Astoria Canyon was formed as a conduit for Columbia River sediment during glacial lowstand, and the stratigraphy of Astoria Fan indicates that canyon incision began as early as 2.58 Ma (Carlson, 1968; Nelson et al., 1970). Holocene sea-level rise from 20 to 7 ka halted canyon incision (Carlson, 1968), and following the Holocene transgression, fine-grained sediment from the Columbia River aggraded a broad northeast-trending mud deposit on the shelf of up to 14 meters thick, referred to as the mid-shelf mud belt (Nittrouer et al., 1979). Over the last century, roughly two thirds of the annual sediment supply from the Columbia River has been retained on the mid-shelf mud belt (Nittrouer et al., 1979; Sternberg, 1986). The southern terminus of the mud belt intersects the head of Astoria Canyon, where canyon bathymetry is believed to capture a significant amount of fine-grained sediment annually, equivalent to ~5% of the Columbia River sediment load (Sternberg, 1986). On seasonal timescales, fine-grained deposits several centimeters thick have been observed on the shelf during summer, but are absent in winter, and are believed to be eroded by winter storms (Nittrouer and Sternberg, 1981). Beyond the shelf break, the slope and canyon regions accumulate modern sediment more slowly, with a majority of modern sedimentation focused on the upper portion of the slope (Carpenter et al., 1981). At depths greater than 500 m within the canyon axis, coarse sediment layers are commonly found in modern deposits from the canyon thalweg, and intermittent coarse sediment layers persist onto Astoria Fan (Carlson, 1968).

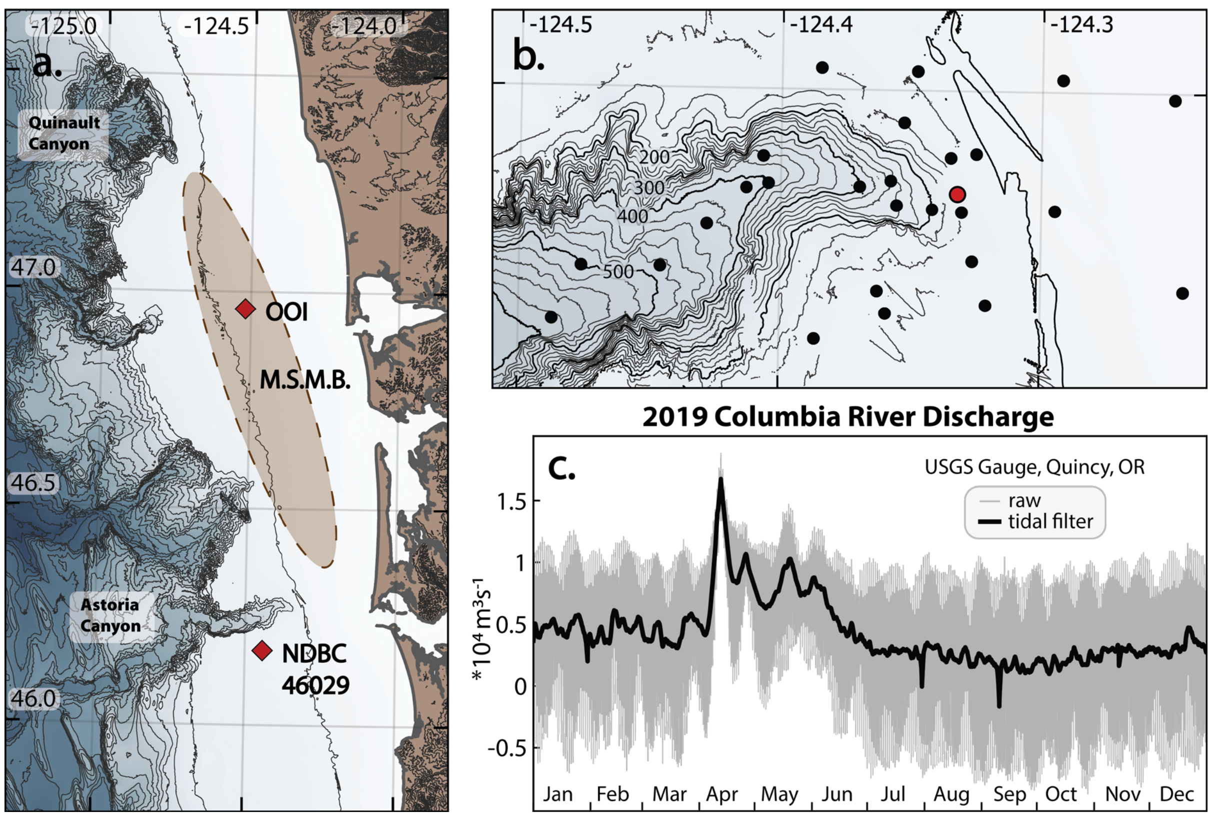

Figure 2.1. *a. Map of the northern Cascadia Margin, including Astoria Canyon and the mid-shelf mud belt, with bathymetry contours at 100 m intervals. b. bathymetry at the head of Astoria Canyon. Data sources are noted, including sediment core locations (black circles), the tripod site (red circle), the National Data Buoy Center Station 46029 and the Ocean Observatories Initiative Washington Shelf Surface Mooring (black diamonds). c. Columbia River hydrograph at Quincy, OR, in 2019 (40-hour low-pass filtered data in black, raw data in gray).*

2.2.2 Sediment supply to the canyon head

The Columbia River is the largest river (670,000 km^2 basin area, 260 km^3 y^{-1} discharge) and the second largest source of fluvial sediment (8 MT; Naik and Jay, 2011) on the west coast of North America. The hydrograph of the Columbia River peaks in spring and summer in the northern hemisphere (Fig. 2.1), driven by high-elevation snowmelt, with lesser peaks in winter driven by rainfall. The Columbia River's natural hydrograph has been altered and sediment supply has been greatly reduced by dams and climate change. Nearly all the reduction in sediment supply is in sand-sized particles, while fine-grained sediment supply has remained largely unchanged (Naik and Jay, 2011).

On seasonal timescales, the plume pathway is controlled by wind stresses and along-shelf geostrophic currents (Hickey et al., 1998). Southerly, downwelling-favorable winds during winter force the plume northward along the coast, whereas northerly winds during summer force the plume to travel southwest or bifurcate into north- and southwest-moving branches (Hickey et al., 2005). Plume sediment concentrations are typically less than 30 mg l^{-1} beyond the river mouth (Sherwood and Creager, 1990; Spahn et al., 2009; Nowacki et al., 2012), and the plume front fluctuates tidally.

2.2.3 Factors impacting sedimentary processes within Astoria Canyon

The surface wave climate in the northeast Pacific Ocean is energetic, with deep-water storm swell annually reaching a significant wave height of 10 m, and interannual maxima reaching 15 m (Allan and Komar, 2002; Allan and Komar, 2006; Ruggiero et al., 2010). These storm events drive strong seabed shear stresses over the continental shelf, capable of resuspending sediment on the outer shelf ~175 hours per year (Sternberg et al., 1986).

The California Current and Undercurrent System flows parallel to regional shelf isobaths over the shelf-incised upper thalweg of Astoria Canyon. Below the canyon rim, steep canyon walls disrupt shore-parallel geostrophic currents, and mean flow is directed approximately east-west along the canyon axis (Hickey et al., 1997; Bosley et al., 2004). Wind stresses drive upwelling- and downwelling-favorable conditions over the canyon with timescales of 2 to 10 days, and associated currents below the canyon rim have been observed with along-axis velocities of 1 m s^{-1}. Currents as deep as 600 m within the canyon maintain a statistical relationship with wind stresses (Hickey, 1997; Bosley et al., 2004).

Bottom nepheloid layers (50 m thick) and intermediate nepheloid layers (200-300 m depth) are observed in the axis of Astoria Canyon (Hickey, 1997; Bosley et al., 2004). In other canyons globally, the breaking of internal tides along slope and canyon bathymetry is known to elevate nearbed shear stress, resuspend seafloor material, and mix sediments high into the water column (Gardner, 1989; Carter and Gregg, 2002; Kunze et al., 2002; Boegman and Stastna, 2019; Maier et al., 2019), contributing to nepheloid layer formation. Tidal currents and internal tides (ITs) are present within Astoria Canyon, amplified by the bathymetry, and nonlinear internal waves (NLIWs) have been observed along the Washington and Oregon shelf (Nash and Moum, 2005; Moum et al., 2007; Alford et al., 2012; Zhang et al., 2015).

2.3 Methods

2.3.1 Hydrodynamic data collection and analysis

A bottom-boundary-layer tripod was deployed into the head of Astoria Canyon at 46.27 N 124.33 W in a nominal water depth of 160 m during the summer of 2019 to observe canyon processes near the annual peak in discharge from the Columbia River. The tripod was deployed on 5 May 2019 and recovered on 12 August 2019. Tripod instrumentation quantified the wave, current, and turbidity parameters relevant to bottom boundary-layer sediment transport, as well as temperature and salinity (see Table 2.1 for details). To understand these values in an annual context, tripod data were supplemented with a year-long record of wave heights and nearbed currents. Supplementary data were obtained from a National Oceanic and Atmospheric Administration buoy (NOAA National Data Buoy Center, 2019), and from the Ocean Observatories Initiative (OOI, Ocean Observatories Initiative, 2019) Washington Shelf Surface Mooring. Both instruments supply concurrent spectral surface wave and meteorological data, and the OOI mooring also recorded nearbed current velocity for a complete year (the year 2016 was chosen for its complete records; details in Table 2.2). The NDBC buoy was located 10 km south of the tripod site, and the OOI mooring was located 81 km north of the tripod site (Fig. 2.1).

Table 2.1. *Instrument deployment details for the canyon head tripod, including sampling frequency and the height above bed of the sampling volume.*

Instrument	Sampling Strategy	mab
RDI 300 kHz ADCP, upward-facing	1 burst / minute (10 profiles at 0.5 Hz)	2
Sentinel V 1 MHz ADCP, downward-facing	1 burst / 5 minutes (90 profiles, 0.5 Hz)	1.3
Sontek 5 MHz ADV	1 burst / 60 minutes (4800 samples, 16 Hz)	0.9
Seabird SBE-37 Microcat T-S Sensor	1 burst / 60 minutes (4800 samples, 16 Hz)	1.05
RBR Concerto CTD	1 sample / 5 minutes	1.35
Campbell Scientific OBS 3+	1 sample / 5 minutes	0.25, 1.9
Sea-Tech Transmissometer	1 sample / 5 minutes	1.35
RBR Virtuoso (Turbidity)	1 sample / 30 minutes	1.55
Tube Sediment Trap		0.35, 1.9

For the summer, seafloor shear stresses were calculated using hourly bursts from the 5 MHz Acoustic Doppler Velocimeter (ADV) mounted 90 cm above bed. First, average current speed was calculated from each hourly current data ensemble, and wave statistics were calculated from each ensemble using PUV wave analysis (more details in Table 2.2). For the winter, wave statistics and nearbed average velocity were calculated from the OOI mooring. Combined wave-current shear stresses were then calculated for all time periods using the Grant-Madsen wave-current interaction model (Madsen, 1994; Wiberg and Sherwood, 2008).

Table 2.2. *Input data and variables for the Grant-Madsen wave-current interaction model (Grant and Madsen, 1979) used to predict bed shear stress within Astoria Canyon head.*

Symbol	Name	Summer	Winter
Ubr	Representative wave-orbital velocity	5 MHz ADV velocity ensemble (PUV method)	OOI Spectral Wave Data (ubspecdat method; Wiberg & Sherwood 2008)
Ω_r	Representative angular wave freq.	5 MHz ADV velocity ensemble (PUV method)	OOI Spectral Wave Data (ubspecdat method; Wiberg & Sherwood 2008)
U_c	Current velocity	5 MHz ADV velocity ensemble, hourly average	OOI ADCP nearbed velocity (lowest cell in velocity profile)
Z_r	Reference height for current velocity	0.9 m	4 m
K_n	Bottom roughness height	3 mm	3 mm

Optical backscatter sensor data were calibrated from nephelometric turbidity units to units of suspended sediment concentration (mg l^{-1}) using the methods of Ogston et al. (2000). The sensors were placed in a tank with a magnetic stir plate and subjected to incrementally increasing suspended sediment concentrations (SSC) while sensors recorded data. Each time sediment concentrations were increased, a water sample was collected, and suspended sediments were filtered, dried, and weighed. Sensor output was calibrated to the mass concentration of suspended sediments using a simple linear fit through the origin and reference values. The sediment used for calibration was collected from the seafloor at the tripod site on the date of recovery. The RBR Virtuoso turbidity sensor provided the best-fit calibration to Astoria Canyon sediments, with an R^2 fit of 0.99.

2.3.2 Sediment core collection and analysis

In August 2019, 24 box cores, each 60 cm long, were collected from the canyon head thalweg, walls, and surrounding continental shelf, in water depths ranging from 60 to 400 meters. Cores were sub-sampled in the field at 2 cm resolution. In the lab, slabs were x-radiographed and further sub-sampled at depth increments of 1 cm. Disaggregated grain size was measured for all samples. Prior to grain size analysis, samples were dispersed using a sodium metaphosphate solution and a sonication bath. Grain size distribution was measured using a Beckman-Coulter LS13-320 Particle Size Analyzer and the sampler completed three measurement periods which were averaged for the final reported distribution. Each sample's individual volume % measurement varied by <10%, consistent with calibration distributions demonstrating size distribution recovery to within 2% of each size class.

Sediment accumulation rates were obtained for each core via ^{210}Pb geochronology using the methods of Nittrouer et al. (1979). Dry sediment samples were spiked with 1 ml of ^{209}Po (10 dpm/ml), and radioisotopes were leached from each sediment sample using 15.8N HNO_3 and 6N HCl. ^{209}Po and ^{210}Po were then plated onto a silver planchet, and the decay of polonium isotopes was measured using an Ortek Alpha Ensemble alpha spectrometer. Supported levels of radioactivity were assumed to be equal to the radioactivity found at the base of cores beyond the layer of logarithmically decreasing radioactivity, and this value was subtracted from each sample's total activity. Where core penetration exceeded the layer of logarithmic decrease, samples had naturally supported activities of ~0.5 dpm g^{-1} on the shelf and ~3 dpm g^{-1} in the canyon, and these values are consistent with previous studies (Nittrouer et al., 1979; Carpenter et al., 1981). These values were used for cores that did not penetrate beyond the layer of logarithmic decrease, as slight non-constancy in levels of supported radioactivity has minimal effect on the calculation of accumulation rate. The decrease of unsupported, or excess, ^{210}Pb activity with depth in each core was fit with an exponential regression and used to calculate a vertical sediment accumulation rate in cm y^{-1}. The conversion to mass accumulation in mg cm^{-2} y^{-1} was calculated by multiplying the vertical sedimentation rate by the dry-bulk density of each sample.

2.4 Results

2.4.1 Hydrodynamics

The canyon-axis currents measured during summer 2019 covaried primarily with nearby wind stresses at NDBC 46029 and tides (Fig. 2.2). Velocities ranged from -70 to 70 cm s^{-1}, where negative velocities denote currents flowing to the west (downslope) along the canyon axis. Peak nearbed shear stresses were driven by downwelling-associated downslope flow (e.g., Fig. 2.2a, year days 130-140, 163-166, 177-182), with nearbed current velocity up to 70 cm s^{-1} and shear stresses as large as 0.14 N m^{-2}. Down-canyon flow events were also accompanied by a decrease in nearbed salinity at the canyon head, and an increase in temperature as large as +0.8 °C. Throughout the timeseries, SSC covaried weakly with shear stress and was elevated during periods of concurrent upwelling and internal wave activity (e.g., year days 143-148, 150-155, 160-163, Fig. 2.2b). SSC was not significantly elevated during periods of strong down-canyon flow, e.g., Fig. 2.2 events at year days 135, 165, 180. Up-canyon flow during internal wave activity was associated with increased salinity and decreased temperature.

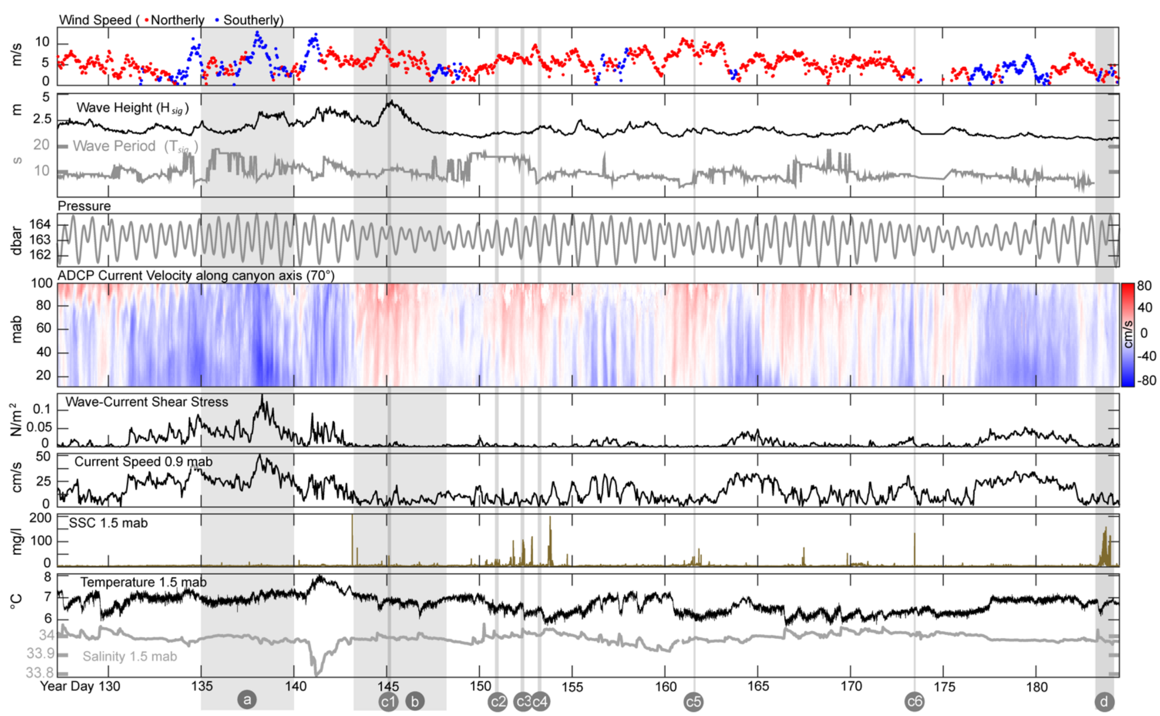

Figure 2.2. *Timeseries from the head of Astoria Canyon from 5 May, 2019 to 3 July, 2019. Wind and wave statistics come from NDBC 46029 and are plotted in red if coming from the north (upwelling-favorable), and blue from the south (downwelling-favorable). ADCP velocity data is plotted in its principal velocity component (which corresponds to the canyon axis), positive values correspond to up-canyon currents. The time periods shaded in gray are expanded in Figures 4 and 5.*

During summer, significant wave heights were typically 2–3 m with a dominant period averaging 8–10 s. Moderate storm events in spring increased dominant swell height to 5 m (Fig. 2.2) and period to 16 seconds. The canyon-head shear stresses generated by waves of this size were <0.05 Pa. The nearby OOI datasets provided a means to calculate bed stress throughout the year, and shear stress magnitudes for the summer season are in agreement, with weak wave shear stresses at 160 m depth (Fig. 2.3a), and current shear stresses consistent in magnitude with those observed in the canyon head (Fig. 2.3b). Stresses of this magnitude are not capable of resuspending most of the grain size distribution at the tripod site (Fig. 2.3d). However, shear stresses at the 160 m depth canyon head site predicted from OOI wave and current data during winter increased up to 1.18 Pa, which could resuspend the complete grain size distribution present at the tripod site (Fig. 2.3c, 2.3d). Stresses capable of resuspending all grain sizes at the tripod site were estimated to occur roughly 48 hours per year (Fig. 2.3d).

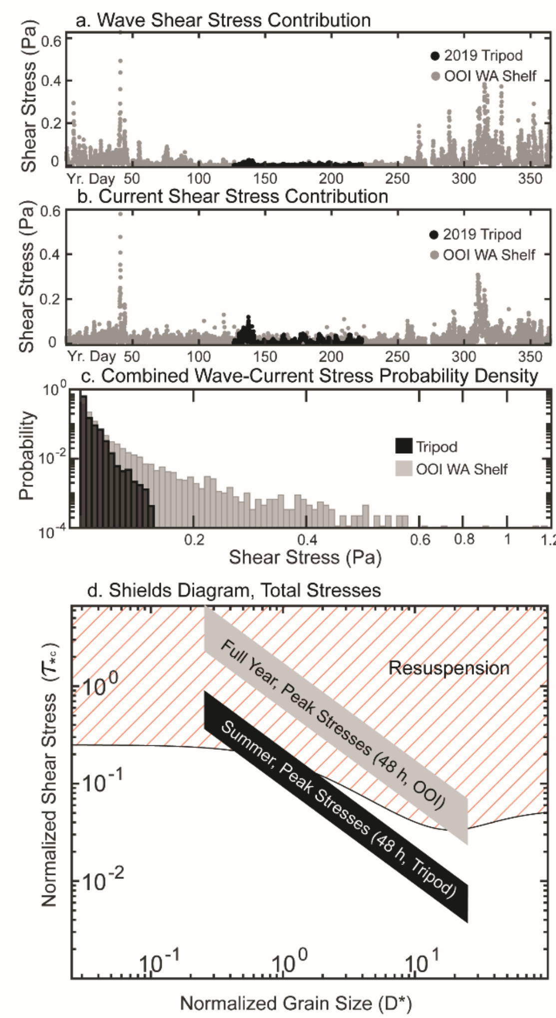

Figure 2.3. *Shear stress computed from the Astoria Canyon tripod deployment (black) and the OOI Shelf mooring (gray). Panels a) and b) depict relative stress contributions from waves and currents respectively, c) the distribution of total stresses, and d) maximum shear stresses from summer and winter on a Shields diagram (Guo, 2020).*

In addition to surface gravity waves, internal tides and nonlinear internal waves (NLIWs) were observed in the ADCP timeseries data (Fig. 2.4). These events were identified by strong velocity signatures over short (< 30 min) timescales. When peak tidal currents coincided with upwelling-favorable conditions there was also evidence of sediment resuspension near the tripod site (Fig. 2.5). The onset of elevated SSC was concurrent with a sharp transition from down-canyon to up-canyon flow, and SSC remained elevated (up to 150 mg l^{-1}) for several hours, including during the downslope phase of the internal tide. A rapid drop in temperature (-0.7° C in 3 h) and increase in salinity was also associated with the upslope phase of the internal tide, and both parameters slowly returned to ambient levels during downslope flow over 12 h. The

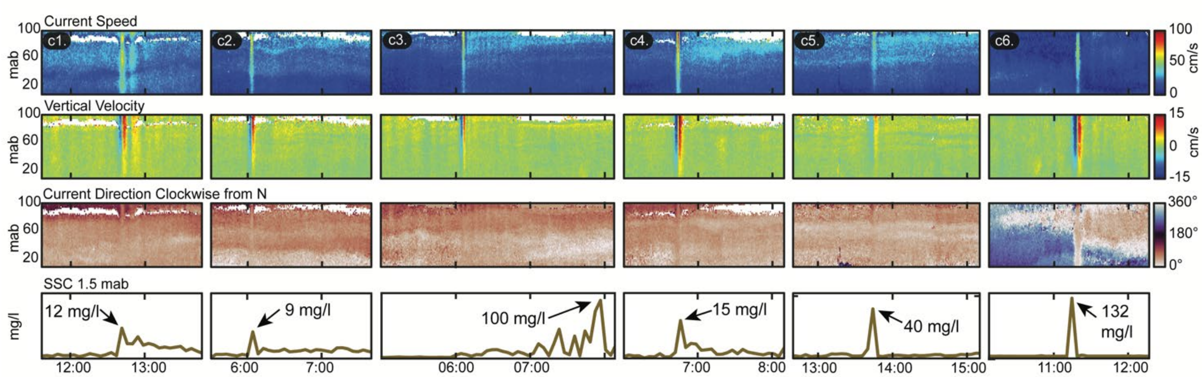

Figure 2.4. *Expansion of time periods c1 through c6 in Figure 2 depicting NLIWs. Top row shows elevated current velocities over a period of 5-10 min. Second row depicts vertical velocity. Note that NLIWs begin with negative (downward) vertical velocity. Third row shows that current directions are all moving to the east at a heading of ~90° from N. Bottom row shows increased suspended sediment concentrations during and after NLIW passage. Concentration scales vary for each event and are defined by the peak annotated.*

local bed shear stress and current speed remained low (<0.05 Pa and 30 cm/s) over the entire tidal cycle.

There were 52 solitary waves and a similar number of NLIW packets identified in the three-month tripod deployment. All the waves were low-mode waves of depression which affected the water column over a period of approximately 10 min. An average amplitude of NLIWs of ~30 m was estimated using ADCP backscatter. These waves most frequently occurred at or slightly after low tide and were associated with elevated SSC (10-15 mg l^{-1}). The largest SSC associated with NLIWs was 130 mg l^{-1} during the summer observation period. The direction of NLIW propagation can be identified using current

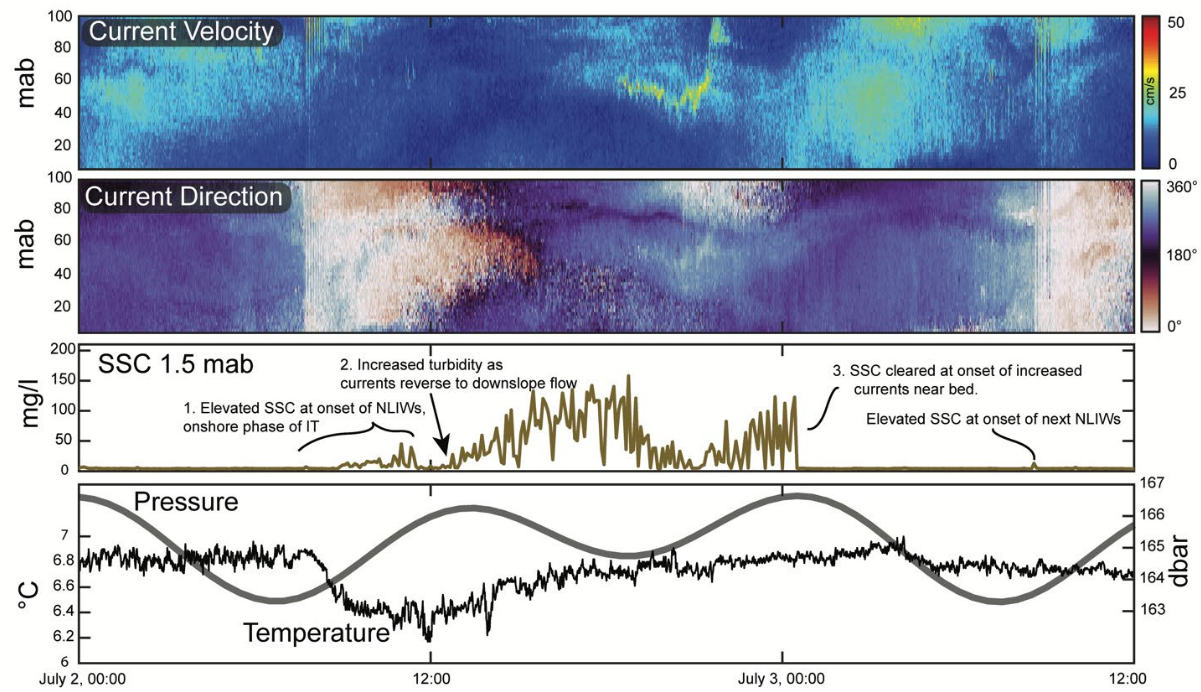

Figure 2.5. *Expansion of time period d in Figure 2, showing conditions during elevated suspended sediment concentrations over a 36-hour period. The onshore phase of the internal tide arrives at approximately 07:00, accompanied by a sharp drop in temperature and slightly elevated SSC. The large increase in SSC was associated with warming temperatures and downslope flow after the passage of the bore.*

orientations during wave passage: mode-1 depression waves drive opposing deep and shallow currents, and wave propagation is in the direction of the shallow current. The NLIWs observed within the canyon head drove nearbed currents to the east, indicating wave propagation west from the shore toward the canyon. In a concurrent synthetic aperture radar image, we document a radial, mode-1, Columbia River plume-associated NLIW near the tripod site (Fig. 2.6).

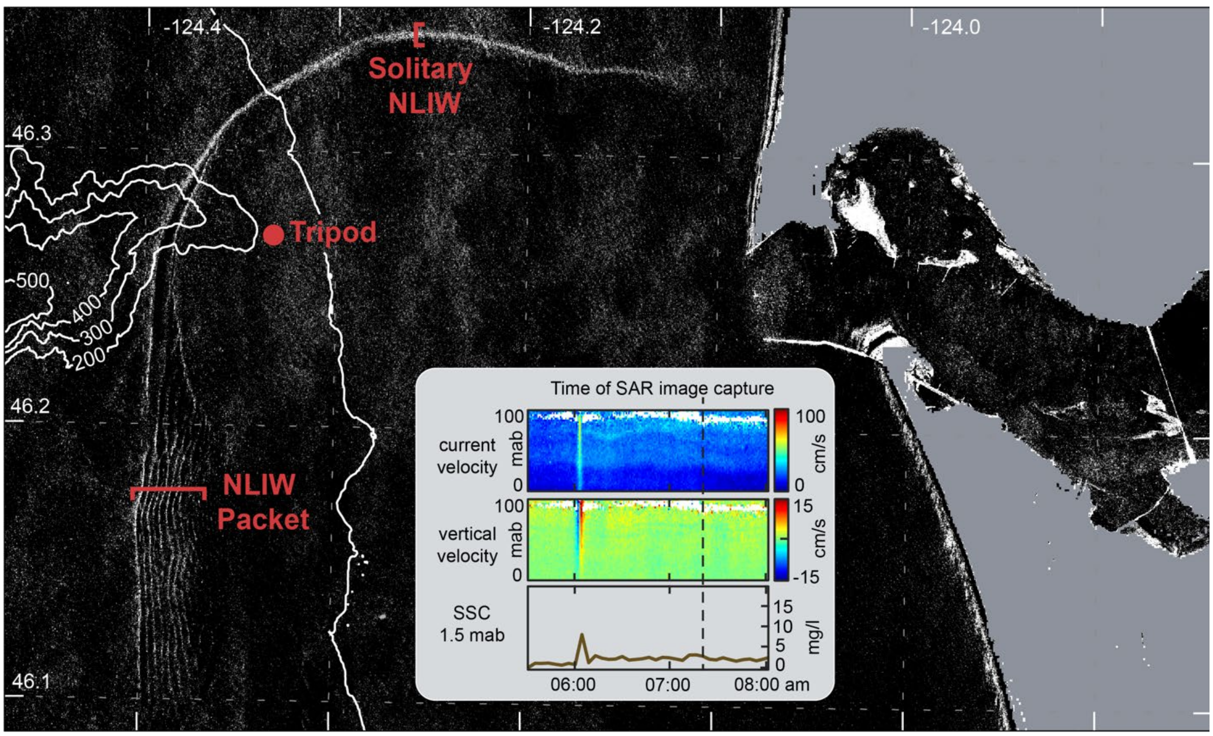

Figure 2.6. *Synthetic Aperture Radar (SAR) image and contemporaneous timeseries data showing Columbia River plume-associated NLIWs traveling over Astoria Canyon during the tripod deployment. Main panel: SAR image taken at 07:21 AM on May 31, 2019 with plume-associated NLIWs. Inset: concurrent ADCP and OBS data collected at the tripod site, documenting the passage of a NLIW of depression shortly before the SAR image was taken. Satellite data from Copernicus Sentinel-1 and the European Space Agency.*

2.4.2 Sedimentology

Average seafloor grain size in the canyon thalweg was medium silt, with 73% silt, 16% clay, and 11% sand by volume (Fig. 2.7). Thalweg sand fraction steadily decreased from 36% to 6% down canyon. There was minimal grain-size variability down-core at the thalweg sites. Sand fraction was dominant along the shelf surrounding the canyon head (70%, Fig. 2.7). Outcrops of consolidated gray clay were cored along the southern rim. Seafloor grain size was similar along the northern shelf rim, with silt and clay increasing with proximity to the canyon walls. Shelf grain size usually decreased slightly down-core. The two sediment traps placed at 0.35 and 2 m above bed collected sediments of identical grain size distribution. The grain size distribution of trap sediment was similar to seafloor samples from the canyon thalweg in deeper water (Fig. 2.7).

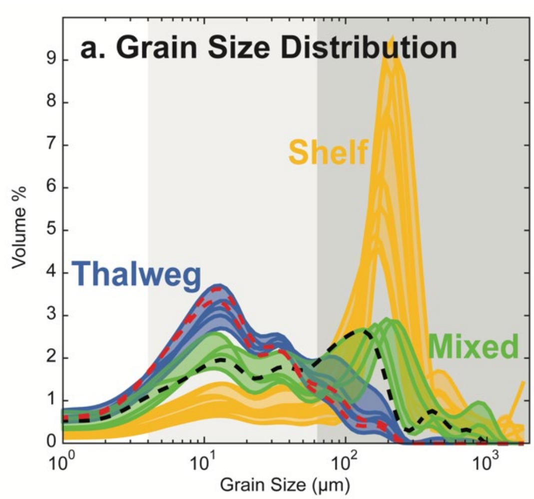

Figure 2.7. *Grain size data from the seabed (upper 5 cm of cores). a) Grain size distributions of seafloor sediment, colored by environment. Dashed lines are the Astoria Canyon tripod seabed sample (black) and tripod sediment traps (red). Gray shading corresponds to clay, silt, and sand size fraction.*

X-radiography of sedimentary structures (Fig. 2.8) showed extensive bioturbation. Physical structures were overwritten in half of the cores. Unaltered physical layering was preserved in core 22 located north of the canyon head. The physical layers that were preserved consist of coarse silt and fine sand. Shell hash and wood were present in cores 17, 18, 19, and 21. The surface mixed layer in the study area varied from 1 to 5 cm below seafloor.

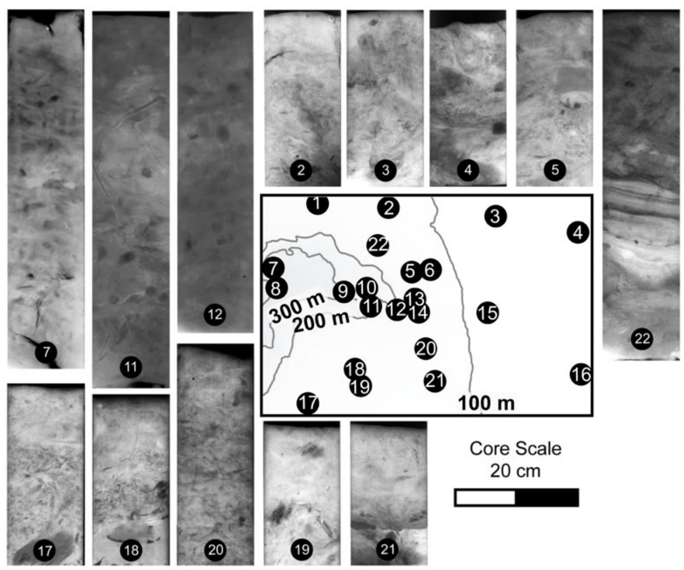

Figure 2.8. *Selected sediment core x-radiographs depicting internal density structure. Darker shades indicate lower bulk density. Biogenic structures are dominant across the study site, with the exception of region where core 22 was collected on the northern shelf rim.*

^{210}Pb accumulation rates from the upper canyon thalweg had an average value of 0.67 g cm^{-2} yr^{-1}. Within the canyon head, core accumulation rates increase with water depth to 500 m depth (Fig. 2.9). Accumulation rates from cores along the north shelf were spatially consistent and averaged 0.24 g cm^{-2} yr^{-1}. Accumulation rates along the south shelf were more spatially variable. The surface mixed layer ranges from 1 to 5 cm below seafloor. A majority of R^2 values for log-linear trendlines were >0.8 indicating interannually consistent rates of accumulation.

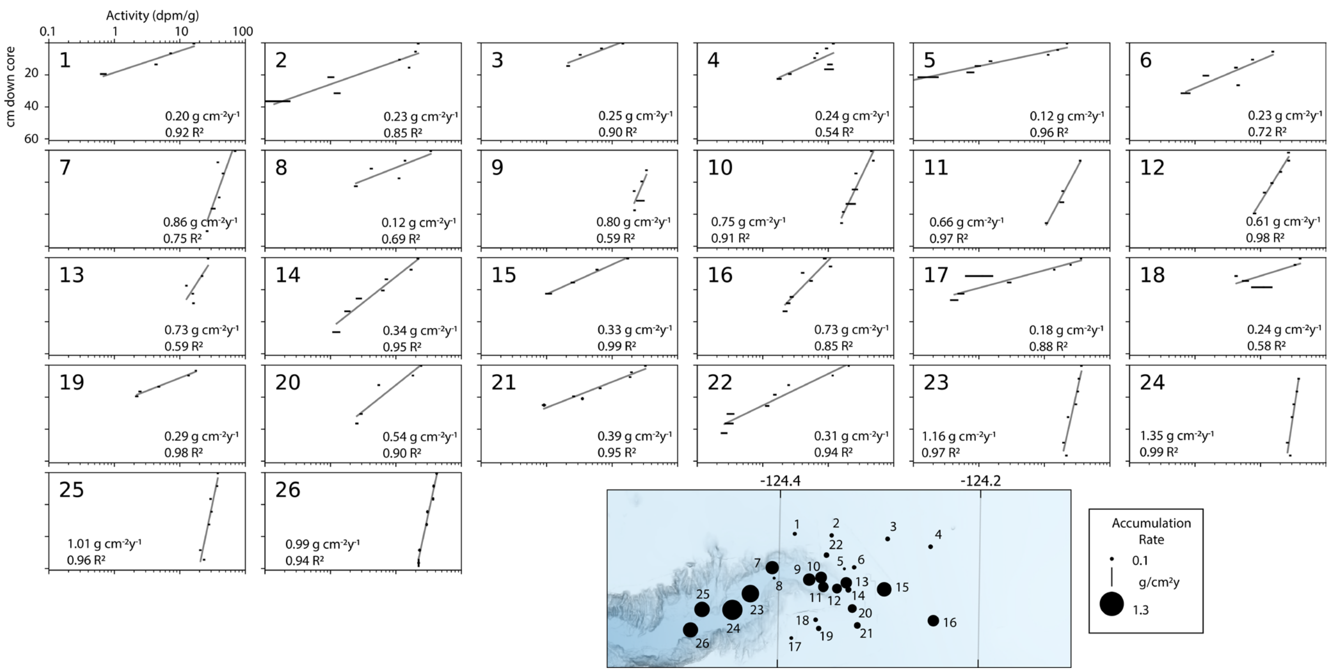

Figure 2.9. *Excess ^{210}Pb profiles along the head of Astoria Canyon and on the surrounding shelf rim, annotated with their accumulation rate and residual fit. Marker size on the inset map is scaled to accumulation rate. Axis limits in all panels are equal and labeled on the upper left panel.*

2.5 Discussion

Observations of sediment transport, grain size and accumulation rates in the head of Astoria Canyon reveal the importance of interacting seasonal sediment supply and ocean energetics in highstand canyon heads. In particular, both winter and summer hydrodynamic processes control sediment transport and accumulation through Cascadia

Margin canyons. Previous studies of similar canyons have emphasized the role of winter storms in driving down-canyon transport (Puig et al., 2004; Thomsen et al., 2017), and processes within Astoria Canyon are consistent with these studies. Storm events produce bed shear stresses that can remobilize the full distribution of seafloor grain sizes, not only on the continental shelf, but also within the canyon head over multiple days each year (Fig. 2.3), and the strong nearbed down-canyon flows associated with southerly winds typical of winter are among the strongest currents in the canyon (Fig. 2.2).

While the importance of winter storms for canyon sediment transport has been emphasized in many studies (e.g., Meiburg and Kneller, 2010; Puig et al., 2013; Normandeau et al., 2020), the summer tripod data provide new insight into the importance of persistent and less-energetic summer events on loading and retaining sediment in the canyon head. During the upwelling-favorable conditions characteristic of summer, internal waves are prevalent, and suspended sediment is periodically transported landward from mid-canyon depths (Fig. 2.2). This upwelling-favorable state provides an important setting for seasonal plume delivery and retention within the canyon head. Although strong internal-wave currents are short-lived, these resuspension events can slow the consolidation process of the recently delivered plume sediment resulting in high porosity, unconsolidated deposits on the shelf (Nittrouer & Sternberg, 1981) and in the canyon head (Fig. 2.5). This preconditioning results in a system with a readily available seabed for subsequent winter storm events to flush sediment down the canyon. Understanding and predicting the magnitude of these loading processes is critical to predicting total down-canyon transport, and studies focused on winter extremes would not capture this fundamental link in the sedimentological cycle.

2.5.1 Summer sediment transport via internal tides and river plume NLIWs

Internal waves play an important role in shaping the morphology of shelf-edge mud deposits (Boegman and Stastna, 2019). The Cascadia Margin exhibits both an active internal wave climate and a large sediment supply, making it a rich site for studies of sediment resuspension and transport by internal waves. The onshore, upslope phase of the internal tide has been identified as a mechanism of sediment resuspension and transport in many canyon and shelf environments globally, and the data from Astoria Canyon support this model and emphasize the seasonal nature of transport processes influencing longer term accumulation. Studies from canyons including Baltimore Canyon (Gardner et al., 1989) and Halibut Canyon (Puig et al., 2013) document elevated SSC associated with the onset of a cold-water bore moving up-canyon, and persistently elevated SSC on the bore's gradual, downslope phase. This pattern initially transports resuspended sediment upslope, contrary to the typical model of exclusively down-canyon sediment transport. Sediment-trap grain size distributions collected at the tripod site resemble those of the thalweg down-canyon (Fig. 2.7) indicating that internal tides initially transport sediment from deposits deeper within Astoria Canyon. However, prior studies suggest that sediment returns down canyon along isopycnal surfaces, generating intermediate nepheloid layers (Gardner, 1989), as have been observed in water-column studies in Astoria Canyon (Hickey, 1997). Internal tides thus play an apparently large role in summer sediment transport within Astoria Canyon and deliver sediment to the canyon head from deeper regions of the canyon over short timescales.

In addition to internal tides, summer sediment transport in Astoria Canyon is directly linked to the Columbia River plume via NLIWs. The canyon head setting near the outer shelf is similar to that of other studies which document resuspension by NLIWs of depression (Quaresma et al., 2007; Zulberti et al., 2020), however the NLIWs observed during summer in Astoria Canyon are generated by the Columbia River, not by remote sources on the continental slope, as confirmed by SAR imagery (Fig. 2.6; Nash and Moum, 2005; Kilcher and Nash, 2010). The observed NLIWs are associated with SSCs from 5 to 130 mg l^{-1} (Figs. 2.4 and 2.6). Thus, the modern Columbia River continues to influence canyon sediment transport by generating NLIWs which travel over the shelf and canyon head. These findings highlight the role of the Columbia River NLIWs as a short-lived yet regularly occurring process that can act to resuspend sediment, transport it shoreward, and inhibit deposit consolidation.

2.5.2 Canyon heads as down-canyon sediment sources

Despite multiple processes acting to promote deposition within the uppermost head of Astoria Canyon during summer, long-term accumulation is greater in deeper regions of this study site (Fig. 2.9). Timeseries observations indicate that fine-grained sediment is deposited and retained in the canyon head over the course of a summer driven by brief upslope currents associated with internal waves and landward flow driven by canyon-confined coastal upwelling. Sediment core data, however, did not constrain the zone of most rapid modern accumulation along the canyon thalweg, as accumulation rates consistently increased to 500 m water depth, the down-canyon limit of sampling. While accumulation rates are consistent with other studies in this area (Nittrouer et al., 1979; Carpenter et al., 1981), the fine spatial resolution presented here highlights this progressive increase between 150 and 500 m water depth. This apparent contradiction between seasonal timeseries and century-scale accumulation suggests that the canyon head is a zone of temporary deposition and ultimately sediment export, i.e., that winter processes are capable of flushing sediment to depth.

The balance between sediment accumulation and export in many highstand canyons depends primarily on the balance between sediment deposition and wave-associated shear stress. Analysis of regional OOI data indicates that the largest storms of each year can resuspend the full grain size distribution of sediment delivered to the canyon head during summer (Fig. 2.1; Fig. 2.3). Many of the large storms along the Cascadia Margin are low-pressure systems which drive southerly winds over the shelf and slope, synchronously affecting several canyon systems. In this region, large waves are typically coherent with southerly winds, increasing both bed stress and the capacity for downslope sediment flux. While the precise winter sediment transport mechanisms remain unknown, it is likely that Astoria Canyon exhibits similar attributes of winter-storm-driven transport to the nearby Cascadia Margin canyons: Quinault, Barkley, and

Eel Canyons (Baker and Hickey, 1986; Puig et al., 2004; Mullenbach et al., 2004; Lamb et al., 2008; Thomsen et al., 2017).

Among the range of plausible transport mechanisms, prior studies have demonstrated the primary importance of nepheloid layers for delivering sediment into canyon systems during storms (Cutshall et al., 1986; Baker and Hickey, 1986; Snyder and Carson, 1986; Sternberg et al., 1986), and our findings are consistent with these studies. Storm-driven down-canyon flows are another likely mechanism which transports wave-resuspended sediment from the canyon head, as canyon axis currents exhibit a strong response to downwelling-favorable wind stresses (Fig. 2.2). Last, while less common, the possibility for downslope transport via sediment gravity flows also exists for Astoria Canyon. SSC observations greater than 150 mg l^{-1} were achieved in the summer timeseries (Fig. 2.2), and lesser concentrations are known to trigger density-driven flow (Puig et al., 2013; Hage et al., 2019). One sediment gravity flow deposit was collected from the Astoria Canyon rim (140 m water depth, Fig. 2.9, core 22), and longer cores from upper Astoria Canyon (>500 m, Carlson, 1968) indicate modern sediment gravity flow activity in this region. These events do not represent the dominant mode of sediment accumulation in this canyon, as they are short-lived and relatively unpredictable events. Such flows are challenging to capture with in-situ deployments, and modeling studies may be useful in quantifying the importance of these events in the total canyon sediment budget.

2.6 Conclusion

The sedimentological and hydrodynamic observations recorded at the head of Astoria Canyon during summer 2019 combined with interannual wind and wave data provide insight into how highstand canyons store and transport sediment under modern conditions. Oceanic processes continue to resuspend and route sediment through the shelf-incising canyon head, supporting the conceptual understanding that even infilling canyon heads remain energetic sites of sediment transport. Sediment transport during summer is driven by internal tides and river plume NLIWs under upwelling conditions, and these processes provide an environment that seasonally loads canyon heads with unconsolidated fine-grained sediment. During winter, the canyon head is subject to large swell and downwelling wind conditions, driving shear stresses that are sufficient to resuspend all seabed sediment for multiple days per year. These conditions can be found in many relatively quiescent canyons on temperate margins globally. As a result, peak rates of sediment accumulation are focused deeper than the canyon head, indicating canyon head sediment export during sea-level highstand.

Submarine canyons throughout the world are often placed on a spectrum between active, energetic sites of sediment flushing and erosion, or quiescent, infilling canyons with minimal transport events. Relative to other canyons globally, Astoria Canyon exhibits traits closer to the quiescent endmember, which is broadly representative of the majority of canyons today. Even so, data from Astoria Canyon suggest that hydrodynamics remain capable of periodic sediment resuspension and transport, and modern stratigraphy from the canyon head suggests sediment gravity flow events do occur, however infrequent. This work demonstrates that multiple processes remain active in canyon systems during sea-level highstand and suggests that other quiescent highstand canyons also may be capable of continued sediment export and density-driven flow triggering.

Chapter 3. FLOOD-DRIVEN TURBIDITE DEPOSITION IN A HIGHSTAND-DETACHED SUBMARINE CANYON

3.1 INTRODUCTION

Submarine canyons transport globally significant volumes of sediment and organic matter across continental margins, creating deposits that record Earth processes over timescales ranging from months to millions of years (Harris and Whiteway, 2011; Rabouille et al., 2019). The primary driver of canyon sediment redistribution is the sediment gravity flow (SGF), a downslope-flowing mixture of water and sediment (e.g., turbidity currents, debris flows). Canyon SGF activity intensifies with proximity to nearshore sediment supply and resuspension processes, and canyon morphology is thus responsive to eustatic sea level. This finding has led to the “highstand dormant” paradigm, which states that canyon processes frequently trigger SGFs during sea-level lowstand but gradually act to infill canyons with fine-grained sediment during highstand (Bernhardt and Schwanghart, 2021; Covault and Graham, 2010; Shanmugam and Moiola, 1988). Recent observations demonstrate complexity within this model, however, as land-detached canyons can trigger SGFs associated with wave events, river floods, and ocean-triggered slope failures (Canals et al., 2006; Heijnen et al., 2022; Liu et al., 2012; Khripounoff et al., 2012; Puig et al., 2004).

In Cascadia, turbidites from canyon systems are believed to represent coseismic submarine landslides triggered by subduction zone earthquakes, and the 300-500 year recurrence of turbidites is interpreted to be the seismic recurrence interval for the region (Adams, 1990; Goldfinger et al., 2012). Within this record, some turbidite deposits have less clear ties to seismic events (e.g., mud turbidites, ash layers, organic layers; Goldfinger et al., 2012; 2013), and the sediment source regions to abyssal stratigraphy are the subject of ongoing study (Hill et al., 2020; 2022). At least one canyon in Cascadia is known to trigger SGFs in association with nonseismic events (Mullenbach and Nittrouer, 2006; Puig et al., 2004).

While SGF deposits offer a useful timeline of prior events, conclusively ruling out the many plausible triggering mechanisms remains difficult without supplementary geologic evidence or timeseries observation (Adams, 1990; Howarth et al., 2021; Nakajima and Kanai, 2000). One useful first-order distinction is whether SGFs are triggered through seismic or nonseismic processes, and prior studies have established common themes between the two processes and products (Guyard et al., 2007; St-Onge et al., 2004; Vandekerkhove et al., 2020). Sediment remobilization by seismic shaking is manifest as sudden failures of sediment sourced from steep marine terrain on the continental slope (Piper and Normark, 2009). By contrast, nonseismic SGFs can remobilize “extrabasinal” sediment sources on the continental shelf or within river basins (Kineke and Sternberg, 1995; Lamb and Mohrig, 2009; Mulder and Alexander, 2001; Puig et al., 2004).

Sedimentary particulate organic matter (POM) origin, age, and degradation represent one means of parsing sediment source regions and making inferences about event deposit triggering over short distances and timescales (Biscara et al., 2011; Hage et al., 2019). In the coastal marine environment, distinct pools of terrestrial and marine POM are mixed and form a gradient from terrestrial to marine across the shelf, slope, and abyssal rise which can be used to distinguish sediment sources (Feng et al., 2013; Hatten et al., 2012; Hedges and Mann, 1979; Prahl et al., 1994). Sedimentary POM is also physically and chemically altered from source to sink, offering insight into the degree of pre- and post-depositional degradation. Last, the terrestrial POM found in the marine environment can be radiocarbon dated, establishing growth age, and thus, a maximum elapsed time between terrestrial source and marine sink. In canyon systems with known connections to fluvial sources, turbidite or SGF deposit POM has been used to characterize the sources to SGF deposits and infer turbidite origin (Biscara et al., 2011; Hage et al., 2019).

Multiple triggers for SGFs in highstand canyons and prominent turbidite records highlight a need to define regions where ocean-driven SGF triggering may be preserved in canyon stratigraphy. Astoria Canyon is chosen to evaluate this question, as it is proximal to multiple potential turbidite inputs including the steep canyon walls, the Columbia River, and the surrounding continental shelf. In this study, we examine whether nonseismic turbidites are preserved within highstand-detached canyon stratigraphy and use turbidite composition to infer turbidity current origins. Our analysis is focused on a detailed interpretation of a representative core with clear turbidite signatures and does not address the spatial extent or distribution of event beds.

3.2 STUDY AREA

The head of Astoria Canyon is located 22 km west of the mouth of the Columbia River, the largest river on the West Coast of the United States by drainage basin area and discharge (Fig. 3.1; Kammerer, 1990). While the river and canyon are coeval over at least 2.6 Ma, Holocene sea-level rise has decoupled sediment transfer between the two systems (Carlson, 1968; Nelson, 1968), and Astoria Canyon now captures only 5% of the fluvial sediment load (Nittrouer et al., 1979; Sternberg, 1986). Today, the canyon is infilling with hemipelagic sediment, and century-scale accumulation rates are generally steady-state (Carpenter et al., 1981; Lahr et al., 2025a; Nittrouer et al., 1979). Turbidites are observed in the upper canyon channel, though turbidite age and origin remain unknown (Carlson, 1968; Barnard, 1978). The physical processes known to redistribute sediment delivered to this canyon are the surface and internal wave field, canyon-enhanced coastal upwelling, and the California Current System (Allan & Komar, 2000; Hickey, 1979; Nash and Moum, 2005; Sternberg, 1986).

The Washington margin has well-documented characteristics of sedimentary POM from terrestrial source to marine sink and exhibits a clear gradient in the properties of stable isotopes and lignin oxidation products (Hedges and Mann, 1979; Prahl et al., 1994). Measurements of the marine end member in this region exhibit enriched $\delta^{13}C_{org}$ (-21‰), low C/N ratio (10), and low-concentration, degraded lignin phenols. Conversely, the terrestrial end-member POM from the Columbia River exhibits depleted $\delta^{13}C_{org}$ (-26‰), high C/N ratios (18), and a high concentration of lignin phenols.

Lignin phenols and stable isotopes in seabed POM are stable over timescales of at least 300 years in marine sediment offshore of Washington (Hedges and Mann, 1979a). The geochemical properties of sedimentary POM in this region thus provide a framework to quantify the relative contributions of terrestrial vs marine sources and make interpretations on modern sediment sources in northern Cascadia.

The Columbia River has a notable history of flood events ranging widely from the Pleistocene Missoula floods to the modern floods of 1894, 1948, and 1964 CE (O'Connor et al., 2020; Rantz and Riggs, 1949; Reynolds et al., 2022), yet the offshore fate of Columbia River flood sediment remains unconstrained. Modern floods observed on the nearby Eel shelf provide a template for flood sedimentation in marine environments: fine lithogenic grain size, negative $\delta^{13}C_{org}$ anomaly (-26‰), high C/N ratio (18), and vascular plant debris (Leithold and Hope, 1999; Sommerfield et al., 1997; Wheatcroft et al., 1996; Wheatcroft and Borgeld, 2000). Rapid bioturbation and physical reworking limit the preservation of flood deposits on the continental shelf (Bentley and Nittrouer, 2003; Leithold and Hope, 1999).

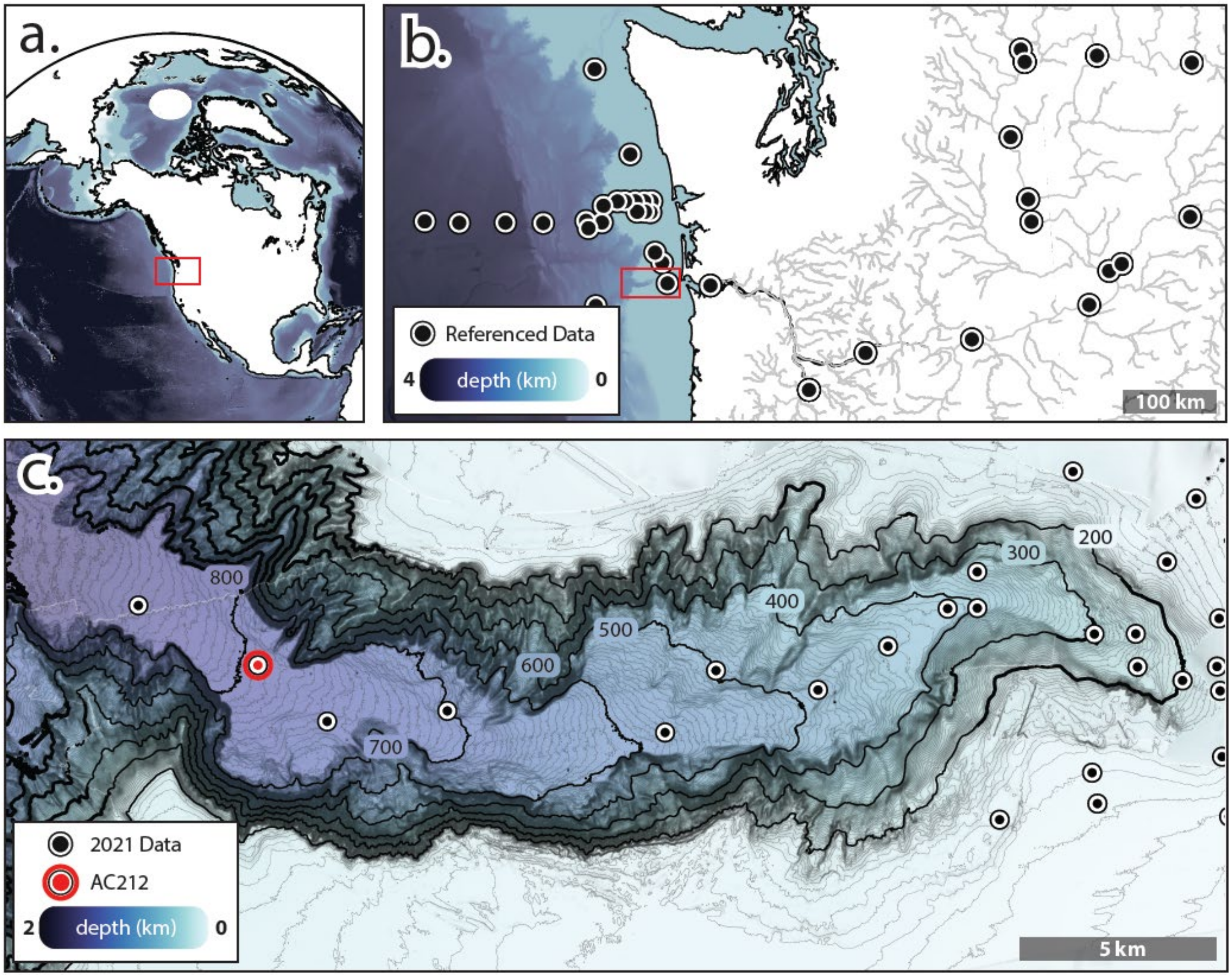

Figure 3.1. *Study area and sampling locations. (a) Global and (b) regional map of the Washington margin and Columbia River. Circles denote locations of sedimentary POM measurements from Hedges et al. (1979a, 1979b) and Prahl et al. (1994). (c) Map of the upper Astoria Canyon showing core locations used in this study.*

3.3 METHODS

A total of 28 sediment cores (5 kasten cores 3 m long and 23 box cores ~50 cm long) were collected in June 2019 and October 2021 from upper Astoria Canyon and the surrounding continental shelf, from water depths of 60 to 900 m (Fig. 3.1). Cores were subsampled at sea and stored at 3°C. This study focuses analytical methods on core site AC212 (Fig. 3.1).

X-ray density scans were collected, and sediment microstructure slides were prepared using the diffusion-embedding technique of Pike and Kemp (1996) and scanned using a Plustek 8100. Grain size was measured at 1 cm intervals down core using a Beckman Coulter LS13-320 particle size analyzer after disaggregation in a sodium metaphosphate solution and sonication.

^{210}Pb geochronology was achieved by alpha detection of the decay product ^{210}Po assumed at equal concentration to ^{210}Pb. ^{210}Po was leached from sediment and measured relative to a known quantity of ^{209}Po spike (Nittrouer et al., 1979). ^{210}Pb activities are corrected for sediment grain size, porewater salt mass, and radioisotope decay between collection and measurement. An age-depth relationship was estimated for core AC212 under constant-flux constant-sedimentation assumptions (CFCS) using the Serac age modeling software (Bruel and Sabatier, 2020). Turbidite intervals identified in sedimentological and geochemical data (see results) were handled as "instantaneous deposits," removing them from the profile prior to computing accumulation rate and establishing depositional age at each horizon.

Sample preprocessing for geochemical methods included desalting with Milli-Q water and freeze drying. For stable isotope analyses, inorganic carbon was removed with 24 h of vapor phase HCl acidification and 24 h of sample drying prior to analysis. Tin capsules were packed with pretreated sediment weighing ~30 mg. Single measurements were made using a ThermoFinnigan MAT 253 mass spectrometer at the University of Washington Isolab. Stable isotope measurements $\delta^{13}C_{org}$ and $\delta^{15}N_{org}$ are reported in ‰ relative to international standards PDB and air, respectively. While acid treatment has been shown to skew $\delta^{15}N_{org}$ signatures (Schlacher and Connolly, 2014), the data interpretations reported here focus on the relative difference between $\delta^{15}N_{org}$ signatures of turbidites and hemipelagite. Measurement of lignin oxidation products followed the CuO methods of Goñi and Montgomery (2000). Briefly, lignin phenol concentrations were measured using a 100 mg aliquot that was oxidized with CuO under basic pH. Following oxidation, lignin phenols were extracted from the solution, concentrated, and measured by paired gas chromatography-mass spectrometry using a Leco Tru-TOF GC-MS.

Radiocarbon age measurements were made on two samples of coarse organic material isolated from turbidite deposits using a 63 µm sieve and deionized water. Samples were dried at 50°C for 48 hours and sent to Beta Analytic; results are reported in calendar years per the IntCal20 calibration (Fig. S3.1).

3.4 RESULTS

All cores collected from the canyon thalweg >300 m water depth were composed of low-variability silt and clay interpreted to be hemipelagite, defined broadly as a fine-grained mixture of terrigenous mud and biogenic remains. The hemipelagite had a median grain size (d50) of ~10 µm, contained <5% sand, and did not exhibit down-core or inter-site trends. Sedimentary structures were limited within hemipelagic material except for intermittent layers of alternating relative density (Fig. S3.2, S3.3).

One kasten core from the channel thalweg contained clear turbidite deposits, whereas others, including several from channel terraces, did not (Fig. 3.1). The turbidite-bearing core, collected at 800 m water depth (AC212), contained two event layers distinguished by grain size, sedimentary structures, radioisotope concentrations, and organic matter composition. The characteristics of the hemipelagite and event layers in this core are described in detail below. AC212 is composed primarily of hemipelagite, but core intervals 48-58 and 133-145 cm below seafloor are distinct and will be referred to as event beds 1 and 2 (E1, E2). E1 and E2 are composed of silt, fine sand, and coarse organic debris with well-preserved sedimentary structures (Fig. 3.2, Figs. S3.4, S3.5). The base of E1 begins with a lamination of fine sand, and alternates between fine grained organic-rich layers and sand laminae (Fig. 3.2b, 3.2d). The base of E2 contains 1-2 cm of fine sediment and coarse organic debris and evolves into alternating sand laminae and graded sequences (Fig. 3.2c). Both coarse layers contain multiple cm-scale normally graded sequences, mm-scale planar lamination, and soft-sediment deformation. Coarse phytoclasts 1-2 cm in length are abundant in low-density laminations (Fig. 3.2g). The sedimentary structures of E1 and E2 indicate deposition by density-driven sediment gravity flows carrying fine-grained particles, i.e., turbidites (Bouma Tb-e, Bouma, 1962).

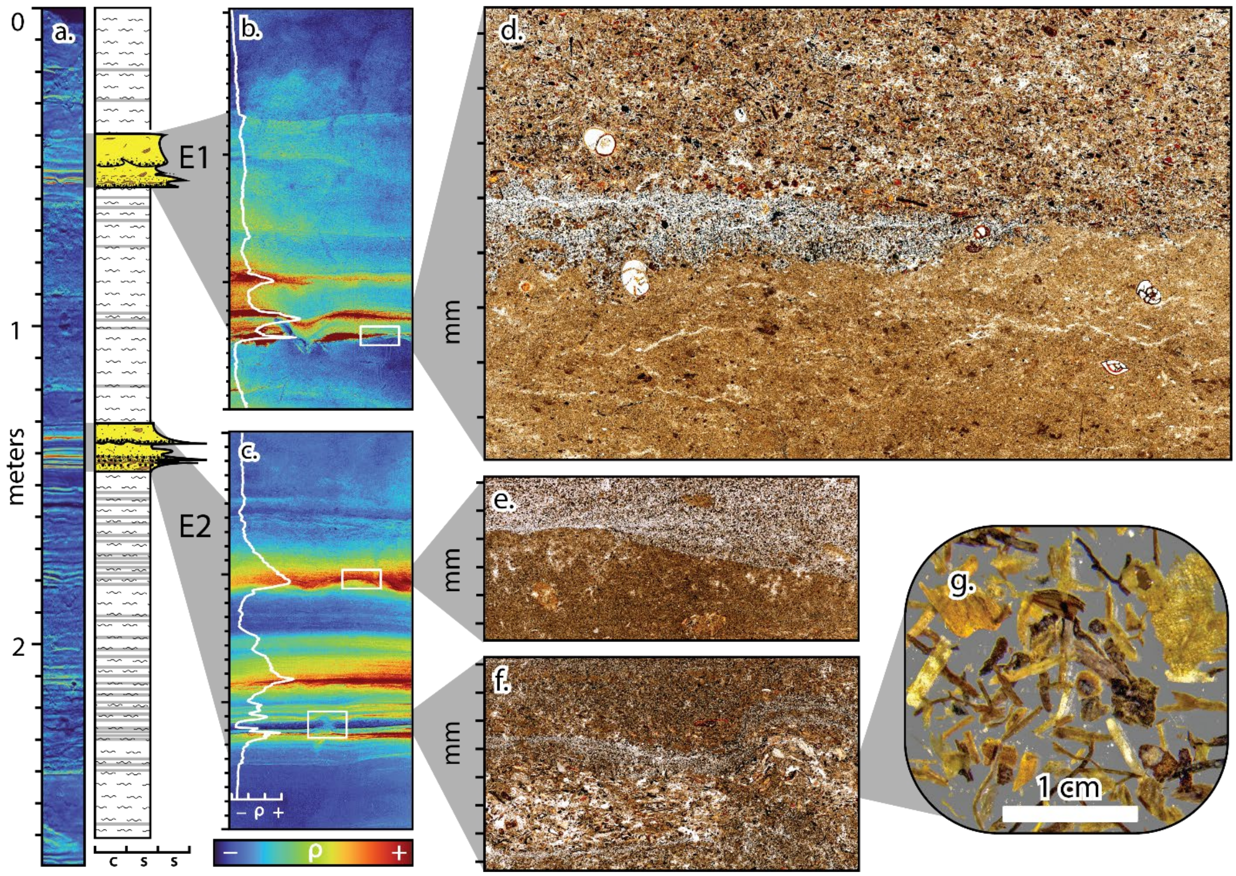

Figure 3.2. *Sedimentological features of core AC212. (a) Down-core relative x-ray density scan and stratigraphic log; the median relative x-ray density is shown as a white line in (b) and (c). Insets (b) and (c) highlight layers E1 and E2, respectively. (d–f) Microstructure images illustrating the basal and internal structures of turbidite layers. (g) Microscope image of the coarse fraction (>63 μm) sieved from layer E2.*

The ^{210}Pb activity of hemipelagic sediment in core AC212 decreases log-linearly from 45 dpm/g at the seafloor to a background level of 1.3 dpm/g at a depth of 205 cm bsf (Fig. 3.3). The slope of a log-linear trendline fit through the excess ^{210}Pb layer is 37.7 (R^2 = 0.96), indicating steady-state accumulation at a rate of 1.2 cm/y. The near-seabed ^{210}Pb profile does not exhibit a surface mixed layer, indicating minimal biogenic mixing at this site. Log-linear decay is clearly interrupted by layers E1 and E2, which have low ^{210}Pb concentrations. Hemipelagic sediment directly above and below layers E1 and E2 exhibits identical activity, indicating preserved steady-state accumulation before and after event deposition. Depositional ages for E1 and E2 were modeled under CFCS assumptions using the Serac age model (Bruel and Sabatier, 2020), and depositional ages are estimated to be 1955±5 and 1901±8 CE, respectively.

The mean percent organic carbon within hemipelagic sediment in core AC212 is 4.1% (SD 0.4%), and within layers E1 and E2, the mean percent organic carbon is 3.6% (SD 0.9%, Fig. S3.6). The mean $\delta^{13}C_{org}$ ratio of hemipelagic sediment in core AC212 is -22.17 (SD 0.42‰), and within layers E1 and E2, mean $\delta^{13}C_{org}$ is -25.35‰ (SD 0.46‰). The mean C/N ratio of hemipelagic sediment in core AC212 is 8.4 (SD 0.17), and within layers E1 and E2, the mean C/N ratio is 13.7 (SD 2.0). Coarse organic material isolated from E1 and E2 for ^{14}C dating exhibits IntCal20 radiocarbon ages of 500±30 and 740±30 ybp, respectively. The concentrations of 12 lignin phenols were also measured down-core in core AC212. In hemipelagic sediment within core AC212, the average lignin phenol values include a total lignin concentration of 1.7 mg per 100 mg OC, a vanillin acid to aldehyde ratio of 0.37, a syringyl to vanillyl ratio of 0.24, and a cinnamyl to vanillyl ratio of 0.12. In turbidite deposits E1 and E2, the average lignin phenol values include a lignin concentration of 6.0 mg per 100 mg OC, a vanillin acid to aldehyde ratio of 0.26, a syringyl to vanillyl ratio of 0.37, and a cinnamyl to vanillyl ratio of 0.09. $\delta^{13}C_{org}$ and $\delta^{15}N_{org}$ were also measured in sediment at the seabed (0-2 cm bsf) of several nearby shelf and canyon core sites (Fig. 3.1 a,b; Fig. 3.4) to provide a comparison between nearby sediment sources. The $\delta^{13}C_{org}$ values for sediment OC at the canyon floor are -21.5 to -23.5‰, and C/N ratios are 8 to 10.5. The $\delta^{13}C_{org}$ values for shelf sediment OC are -23 to -24.5‰, and C/N ratios are 10 to 13. Average percent organic carbon for canyon and shelf sediment are 4% and 1%, respectively.

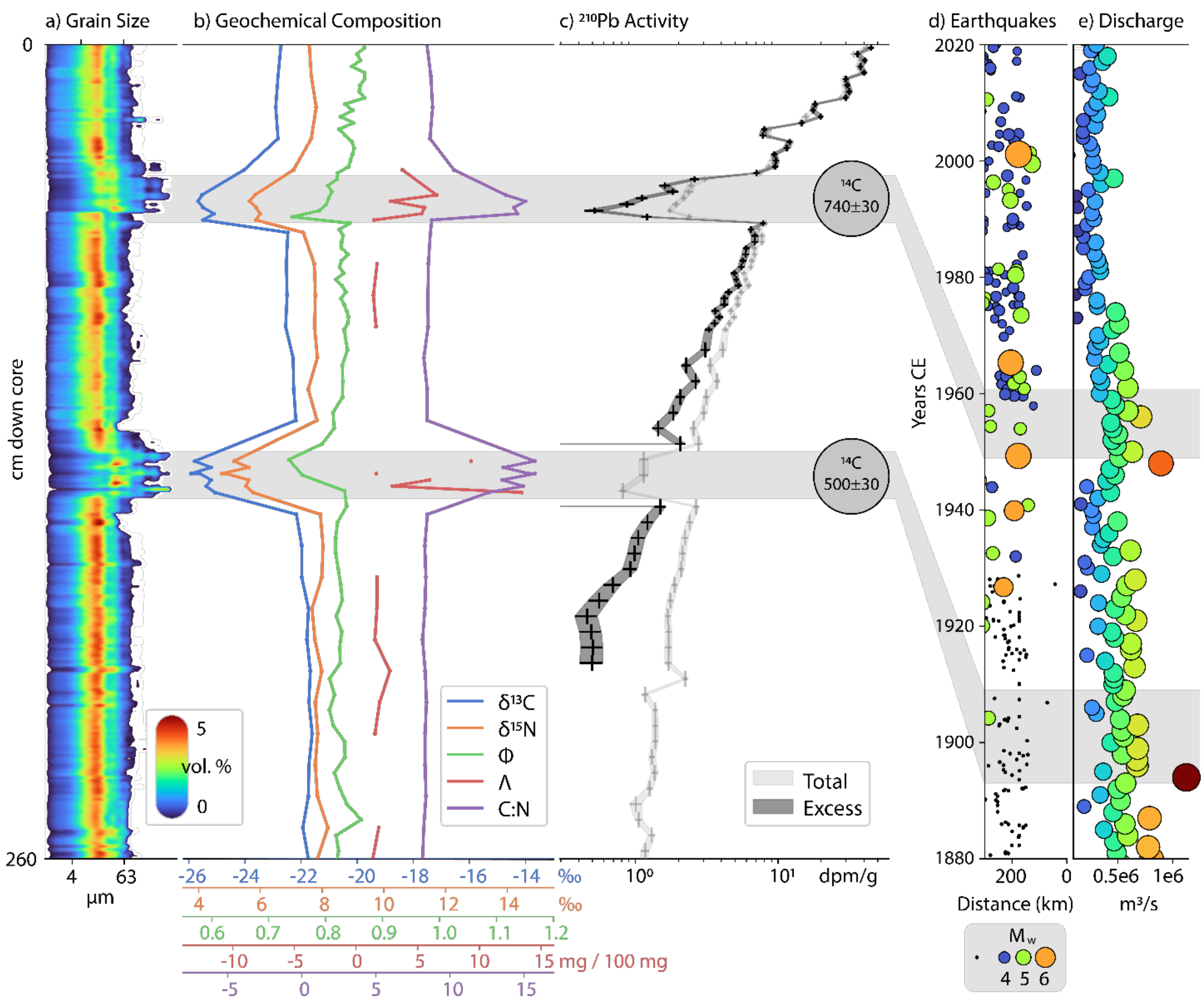

Figure 3.3. *Sedimentological, geochemical, and radioisotopic data for core AC212. (a) Down-core grain size distribution. (b) Geochemical composition including $\delta^{13}C_{org}$, $\delta^{15}N_{org}$, porosity (Φ), lignin concentration, and atomic C/N ratio. (c) ^{210}Pb activity profile. (d,e) Chronologies of local earthquake events and maximum annual discharge of the*

Columbia River; data are from USGS (2023a and b). Marker color and size in (d) denote earthquake magnitude, black markers are historical earthquakes with undetermined magnitude; marker color and size in (e) denote discharge magnitude.

3.5 DISCUSSION

3.5.1. Identifying flood turbidites: evidence and conceptual model

Despite several plausible turbidite origins, layers E1 and E2 can be clearly related to modern river floods based on sedimentology (x-radiographs, microstructure, grain size), geochemical composition (C_{org}, N_{org}, ^{210}Pb), and age (^{210}Pb, ^{14}C). Layers E1 and E2 are 10-20 cm thick, silt-dominant event deposits with sedimentary structures consistent with turbidite sequences (e.g., Bouma Tb-e), including graded sequences, an erosive internal contact, planar laminations containing coarse organic debris and load structures (Fig. 3.2). Turbidite ^{210}Pb depositional ages closely align with flood events: layer ages for E1 and E2 are consistent with the ages of the two largest historical flood events (Fig. 3.3). Turbidite ^{210}Pb activity is uniformly depressed, and hemipelagite ^{210}Pb activity is identical above and below deposits, indicating that each turbidite was deposited as a single event (e.g., Kenney et al., 2022; Burnett et al., 2023). The composition of turbidite sedimentary organic matter approximates terrestrial end-member signatures from the Columbia River, and all geochemical measurements of turbidite material are distinct from the hemipelagite accumulating on the adjacent canyon floor and shelf (Fig. 3.4 and references therein). Compositional differences are present not only in bulk organic isotope signatures, but also within the lignin fraction: turbidite lignin is more abundant, nondegraded, and contains a higher proportion of angiosperm wood (Fig. 3.4). Terrestrial organic debris ^{14}C ages are <1 ka (Fig. 3.3); in this region, comparable ^{14}C values are observed in modern sediment discharged from the Columbia River (Feng et al., 2013). Critically, these recent ^{14}C ages indicate that relict, pre-Holocene sediment deposits are not the primary sediment source for turbidites. We infer from the overall geochemical signature that the organic matter in turbidites has not aged along the shelf and reflects material moved rapidly from the coastal zone to the slope without extensive on-shelf storage and degradation (e.g., Keil et al., 2004).

Given the evidence for rapid river-to-canyon sediment transport, layers E1 and E2 may represent hyperpycnal flow (Mulder and Alexander, 2001; Mulder and Chapron, 2012; Mulder and Syvitski, 1995; Mulder et al., 2001a; 2003; Zavala and Arcuri, 2016; Zavala, 2020). Turbidite ^{210}Pb activity is depressed relative to hemipelagite sediment delivered under relatively steady-state conditions, indicating sediment transport with minimized exposure to water masses rich in ^{210}Pb. While these turbidites could be derived from remobilization of flood deposits initially emplaced on the shelf, temporary deposition would permit bioturbation and incorporation of marine organic carbon, diluting terrestrial biomarker signals (Leithold and Hope, 1999). In addition, the observed sedimentary structures are characteristic of hyperpycnites, specifically multiple graded pulses, organic laminae, and a reverse-graded base, as observed in E2 imagery (Fig. 3.2; Biscara et al., 2011; Zavala & Pan, 2018). Adopting the classification of Piper and Normark (2009), the turbidites observed here fit the characteristics of "direct freshwater flow" deposits, namely "muddy-hypopycnal plume" or "muddy hyperpycnal plume" turbidites. Regardless of the precise pathway, our interpretations highlight a dependence of event bed formation upon river discharge and demonstrate that the modern Columbia River remains capable of bridging the gap between river and submarine canyon.

3.5.2. River floods drive turbidite deposition in highstand canyons

In this highstand canyon setting, evidence exists for flood-associated turbidity currents at least once per century, a process previously thought to be inactive or limited in shore-detached canyons that lie outside the main littoral cell (Shanmugam and Moiola, 1982, 1988). This apparent contradiction highlights the complexity within the depositional environment of highstand submarine canyons and supports the growing number of studies reframing highstand canyon sedimentation on a spectrum between active and dormant (Heijnen et al., 2022; Lahr et al., 2025a; Mullenbach and Nittrouer, 2006; Puig et al., 2004). Of the numerous sediment gravity flow observations related to floods, only some are related to hyperpycnal plumes, while others are triggered by dilute plume conditions or seabed preconditioning, highlighting the complex initiation mechanisms acting beyond river mouths (Ayranci et al., 2012; Hizzett et al., 2018; Wright and Nittrouer, 1995). These studies of dilute plume triggering support the hypothesis that flood-related stratigraphy is possible offshore of riverine sources despite river-canyon decoupling and an often-low suspended sediment concentration.

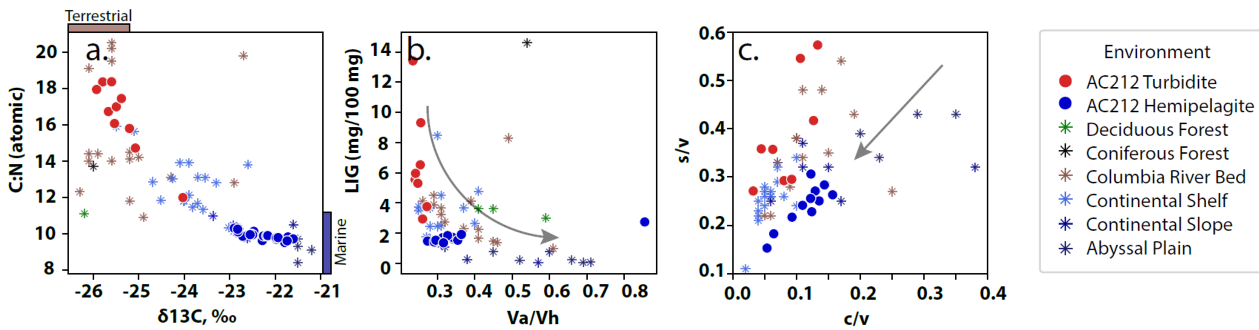

Figure 3.4. *Comparison of geochemical parameters from core AC212 with those from sediment source regions within the Columbia River Basin and Cascadia margin. Circles represent data from core AC212, with red indicating turbidite intervals and blue indicating hemipelagite intervals. Stars denote seabed sample data from Hedges et al. (1979a, 1979b), Prahl et al. (1994), and seabed sites from this study; sampling locations are shown in Fig. 3.1a and 3.1b. Terrestrial and marine end-members for organic matter are denoted in (a) with brown and blue boxes, and (b) and (c) contain arrows indicating the vector for degradation of lignin.*

Over longer timescales, this updated understanding of canyon sediment transport also impacts geochemical flux estimates and the interpretation of event stratigraphy. The two turbidites account for approximately 12% of the total mass and 11% of the organic carbon accumulated over the full core interval (>200 y), demonstrating the outsized contribution that flood turbidite deposition can provide to the seabed. This preservation of coarse, modern, and terrestrial organic matter located 41 km offshore and at 800 m depth also highlights that flood processes represent an efficient, concentrated pathway into the marine environment. While the overall extent and downslope limit of the E1 and E2 deposits are not constrained in this study, examples globally show that related flows can reach abyssal depth (Bourget et al., 2010; Nakajima, 2006). It is possible that these floods, and the larger flood events which have occurred throughout the Holocene, have generated turbidite stratigraphy at greater depth. This suggests a greater downslope flux of POM than is accounted for via steady-state processes alone.

3.6 CONCLUSIONS

This study provides the first evidence of modern, nonseismic sediment gravity flow activity in a northern Cascadia submarine canyon, demonstrating significant complexity within the highstand dormant paradigm. Even when decoupled from the shoreline, sediment gravity flows related to coastal forcing reach at least intermediate depth in submarine canyons, demonstrating a continued connection between highstand canyons and hydro-sedimentary processes. More specifically, the link between turbidites and river floods highlights the importance of fluvial processes in cross-margin sediment transport and the accumulation of sediment and organic matter in deep marine stratigraphy. Turbidity currents may have been triggered directly by hyperpycnal flows or by preconditioning via flood sedimentation, underscoring the broad range of fluvial, oceanographic, and tectonic processes that build stratigraphy on active margins. Given the importance of submarine canyon deposits in paleoseismic reconstructions, distinguishing between seismic and nonseismic turbidites is critical, and this study constrains turbidite origin via the synthesis of lithogenic, radioisotope, and organic matter tracers. This methodology provides a powerful framework for parsing turbidite origins in any location where compositional gradients exist between source and sink.

Unresolved sediment transport pathways within canyons, as highlighted in this study, remain a key gap that precludes a complete view of modern canyon functioning.

Chapter 4. CANYON HEADS PROVIDE A RECORD OF SEDIMENT GRAVITY FLOWS OVER THE SEISMIC-INTERSEISMIC CYCLE

4.1 Introduction

Critical environmental histories are interpreted from cores within submarine canyon systems, including turbidite records, which are among the longest temporal archives and most trusted paleoseismic proxies for seismic geohazard and recurrence (Goldfinger et al., 2012; Howarth et al., 2021; Talwani & Cox, 1985). The conceptual model is that sediment is flushed through canyon systems into the abyssal ocean in response to earthquake triggering (Goldfinger et al., 2012; Howarth et al., 2021), yet highstand-detached canyons are otherwise sedimentologically inactive (Shanmugam & Moiola, 1982, 1988), and this results in the deposition of widespread, seismically-triggered event beds in the abyssal ocean. Importantly, this model has been inferred almost entirely from distal deposits spanning multiple Holocene earthquake cycles, with little direct evidence from the proximal canyon reaches where sediment gravity flows are thought to be initiated. Turbidite interpretations are thus limited by both the state of our understanding of the canyon response to major triggering mechanisms and our ability to infer deposit origin. Recent studies have documented exceptions to the seismoturbidite conceptual model (Hill et al., 2022, 2026; Piper & Normark, 2009; Puig et al., 2004) and questioned whether canyon stratigraphy can provide reliable event histories (Bailey et al., 2021; Nieminski et al., 2024). One primary complication is that canyon sediment routing is influenced by oceanic processes on the shelf and coast—e.g., oceanic storms, dense shelf water cascading, and river floods (Bailey et al., 2021; Heijnen et al., 2022; Liu et al., 2012; Mulder et al., 2003; Puig et al., 2004)—and these processes generate turbidite stratigraphy that may complicate core chronologies (Goldfinger et al., 2013). Additionally, uncertainty remains regarding the flow paths and processes that generate seismoturbidites in the abyssal ocean, with recent studies identifying the deformation front as a major source of turbidite sediment (Hill et al., 2022, 2026). While there is a clear need to validate hypotheses of margin flushing in response to major triggers, the opportunities to test assumptions remain rare, as they require well-constrained, major triggering events and contemporaneous evidence of sediment gravity flow activity. The upper reaches of highstand submarine canyons are promising environments for well-preserved, century-scale chronologies, due to enhanced sedimentation rates from off-shelf transport processes and reduced bioturbation associated with upper-slope oxygen minima.

The Cascadia subduction zone preserves one of the world's best-constrained paleoseismic records, with turbidite chronologies indicating that ~M9 earthquakes occur every 200–500 years. The most recent subduction zone earthquake on 26 January 1700 CE is independently constrained by written tsunami records, coastal subsidence, and regionally correlated abyssal turbidites, providing an unusually precise date for evaluating sedimentary archives (Atwater et al., 2016; Atwater & Yamaguchi, 1991; Goldfinger et al., 2012; Satake et al., 2003; Yamaguchi et al., 1997). The central Cascadia margin is also the site of long-term records of interseismic forcing events, including a

~350-year dendrochronological reconstruction of Columbia River discharge and river gauge observations extending to the nineteenth century. Historical timeseries records constrain the timeline of major disturbance over the 300-y seismic-interseismic cycle and provide a rare opportunity to directly compare canyon sediment routing with known triggering events. Astoria Canyon, located along the central Cascadia margin, is uniquely suited for this test because it is proximal to the well-studied Columbia River—the largest river in Western North America by discharge—and largely isolated from crustal and transform-fault seismicity, minimizing ambiguity between nonseismic triggers, crustal earthquakes, and subduction zone earthquakes. While Astoria Canyon formed as a conduit for Columbia River sediment, the canyon head is now detached from the shoreline (25 km offshore, 150 m water depth) and receives only ~5% of the modern Columbia River sediment supply (Sternberg, 1986). As a highstand-detached canyon with independently constrained records of both seismic and oceanic forcing, Astoria Canyon provides a natural laboratory for testing how sediment is mobilized, routed, and preserved during major earthquakes and the interseismic period.

Here we show that stratigraphy from the upper reaches of a highstand submarine canyon preserves a high-resolution record of sediment transport throughout the most recent seismic-interseismic cycle. We identify two distinct classes of event deposits with characteristic sedimentological and geochemical signatures that can be independently linked to historical earthquakes and floods, providing a rare validation of submarine canyon stratigraphy against known triggering events. These observations reveal distinct sediment-routing pathways associated with seismic and interseismic forcing and demonstrate that substantial volumes of sediment are retained within the upper canyon during sea-level highstand. Together, our findings indicate that connectivity between upper canyon systems and the abyssal ocean may be more limited than assumed by the prevailing canyon-flushing model, and stratigraphy from upper canyon systems can be leveraged as a short-timescale, well-constrained test of assumptions regarding seismic and interseismic gravity flow routing.

4.2 Methods

4.2.1 Core collection and imaging

Forty-nine sediment cores, sparker multichannel seismic data, and multibeam bathymetry were collected from the upper 50 km of Astoria Canyon targeting the floor and wall environments in water depths from 100–1400 m over 5 cruises between 2019-2024 (Fig. 4.1), prioritizing the region of enhanced sedimentation rates and the minimum in bottom water oxygen. Sediment was collected using a variety of coring devices (piston, gravity, multi, box). Gravity and piston cores were sectioned into 1.5 m segments upon collection and stored at 3°C. Cores were transported to Geotek X-ray CT scanning facilities at the Pacific Coastal and Marine Science Center (model RXCT) and the mobile unit operated by the National Science Foundation Marine Rock and Sediment Sampling Group (model VXCT). CT scan resolution ranged from 69 µm to 327 µm. Imagery of down-core orthogonal planes at 90 and 180 were produced by computing the median CT number normal to the plane within a 1 cm-thick scanning volume. Cores were then split, line-scan imaged on a Geotek multi-sensor core logger track, logged visually, and subsampled at 2 cm for analysis.

4.2.2 Event deposit identification

Event beds were identified within cores using a combination of CT density structure, ^{210}Pb radioisotope concentration, organic matter composition, and sediment grain size distribution. X-ray computed tomography (CT) scans were collected to characterize internal density structure and identify the sedimentary structures associated with event deposition, including turbidity currents, debris flows, and other forms of marine sediment gravity flows. CT intensity was also used as a proxy for whole-core sediment density, and median density profiles were extracted across event deposit intervals for comparison between deposits. Bulk sediment organic geochemistry was measured to characterize sediment source and distinguish between marine- and terrestrial-derived deposits. Sediment samples were freeze dried, homogenized, and acidified using vapor-phase HCl to remove inorganic carbon prior to stable isotope analysis. Measurements of δ^{13}Corg, δ^{15}Norg, organic carbon and nitrogen, were performed using a ThermoFinnigan MAT 253 isotope ratio mass spectrometer, and atomic C:N ratios were calculated from elemental concentrations. The stable isotope composition of organic carbon and nitrogen is reported in per mille relative to international standards VPDB and air, respectively. Grain size analysis on core sections was performed on a Beckman-Coulter LS13-320. Deposits were then classified into two contrasting categories. Type-1 deposits were characterized by thin, graded, laminated turbidite beds with low excess ^{210}Pb activity and terrestrial organic matter signatures including depleted $\delta^{13}Corg$ values (-25‰ VPDB) and elevated C:N ratios. Type-2 deposits were characterized by thick, compositionally heterogeneous intervals containing sheared muds, mud clasts, debris-flow fabric, and marine-derived organic matter signatures (C:N ~8, $\delta^{13}C_{org}$ -21.5‰ VPDB, Fig. 4.3).

4.2.3 Geochronology

The geochronological techniques used to determine sediment accumulation rates and event bed depositional ages include ^{210}Pb dating and an age-depth relationship estimated from seasonally laminated sediment. ^{210}Pb measurements were performed via the alpha detection of ^{210}Po assumed at equal concentration to ^{210}Pb after correcting for grain size, salt mass, and radioactive decay between collection and analysis. Outside the oxygen minimum zone (dissolved oxygen >0.2 ml l^{-1}) the constant-flux constant-sedimentation assumptions were used to compute sediment accumulation rates, consistent with prior work in the area.

Within the oxygen minimum zone (dissolved oxygen <0.2 ml l^{-1}), age-depth relationships were obtained using the constant-activity (CA) model under the assumption that the initial concentration of ^{210}Pb in sediment is constant at each core site and post-depositional mixing is negligible. The CA model assumptions were verified using supporting information from density scans, sediment traps, and stratigraphic event beds. Density scans confirm minimal post-depositional mixing and the preservation of horizontal laminae. Sediment traps collected modern sediment near the seabed in

Astoria Canyon at 180, 500, and 1100 m water depth between March 2023-2024. Sediment trap ^{210}Pb activity demonstrates a strong linear relationship with water depth (R^2 0.92) despite spatially variable accumulation rates across the study area. Physically, this indicates that at this site, the initial concentration of unsupported ^{210}Pb in sediment is controlled primarily by water depth and not by the observed variability in rates of hemipelagic sedimentation and particle scavenging. The linear regression of sediment trap ^{210}Pb activity was then used to estimate the initial ^{210}Pb concentration along the canyon floor, and trap-defined initial concentrations for each core were used to compute the depositional age of turbidite event beds. This method accounts for the potential non-recovery of unconsolidated, high-porosity sediment near the seabed.

Two turbidite event beds were deposited recently enough to be contained within the region of excess ^{210}Pb in several cores from the oxygen minimum zone, and the depositional age of these deposits is constrained. ^{210}Pb activity is depressed within turbidite intervals, and hemipelagic intervals above and below turbidites are log-linear with no offset in activity, indicating negligible erosion by the flow. Identified event beds were treated as instantaneous deposits and excluded from age–depth calculation by removing the corresponding depth intervals and shifting all underlying ^{210}Pb measurements upward by the thickness of the removed interval(s). ^{210}Pb activity at the turbidite horizon was then interpolated from overlying and underlying points and compared with the initial activity at deposition to establish a depositional age. The mean ages of these turbidite horizons are 1900 ± 13 and 1950 ± 7, which overlap in age with the 1948 and 1894 floods. Estimated depositional ages for event stratigraphy outside the layer of excess ^{210}Pb were obtained by back-propagating the mean ^{210}Pb vertical accumulation rate from the earliest chronostratigraphic marker dateable with ^{210}Pb, in this case, the 1894 turbidite event bed.

4.3 Results and Discussion

4.3.1 Upper canyon stratigraphy as a record of one seismic–interseismic cycle

Upper Astoria Canyon contains a zone of rapid sediment accumulation and limited bioturbation preserving a continuous, high-resolution stratigraphic record across the most recent seismic-interseismic cycle. The location of the canyon depocenter within Astoria Canyon and recently deposited sediment gravity flow event beds was determined from 49 cores collected in the upper reaches of the canyon between 150-1400 m water depth (Fig. 4.1a). Century-scale sediment accumulation rates are steady-state and vary predictably with depth, increasing to a maximum value of 1.2 cm y^{-1} at 600 m water depth and 34 km offshore, and decreasing beyond this, with little modern sediment accumulating beyond the shelf incised channel. This zone of enhanced accumulation intersects a severe oxygen minimum zone between 700–900 m water depth (<0.2 ml l^{-1}), which limits bioturbation and preserves physical depositional structures. Computed tomography (CT) density structures within this zone reveal intermittent preservation of cyclical density laminations with a mean wavelength matching the ^{210}Pb vertical accumulation rate, i.e., varves (Fig. 4.1). This unique setting allows precise age control using a combination of dating methods including a ^{210}Pb

constant initial concentration age model, down-core extrapolation of the mean ^{210}Pb sediment accumulation rates, and an algorithm for estimating age based upon varve laminae. This combination of methods permits event bed age control over a ~320 y time period, the most recent seismic cycle.

Three primary sediment gravity flow event beds are present in cores over the age-controlled time period, and these layers are correlatable across a ~12 km region of the canyon floor (Fig. 4.1). Event beds are distinguishable from background sedimentation due to increased CT density, sedimentary structures consistent with sediment gravity flow deposition, increased lithogenic grain size, and reduced ^{210}Pb activity within the excess ^{210}Pb layer where the deposit is sufficiently modern. Within the event beds identified, we observe two distinct types: centimeter-scale "Type-1" deposits indicative of dilute sediment gravity flows, and meter-scale "Type-2" deposits indicative of dense, multi-phased flow. Type-1 deposits are thin (<15 cm)

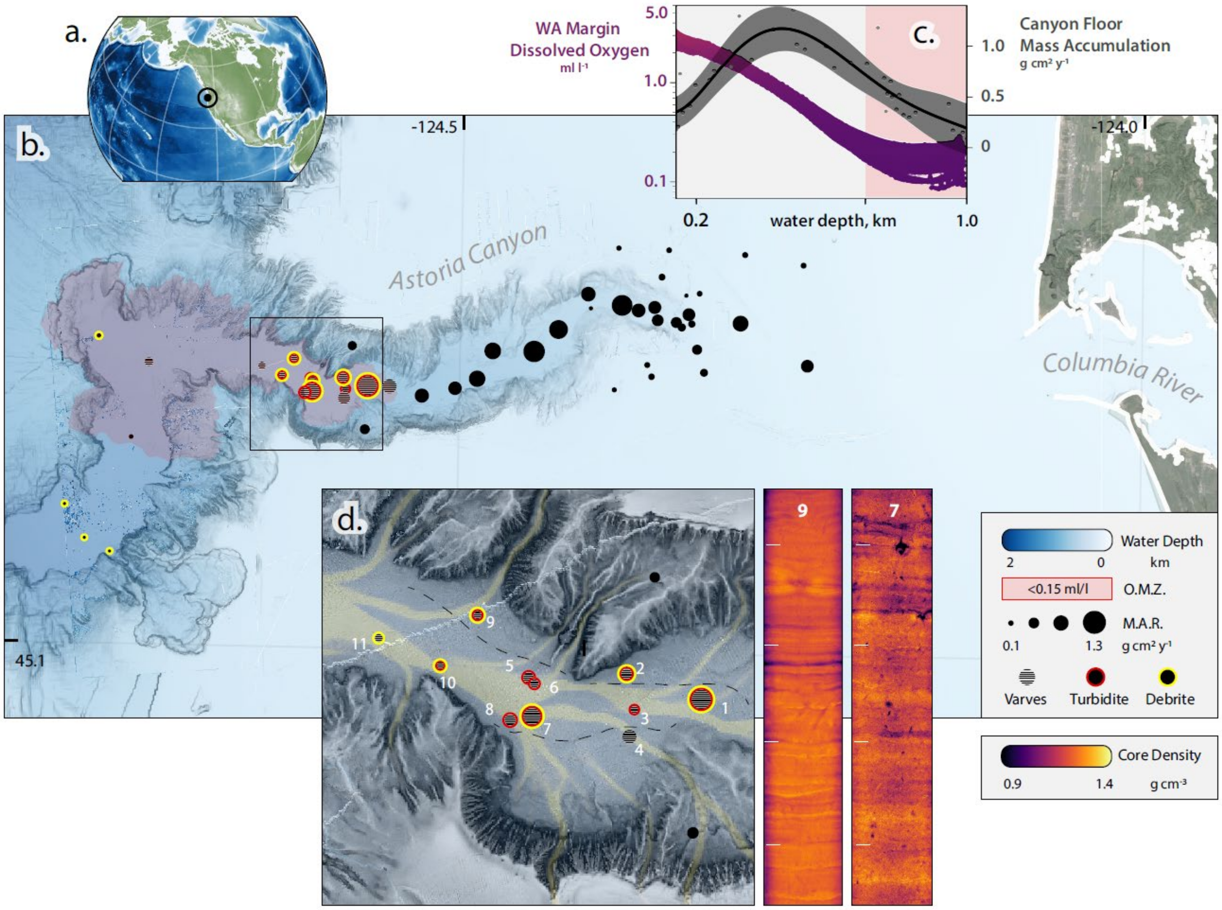

Figure 4.1. *Morphology and depositional environment of Astoria Canyon, northern Cascadia Margin, including sediment core locations and the position of the oxygen minimum zone. (a) Global setting, (b) regional bathymetric map and regions of suboxic canyon bottom water, symbols indicate core locations, accumulation rates, event deposits. (c) Position of the oxygen minimum zone relative to sediment accumulation rates, with suboxic conditions shaded red. (d) Inset of core locations, and density structure of laminated hemipelagic sediment.*

deposits of silt and sand, graded and internally laminated, with low excess ^{210}Pb activity and organic matter dominated by fresh terrestrial inputs (e.g., −26‰ $\delta^{13}C_{org}$, C:N > 14). In contrast, the Type-2 deposits are 20–200 cm thick, with an upper unit composed of coarse turbidite sand and a lower unit composed of highly deformed fine-grained sediment. The upper turbidite unit within Type-2 deposits is 10-20 cm thick and exhibits a variable number of density pulses across cores (Fig. 4.2). The lower unit of Type-2 deposits can be >150 cm thick and can exceed core

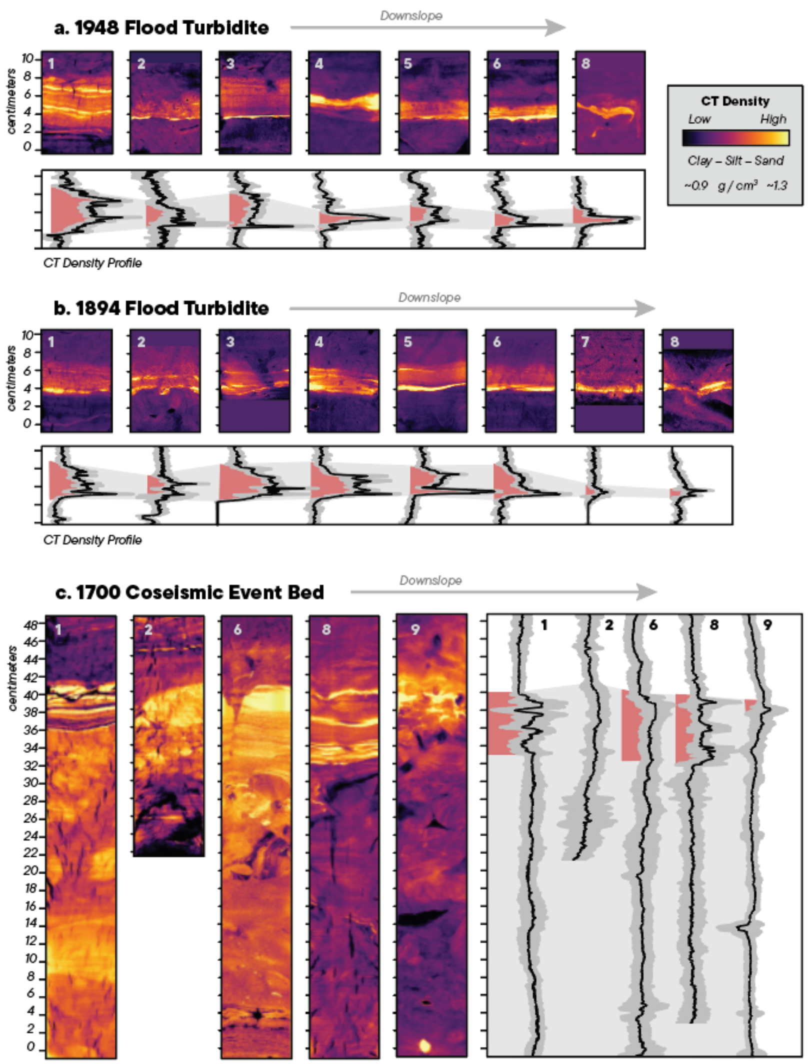

Figure 4.2. *Density structure and downslope evolution of event beds from a single known triggering mechanism. Panels a and b align the turbidite layers attributed to modern floods of the Columbia River (1894, 1948). Density structures vary within each flood layer and exhibit between 1-4 density pulses. Panel c aligns the upper interface of the event beds connected to the 1700 earthquake; these beds are composed of cohesive mud that is sheared and broken into clasts and topped with multi-pulsed sand laminae. There is no consistent thickness or density structure evolution observed downslope.*

recovery in places, with sedimentary structures that indicate shearing and brecciation in high-density flows (e.g., a grain-supported debris flow, debris avalanche, or slide; Tripsanas et al., 2008). Unlike Type-1 deposits, the Type-2 deposits are consistently composed of marine rather than terrestrial organic matter (Fig. 4.3), similar to the signatures of modern hemipelagic sediment accumulating in the canyon and slope.

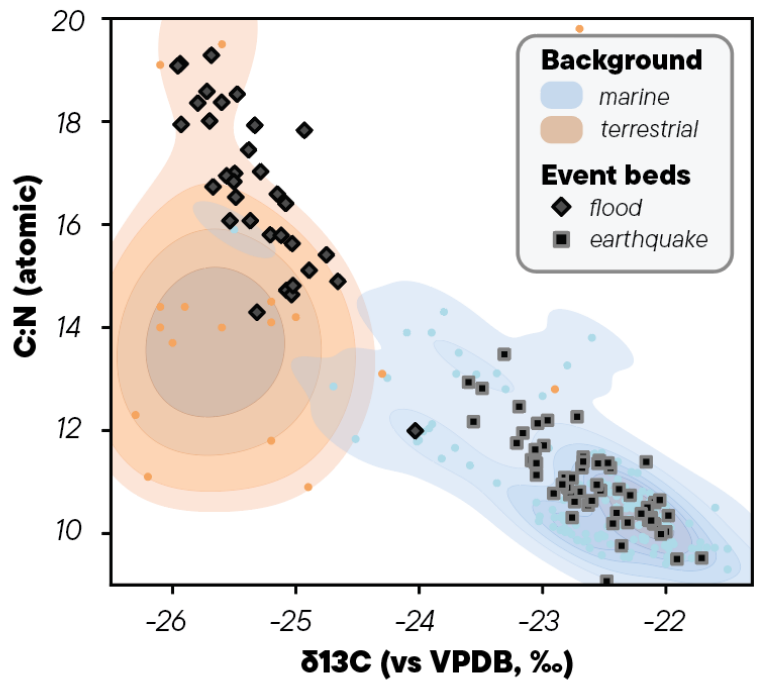

Figure 4.3. *Stable isotope signatures of bulk sediment organic matter in flood turbidites vs coseismic debris flows. Flood turbidites exhibit a $\delta^{13}C$ vs C:N signature consistent with terrestrial end-members from the Cascadia Margin (tan), whereas coseismic deposits are composed of marine material (blue).*

Event bed geochronology indicates mean depositional ages of 1950 and 1890 for the upper, Type-1 event beds, and 1700 for the third and deepest event bed recorded. These ages are synchronous with three of the largest-magnitude, independently recorded sediment transport events on the northern Washington margin: the largest recorded floods of the Columbia River (1894, 1948), and the most recent Cascadia Subduction Zone Earthquake (1700). Older event beds were also present in upper canyon stratigraphy; their geochemistry and structure are presented, but these event beds are not attributed to specific triggering events. This 320-y stratigraphic section is interpreted to be a high-resolution and continuous record of canyon sedimentation over one complete seismic-interseismic cycle.

4.3.2 Distinguishing oceanic from seismic event deposits within canyons

The preservation of recently deposited turbidites in Astoria Canyon and connection to independently recorded triggering events allows us to identify the primary features of intermingled deposits from distinct triggering origins. “Type-1” deposits are identifiable as flood-associated turbidites: depositional ages align with the timing of major river floods, density structures are consistent with fluvial deposits globally (Biscara et al., 2011; Liu et al., 2012; Mulder et al., 2003; Puig et al., 2004; Zavala, 2020), and organic matter geochemical signatures are consistent with the signatures of terrestrial end-members in this region. These deposits represent turbidity currents sourced from flood-stage river sedimentation, likely via settling and short-term deposition which preconditions the seabed for subsequent flow triggering during energetic oceanic events. These deposits demonstrate that the combination of age, sedimentary structure, and geochemical signature (Lahr et al., 2025) can be diagnostic of origin, and organic matter composition provides a practical tool for the attribution of event beds in settings where multiple triggering mechanisms are active. The presence of Type-1 deposits also reinforces that highstand-detached canyon channels are not entirely dormant during the interseismic period. Highstand canyons are known to initiate sediment gravity flows through a range of meteorological, oceanic, and fluvial processes, and the Type-1 deposits observed here demonstrate that these processes leave distinct, identifiable signatures in long-term stratigraphic records.

In contrast to Type-1 flood deposits, the Type-2 deposits in this location are interpreted to be the product of major sediment remobilization by strong ground motion associated with earthquakes including the 1700 Cascadia Subduction Zone earthquake. Type-2 deposits were identified as earthquake-derived mass transport deposits (MTDs): deposits exhibit depositional age consistent with the 1700 earthquake or prior events, density structures are consistent with cohesive MTDs (Tripsanas et al., 2008), and sediment is primarily fine-grained with an organic matter geochemical signature consistent with marine sediment in the canyon. The MTDs observed in shallow regions of the canyon include sheared and contorted beds of weakly consolidated mud, and MTDs slightly deeper within the study area exhibit sections of clast-supported conglomerate (Fig. 4.4). These depositional structures confirm multiple high-density flow processes supporting downslope motion, including both brecciation and ductile deformation (Fig. 4.4). Clast-rich Type-2 deposit textures near major slide scarps indicate the mass transport of well-compacted relict material (Fig. 4.4), while ductile deformation structures shallower in the canyon indicate the remobilization of recently deposited hemipelagic sediment with low shear strength (e.g. at 750 m water depth; Fig. 4.4a-c). Several Type-2 deposits are topped with laminated turbidite sand (Fig. 4.2c), indicating a synchronously generated turbidity current, though not all deposits exhibit this turbidite layer (e.g., Fig. 4.4). Taken together, these deposits are indicative of widespread sediment gravity flows in the form of high-deformation slides, viscous debris flows, debris avalanches, and turbidity currents (Tripsanas et al., 2008). These structures are linked only to subduction zone earthquakes, as multiple <M6 earthquakes have occurred in this region and are not associated with Type-2 deposits, and oceanic processes are unable to produce Type-2 deposits, as they remobilize surficial hemipelagic sediment in comparatively low-density flows. Type-2 deposits are also distinct from conventional abyssal seismoturbidite deposits (Goldfinger et al., 2012) in the region, as deposit thickness is an order of magnitude larger, material composition is primarily fine-grained, and sedimentary structures indicate high-density flow behavior.

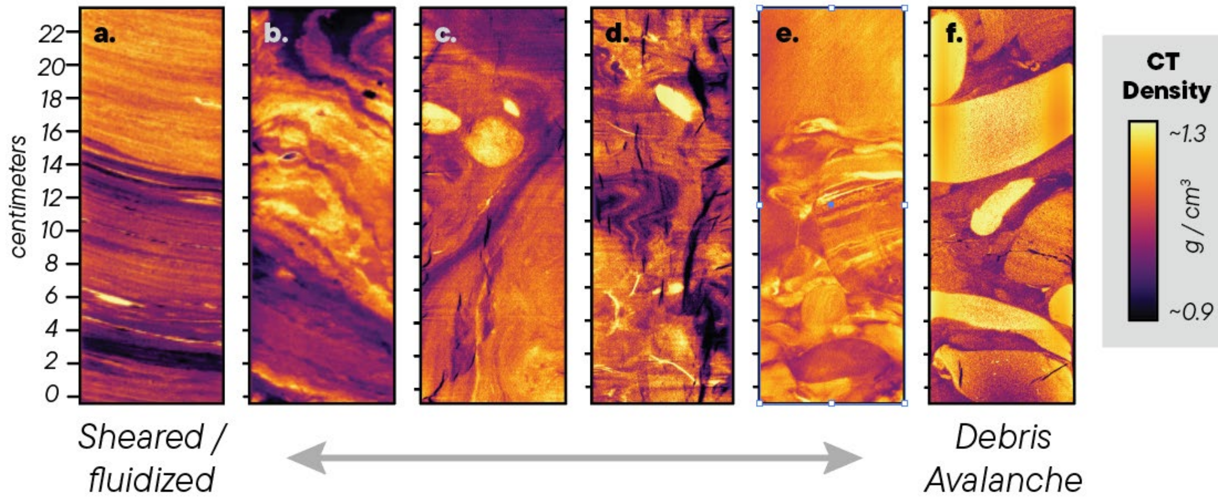

Figure 4.4. *Continuum of deformation textures in submarine mass-transport deposits. Panels arranged from sheared, ductile sediment deformation (left) to clast-dominated, blocky fabrics characteristic of debris-avalanche deposits (right). Intermediate panels capture mixed regimes in which deformation, clasts, and the partial preservation of primary structure coexist. This sequence emphasizes the range of high-density flow behaviors active over small spatial scales during mass wasting events.*

4.3.3 Upper canyon accumulation over multiple seismic cycles

Prior studies of the Cascadia Margin have suggested major canyon head sediment remobilization during subduction zone earthquakes, and the Type-2 deposits observed in Astoria Canyon are the first data to confirm this phenomenon. This new evidence also prompts a fundamental question: do coseismic sediment gravity flows flush sediment into the deep ocean, or infill the upper canyon channel? Only a few well-documented canyon systems have a measured coseismic event response, and Kaikōura Canyon is the best-documented example, where an earthquake removed tens of meters of canyon floor infill. The Kaikoura event flushed the majority of sediment into the deep ocean, and today, only a small sediment volume remains in the upper channel (Howarth et al., 2021; Maier et al., 2024; Ribó et al., 2024). The Astoria Canyon record provides a contrasting example, as the 1700 seismic event is associated with the deposition of meter-scale MTDs rather than flushing the channel, and oceanic processes continue to load the slope and upper canyon. While the presence of thick intervals of Type-2 deposits demonstrates meter-scale sediment retention, core data alone do not resolve the balance of erosion and deposition. To more comprehensively assess the degree of canyon flushing, seismic reflection and multibeam data were collected and confirm the presence of >100 m of sediment infill in the floor of the canyon where Type-2 deposits are observed. Specifically, the canyon floor between 700-900 m exhibits up to 120 m of sub-parallel laminae indicative of successive MTDs (Fig. 4.5). These MTD sequences are located on a seafloor gradient of ~0.5°, which is among the lowest-gradient settings found in the upper canyon environment in Cascadia. While it is possible this morphology promotes deposition rather than efficient sediment bypass, depositional thresholds are not only related to slope and instead relate to properties of both the flow and the seabed (Crisóstomo-Figueroa et al., 2020; Pohl et al., 2020; Stevenson et al., 2015; Sumner et al., 2012). This material is likely to have been emplaced during the Holocene, as Astoria Canyon was the primary conduit for the Missoula Floods, 15–13 kya, which are among the largest sediment discharge events known globally and are events known to erode the seafloor, even at abyssal depth (Normark & Reid, 2003). The mass transport deposits observed in cores and seismic are not evidence for the downslope evolution of a single major, erosive flow. Instead, these deposits represent a mosaic of locally failed sediment which accumulates over multiple seismic cycles on a shallow canyon floor gradient (Tripsanas et al., 2008). Overall, the presence and structure of Type-2 deposits provides two key insights: 1) coseismic gravity flows in the canyon head do not only initiate turbidity currents, but also debris flows and avalanches of fine-grained material, and 2) earthquake-triggered flows can not only flush, but also infill canyon channels, likely over multiple seismic cycles.

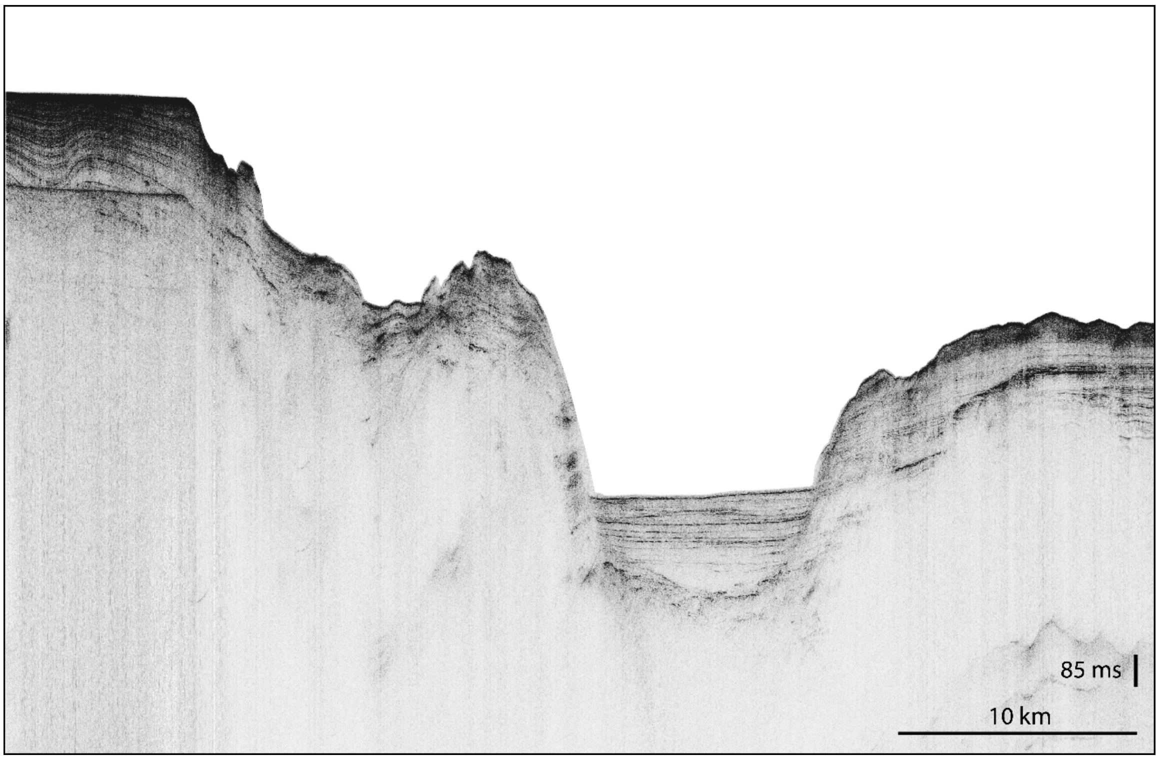

Figure 4.5. *Sub-bottom structure and bathymetric morphology of the upper canyon floor. Left panel: sub-bottom structure of Astoria Canyon at 1100 m, including 150 m of MTD channel infill. X-dimension scale units are kilometers, Y-dimension scale units are milliseconds.*

4.3.4 Implications for sediment gravity flows on active margins

Here we show that upper canyon channels preserve a chronology of sediment gravity flows that can be verified against known triggering events, and this environment can advance longstanding questions of canyon infilling and flushing across active margins. In this case, Astoria Canyon provides a record of sediment gravity flow routing across the most recent seismic-to-interseismic cycle on the Cascadia margin which updates assumptions regarding nonseismic gravity flows, coseismic flows, and the evolution of canyon morphology.

First, while highstand-detached canyons are thought to be dormant between earthquakes, flood-associated sediment gravity flows are shown to enter canyon systems and generate deposits during the interseismic period. With this in mind, accurate stratigraphic interpretations in canyon systems—including those that are highstand-detached—require a framework for distinguishing the event beds of seismic and nonseismic origin. In this study, event bed composition is distinct, and flood turbidites can be consistently differentiated from coseismic deposits on the basis of their organic carbon signatures and sedimentary source. The addition of quantitative measurements of sedimentary organic matter to more traditional analyses of turbidite fingerprinting can provide a reliable and consistent basis for distinguishing flood from earthquake triggering and identifying false positives in seismoturbidite records.

Second, this study provides the first evidence confirming that subduction zone earthquakes trigger sediment gravity flows in Cascadia margin canyon heads and reveals that coseismic flows are initiated as slides and debris flows of largely fine-grained sediment. These deposits exhibit significant differences with the abyssal seismoturbidite record, as abyssal seismoturbidites are centimeter-scale sandy deposits representing turbulent flows, but seismic deposits in the upper canyon are mostly characterized by meter-scale sequences of silt and clay transported in high-density, nonturbulent flows. This updated view of earthquake-driven transport necessitates consideration of several additional physical processes that facilitate downslope motion and highlights that a single-phase understanding of sediment gravity flow routing (i.e., solely turbidity currents) fails to account for the majority of the sediment redistributed during an earthquake. Further, these findings underscore that the near-surface sediment available in highstand canyons is primarily fine-grained silt and clay, especially along the channel floor, and this feature of highstand canyons can limit the entrainment of sand into turbidity currents, dampening ignition and runout. Taken together, the variable flow structure, minimal sand content, and upper-canyon deposition of these flows suggest that coseismic flows in some canyons are limited in runout and instead settle as a patchwork of local failures in the canyon floor. This conclusion supports recent evidence that Cascadia's deep-water turbidite records may also be sourced from deep-water sources near the deformation front (Hill et al., 2022, 2026).

Last, the >100 m thick sequence of stacked MTDs preserved on the canyon floor indicates that seismic flushing of the upper channel remains incomplete over multiple seismic cycles. While some submarine canyons are known to flush sediment into the deep ocean during major earthquakes (Howarth et al., 2021; Mountjoy et al., 2018; Piper et al., 1999; Ribó et al., 2024), long-term sediment retention within Astoria Canyon demonstrates that earthquake-driven flushing is not ubiquitous across canyon systems. Instead, the balance between erosion, deposition, and sediment bypass by sediment gravity flows in the upper canyon appears to be inconsistent. In Astoria Canyon, an anomalously low channel gradient between 600 and 1100 m water depth likely promotes deposition and retention of earthquake-remobilized sediment, highlighting long-term feedbacks between pre-existing canyon morphology and sediment gravity flow routing. Consequently, canyon systems on active margins may experience fundamentally different sediment routing and depositional patterns dependent upon both geomorphic configuration and flow properties. These observations indicate that while subduction zone earthquakes do remobilize large volumes of fine-grained sediment, they may not efficiently transfer that material to the deep ocean. Rather than acting as simple conduits during major earthquakes, channel morphology can aid downslope flows or provide resistance to their propagation which creates long-lived sediment reservoirs and controls the balance between infilling and flushing over multiple seismic cycles.

Rather than passively storing sediment between earthquakes and flushing it to the deep ocean during seismic events, the upper canyon remains active throughout the seismic cycle and regulates whether gravity flows are transmitted, transformed, or retained. In Astoria Canyon, nonseismic sediment gravity flows continue to enter the canyon, subduction earthquakes initiate several modes of sediment transport beyond turbidity currents alone, and coseismic remobilization results in channel infilling and not efficient sediment export. These observations demonstrate that channel morphology exerts a fundamental control on the routing, transformation, and retention of sediment on active margins. By preserving a century-scale stratigraphy recording the early evolution of sediment gravity flows and allowing comparison with historical triggering events, upper canyon heads provide a critical bridge between modern process observations and the abyssal stratigraphic record. Expanding observations in these settings is a useful future direction for refining paleoseismic reconstructions and developing predictive models of sediment routing across active continental margins.

Chapter 5. DOES HIGHSTAND SUBMARINE CANYON SEDIMENT TRANSPORT REFLECT SYNOPTIC FORCING? EVENT MAGNITUDE AND SYNCHRONEITY IN CANYONS >120 KM APART

5.1 Introduction

Submarine canyons distribute globally significant volumes of sediment, organic particulates, and dissolved nutrients across continental margins (Maier et al., 2019; Puig et al., 2014; Talling et al., 2024). The processes that act within canyons build the largest sedimentary deposits on Earth, with implications for global-scale sediment budgets, carbon and climate, and biological productivity (Curray et al., 2002; Galy et al., 2007; Hilton & West, 2020; Kao et al., 2014). Further, the sediment stratigraphy generated by processes within submarine canyons provides a rich environmental record that scientists leverage to infer past climate, sea level, and event histories from earthquakes, floods, and marine storms (Adams, 1990; Goldfinger et al., 2012; Mulder et al., 2001b; Okutsu et al., 2019; Paull et al., 2014). While the hydrodynamic processes acting in submarine canyons are the pump that underpins this major redistribution of sediment across continental margins, observational studies from submarine canyons are comparatively rare due to the remote and challenging nature of in-situ data collection.

Submarine canyon channel morphology is created and maintained in part by sediment gravity flows, mixtures of sediment and water which flow downslope due to their excess density (e.g., dilute turbidity currents, debris flows). Sediment resuspension from the seabed is the critical “first step” where a density instability is formed and a gravity flow may propagate. Over long timescales, conditions during sea-level lowstand are known to supply and resuspend sediment in canyon heads, leading to the view of canyons as “active” with gravity flows ubiquitous during lowstand—and conversely—dormant during highstand with the majority of sedimentation associated with intermediate and bottom nepheloid layers (Gardner, 1989; Hickey et al., 1986). Today, approximately 80% of canyons are considered detached from shore (Bernhardt & Schwanghart, 2021), yet recent monitoring has shown an ever-increasing number of oceanic and tectonic events can resuspend sediment which evolves into downslope-flowing sediment gravity flows within the bottom boundary layer. Of the several documented triggers for sediment gravity flows, major oceanic storms (Puig et al., 2004), flood-stage river discharge (Mulder & Syvitski, 1995; Parsons et al., 2001), and sediment slope failure (Clare et al., 2016; Howarth et al., 2021; Piper & Normark, 2009) are among the primary mechanisms known to redistribute sediment and trigger sediment gravity flows in marine settings. Sediment resuspension remains a key process underpinning assumptions of canyon activity, and too few observations of canyon resuspension events limit our understanding of canyon activity.

Because seabed resuspension and gravity flow triggering are driven by meteorological phenomena including storms and floods, it is necessary to understand the spatial scale over which these disturbances act. The storm systems that modulate waves, currents, pressure and precipitation are often not localized phenomena, as individual storm footprints commonly exceed 100 km along continental margins, and major, “synoptic” scale storms, e.g., extratropical cyclones, are manifest on the order of 1000 km. These systems enhance the wind stress, wave fields, and pressure gradients that transmit energy to the seabed over large portions of continental margins. As a result, the physical mechanisms responsible for sediment resuspension are often spatially continuous over many submarine canyons at any given time (average canyon spacing ~30 km; Harris & Whiteway, 2011). This basic scaling implies that, in the absence of strong local controls, seabed disturbance may occur synchronously across multiple canyon systems within the scale of regional forcing.

The Cascadia margin provides a natural test case to evaluate whether sediment transport processes can be generalized across canyon systems subject to similar external forcing, yet with dissimilar morphology and fluvial influence. The northward limit of the Washington margin is incised by the broad, steep head of Quinault Canyon, whereas the southern limit of the margin is incised by the narrow, low-gradient head of Astoria Canyon. This margin experiences strong and well-characterized oceanic forcing, yet observations of sediment transport within submarine canyons remain limited (Allan & Komar, 2000; Allen & Hickey, 2010; Carson et al., 1986; Hickey et al., 1986; 1997; Tillotson & Komar, 1997). The sedimentary record from the base of this margin is classically interpreted to reflect coseismic turbidity currents, and one of the key “tests” of this record is the confluence test, where synchronous sediment gravity flow activity across canyons reaches the abyssal ocean (Goldfinger et al., 2007, 2012, 2017). Recent evidence points to nonseismic triggering also occurring under modern conditions and a key unresolved question is whether the scale of nonseismic disturbances is also sufficient to generate synchronous transport events across the tributary canyon systems used in the confluence test (e.g., ~100 km scale). The uncertainty between stratigraphic interpretation and water column observation creates a fundamental ambiguity in how turbidite records are interpreted. At present, it remains unclear whether oceanographic processes produce synchronous resuspension across adjacent canyons, or if sediment transport is inherently asynchronous despite shared forcing, with direct implications for the interpretation of the turbidite record.

To address the potential for ocean-driven sediment transport events in adjacent highstand-detached canyons, we use concurrent hydrodynamic observations from two Cascadia canyons to evaluate the timing and structure of nearbed processes and sediment transport. Broadly, our objective is to quantify the degree to which sediment transport events are active under sea-level highstand and temporally coupled across canyon systems >100 km apart. Specifically, we address whether oceanic processes in highstand canyon heads 1) resuspend a substantial mass of sediment into the bottom boundary layer and move it deeper into the canyon, 2) produce temporally synchronous nearbed transport in canyons >100 km apart, and 3) generate the excess nearbed density required to initiate density-driven sediment gravity flows.

5.2 Materials and Methods

5.2.1 Field Program

The Cascadia Canyons program collected a coordinated set of oceanographic and sedimentological observations on the Cascadia margin within Astoria and Quinault submarine canyons from March 2023 to April 2024. The experimental design targeted the quantification of nearbed hydrodynamics, suspended-sediment transport, and seabed properties over a complete annual cycle, capturing both quiescent summer conditions and energetic winter forcing. Three instrument platforms were deployed along the upper reaches of each canyon axis, including canyon head (~200 m; AHT, QHT, Fig. 5.1), mid-canyon (~500 m; AMM, QMM), and deep (~1200 m; ADT, QDM) sites. Exact deployment depths and platform configurations are provided in Table 5.1. Sedimentological data were also collected, including sediment cores and time-marked sediment trap samples, providing constraints on grain size, seasonal-to-century-scale accumulation rates, and sediment erodibility. Field operations were supported over four cruises aboard research vessels R/V Sikuliaq (deployment, recovery), R/V Sproul (maintenance), and Swift Responder (recovery).

5.2.2 Instrument Platforms and Oceanographic Data

At each canyon “Head” site (AHT, QHT), benthic tripod platforms were deployed to obtain physical measurements within the bottom boundary layer and minimize flow disturbance. The canyon-head tripod platforms were equipped with sensors including the following: 300-kHz (Teledyne, upward-looking) and 2-MHz (Nortek, downward-looking) acoustic doppler current profilers, 2-MHz acoustic doppler velocimeters (Nortek), multi-frequency acoustic backscatter sensors (Echologger, AquaTec), and multiple temperature, salinity, pressure, and turbidity loggers, and in-situ particle-size analyzers (RBR, Seabird, Sequoia). All sensors logged data at 30-min resolution or higher frequency. A comprehensive table of the sensor sampling protocol can be found in Table 5.1. Deployment duration for the canyon-head sites was programmed for a 6-month deployment duration.

The "Mid" and "Deep" site locations were primarily monitored using taut-wire moorings equipped with similar instrumentation (AMM, QMM, QDM), with one exception at the Deep Astoria site which was instrumented using a free-ascent benthic tripod with weighted, releasable feet (ADT). Mid and Deep site platforms were equipped with sensors including the following: 300-kHz (Teledyne, downward-looking) acoustic doppler current profilers, multi-frequency acoustic backscatter sensors (Echologger, AquaTec), and multiple temperature, salinity, pressure, and turbidity loggers (RBR, Seabird). All sensors logged data at 30-min resolution or higher frequency. A comprehensive table of the sensor sampling protocol can be found in Table 5.1. The Mid and Deep sites were programmed for a 12-mo deployment duration.

5.2.3 Oceanographic Data Analysis

Several additional data sources were used to provide context for the oceanographic conditions forcing currents and sediment transport during the deployment period (Fig. 5.1). These sources include National Oceanic and Atmospheric Administration (NOAA) buoys and tide stations (46029, 46041; 9437540, 9440581, 9440910, 9441102, 9442396; NOAA, 2024), Ocean Observatories Initiative (OOI) Washington Endurance Array sites (Shelf Surface Platform and Offshore Multi-Function

Node; National Science Foundation Ocean Observatories Initiative, 2024), United States Geological Survey river discharge stations (14246900, 12031000, 12041200, 12040500, 1203951610; U.S. Geological Survey, 2024). LiveOcean model output at each instrumentation site was also obtained to assess water density stratification state throughout the timeseries (https://faculty.washington.edu/pmacc/LO/LiveOcean.html; MacCready et al., 2021).

Combined wave-current bed shear stresses were calculated for all time periods using the Grant-Madsen wave-current interaction model (Madsen, 1994; Wiberg and Sherwood, 2008). The model was forced using the following parameters: ADCP current velocity near the seabed (U_c) with measurement height (Z_r) between 0.5 and 5 meters above bottom (mab), NDBC significant wave height measurements (Astoria Canyon sites were modeled using data from site 46029, Quinault Canyon sites were modeled using site 46041; Fig. 5.1) and a bottom roughness height (k) of 3 mm.

Time periods of elevated suspended sediment were identified from acoustic doppler current profiler echo intensity following range correction to relative backscatter. ADCP echo intensity was used because it is the most complete and uniform estimate of suspended sediment concentration (SSC) across sensor platforms. The range-correction equations used to compute relative backscatter from raw echo intensity remove the baseline RSSI, correct for two-way transmission losses as a function of slant range, and convert the result to decibels (dB). Relative sediment flux was computed as the product of relative backscatter and the primary current velocity.

A robust estimate of suspended-sediment mass concentration was possible at site AHT due to the presence of an ADCP, an acoustic backscatter sensor, and a laser scatterometry sensor. This estimate was computed from an acoustic backscatter timeseries (Aquatec 1000R) calibrated to a mass concentration. Mass concentration was computed as the product of the effective density for flocculated fine-grained sediment (0.5-1.5 g cm^{-3}; Dyer & Manning, 1999; Fox et al., 2004; Mikkelsen & Pejrup, 2000) and volume concentration measurements from a Sequoia Instruments Laser In-Situ Scattering and Transmissometry model 200X, processed using the Sequoia Irregular Grain Size Model. Both instrument sampling volumes were located at 50 cm above bottom (cmab). The ABS record was chosen as the primary record due to maximum temporal coverage and a measurement technique which is robust to biofouling. The time period selected for calibration was 3 Dec 2023 to 14 Jan 2024. This date range was chosen for two reasons: 1) the time period minimizes the effects of biofouling, as it was shortly after deployment and biological activity was lesser during winter, and 2) the date range encompassed major sediment-transport events. The calibration linear fit was 0.79.

The temporal synchroneity of oceanic forcing and canyon response was measured across sites by computing the Pearson correlation coefficient at zero lag after applying a low-pass filter and interpolating to a common time base. In order to isolate the subtidal processes expected to be spatially widespread, a 40 h, 2^{nd} order Butterworth low-pass filter was applied. The filtered timeseries were then downsampled from their native 3-30 min sampling interval to a common time base informed by an estimate of the temporal decorrelation timescale. The decorrelation timescale (τ_e) was defined as the e-folding timescale, corresponding to the first lag at which the autocorrelation decayed below $\frac{1}{e} = 0.37$, a standard practice for empirically determining decorrelation timescales (e.g., Jacobs et al., 2021; Kuhn et al., 2019). τ_e within the study area ranged from 40-80 h. Based on these estimates, all timeseries were resampled to 12-hour intervals which were sufficiently coarse to reduce sample redundancy in filtered signals yet preserve event variability. The resulting decorrelation timescales are consistent with storm processes and synoptic-scale variability on continental shelves, which typically occur on timescales of 2-5 days.

The likelihood of density-driven flow was evaluated using a Chezy-based parameter space for flow velocity based upon the linearized Chezy equation (Flores et al., 2018; Traykovski et al., 2007; Wright et al., 2001).

$$U = \sqrt{\frac{H * g' * \sin(\alpha)}{C_d + E_t}}$$

where U is the layer-averaged current speed (m s^{-1}), H is the thickness of the high-concentration layer (m), g' is the reduced gravity (m s^{-2}), α is the seabed slope angle, C_D and Et are seabed and upper surface drag coefficients, respectively (0.003 and 0.001; Flores et al., 2018; Traykovski et al., 2007; Wright et al., 2001).

5.2.4 Sedimentological Data and Analysis

A total of 70 gravity cores and multicores were collected during field operations. Gravity cores were sectioned into 1.5-m sections and stored for x-ray computed tomography (CT), subsampling, and compositional analyses (grain size, ^{210}Pb radioisotope measurement). Multicores were reserved for subsampling at 1-cm intervals, CT scanning, and Gust erosion microcosm system (UGEMS) shear stress experiments. All samples were stored at 3°C immediately following collection. Multicores were transferred upright and undisturbed from the corer into the UGEMS system, which applies spatially uniform bed shear stress via a rotating disk (Gust & Muller, 1997). Shear stress was increased stepwise (e.g., 0.05–0.6 Pa, 20 min per step) while sediment-free seawater was continuously pumped into the chamber and effluent turbidity was measured in real time. Suspended-sediment concentrations were determined from calibrated turbidity measurements and integrated over each stress step to estimate mass eroded. Critical shear stress for erosion was defined as the stress at which turbidity exceeded a threshold corresponding to sustained sediment resuspension.

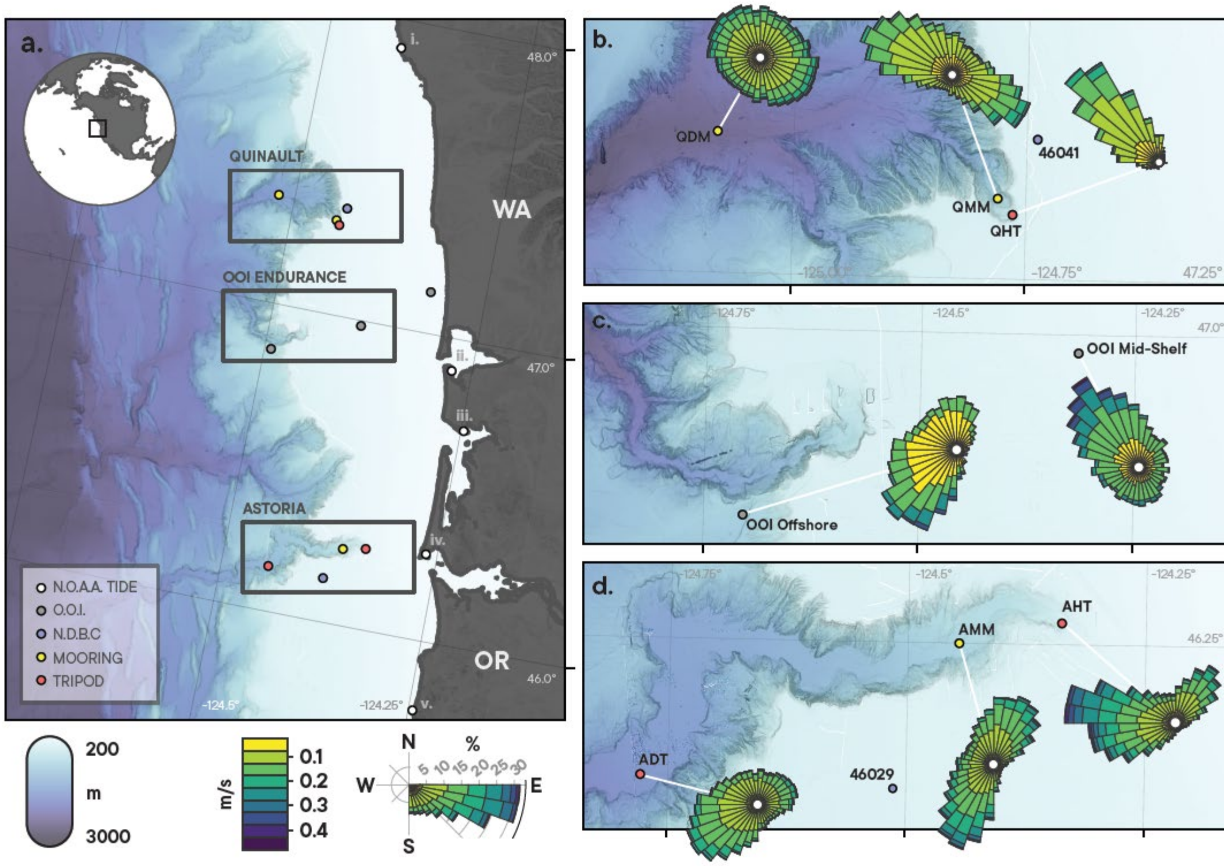

Figure 5.1. *Study area, observation sites, and nearbed flow structure. (a) The location of the Washington margin study area is shown with a global inset and regional bathymetry, including all observational sites. (b–d) Rose diagrams show nearbed currents (~5 m above bottom) at representative sites, where arm length indicates the percentage of observations from each direction and color represents current speed, with darker color corresponding to greater velocity.*

5.3. Results

5.3.1 Annual Dataset of Regional Forcing and Canyon Response

The temporal structure of meteorological and oceanic forcing observed during the deployment period was consistent with the climatology from the region: summer conditions were associated with moderate wave climate (significant wave height 2-4 m) and surface wind (1-7 m s^{-1}), and southward wind promoted a weakly negative and fluctuating subtidal water-level anomaly at the coast (Fig. 5.2). The months of May and June corresponded to the annual

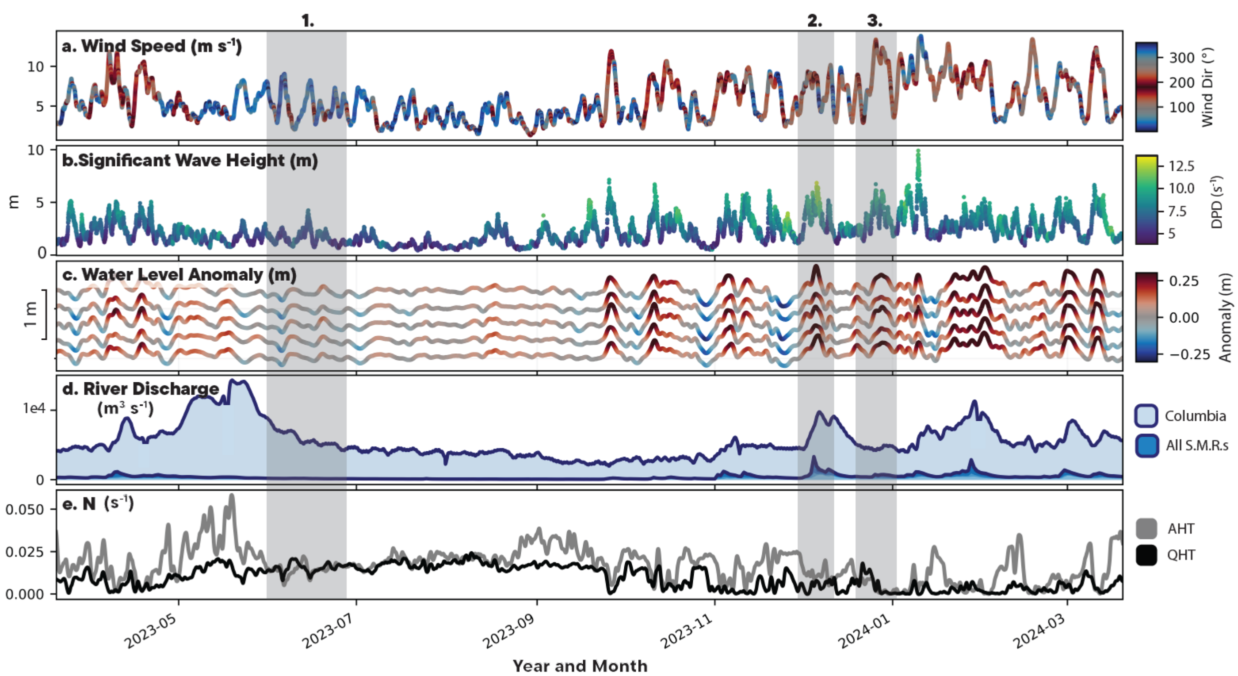

Figure 5.2. Regional physical forcing. *Panels a–e show timeseries of key forcing, and panels f–k cross-plot timeseries at northern and southern sites. All data are 40-h low-pass filtered except wave statistics. (a, b) Wind and wave conditions from NOAA station 46041. (c) Water level anomaly from stations i–v from top to bottom, respectively (Fig. 5.1). (d) River discharge from U.S. Geological Survey gauges: Columbia River (light blue) and small mountainous rivers (dark blue; Chehalis, Queets, Quinault, Hoh). (e) Median*

upper-ocean buoyancy frequency (N) from LiveOcean at AHT and QHT. Time periods associated with elevated SSC are highlighted in gray and labeled 1-3.

maximum in the Columbia River freshwater discharge. Strong density stratification in the upper ocean (median buoyancy frequency N as large as ~0.05 s^{-1} for the upper 30 m of the water column) was also predicted by LiveOcean model output during summer. Winter ocean conditions were comparatively energetic and associated with northward surface wind up to 17 m s^{-1}, episodic positive coastal water level anomalies up to +0.5 m, significant wave height events with a maximum of 9.8 m, and a diminished upper-ocean stratification state (N ~0 s^{-1}).

5.3.2 Bottom Boundary-Layer Hydrodynamics and Shear Stress

Mean currents on the continental shelf seasonally transition from southward in summer to northward in winter. Shelf currents near the seabed (0-10 mab), however, were more consistently oriented in the northward direction (315°). Within submarine-canyon bathymetry, the principal axis of nearbed currents was oriented perpendicular to axial isobaths, and the greatest degree of directional focusing was in canyon sites at 500 m water depth (Fig. 5.1b-d). Nearbed current velocities were greatest at canyon-head sites, where down-canyon flow as great as 40 cm s^{-1} was observed. At most sites, nearbed currents are asymmetric, and downslope-oriented flow is dominant (Fig. 5.1b-d). A mean-flow profile was computed from each rotated current-velocity timeseries, and notably, all but one record exhibits a net-downslope flow direction in the lowermost ~10 meters of the water column, with a mean velocity magnitude ranging from 0.5 to 5 cm s^{-1} (Fig. 5.3i-p). In all cases, mean flow higher in the water column is less strongly downslope, and in several cases, the mean flow in the overlying water column is oriented onshore (Fig. 5.3i-p). Across-isobath currents at canyon-head sites are in phase with along-shelf currents, particularly during summer.

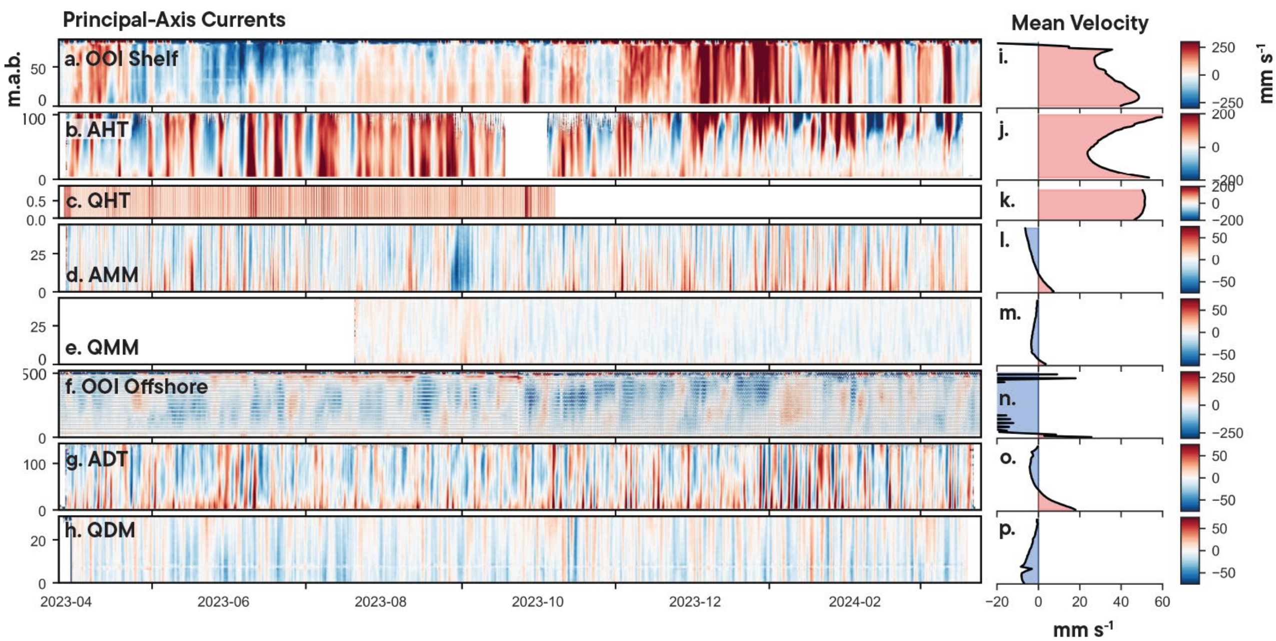

Figure 5.3. Subtidal current structure in the lower water column. *Panels a–h show current profile timeseries plotted from height above bottom (mab). Panels i–p show the corresponding mean velocity profile over the full record for each site. Current velocities are 40-h low-pass filtered and rotated to the principal flow direction in the bottom boundary layer, which is isobath-parallel at the shelf site (a) and isobath-perpendicular at slope and canyon sites (b–h).*

The modal grain sizes of the canyon floor at all of this study's observation sites and the continental shelf are 10 µm and 110 µm, respectively (Lahr et al., 2025a). The minimum critical seafloor shear stress (τ_{crit}) required to resuspend sediment of these grain sizes is 0.09 and 0.2 Pa, respectively, as estimated by the Shields critical stress equation (Guo, 2020; Shields, 1936). This threshold estimate was supported by core-top UGEMS erosion measurements, which exhibit significant erosion at threshold values between 0.1 and 0.2 Pa. The wave-current interaction shear stress computed from currents and waves is greatest on the continental shelf, where storm conditions reach >2 Pa, greatly exceeding τ_{crit} (Fig. 5.4). Maximum shear stresses at canyon-head sites reach 0.8 Pa, and values sharply decrease moving into deeper sites. Within mid- and deep-canyon-head sites, shear stress is <0.1 Pa, insufficient to resuspend sediment. This indicates that local resuspension is unlikely to be the dominant sediment source at mid- and deep-canyon sites.

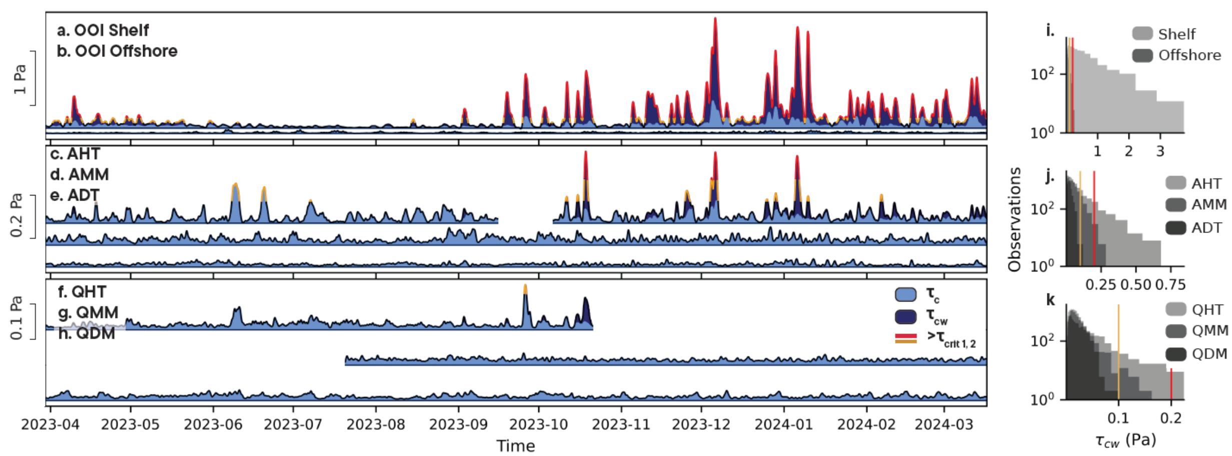

Figure 5.4. Nearbed shear stress timeseries and distribution. *Panels a–h show timeseries of current-only shear stress (τ_c; light blue) and combined wave–current shear stress (τ_{cw}; dark blue) at all sites. Red and yellow outlines indicate periods when τ_{cw} exceeds the critical shear stress threshold (τ_{crit} > 0.1 and 0.2 Pa). Panels are grouped by region: OOI sites (a–b), Astoria Canyon (c–e), and Quinault Canyon (f–h). Panels i–k show histograms of τcw for OOI sites (i), Astoria Canyon (j), and Quinault Canyon (k), with vertical lines indicating τcrit.*

5.3.3 Sediment Resuspension and Transport

On the continental shelf, SSC is greatest near the bed and within the lowermost 20 m of the water column. SSC increases and remains persistently elevated during winter months (e.g., Fig. 5.5; November 20-30 and December 1-30) contemporaneous with high-energy wave conditions and greater river discharge. Within canyon-head sites, SSC is also increased during winter conditions, often throughout the water column, and events are cleared from the site within 1-5 days of peak storm conditions. SSC at canyon-head sites is also elevated for 1-4 day periods in summer during transitions from sustained upwelling- to downwelling-favorable winds (e.g., Fig. 5.5; June 7-12, 19-22). Deep-canyon sites (ADT, QDM) and the OOI Offshore site do not increase during these time periods: while increased SSC events are present, they differ from one another (ADT and OOI are persistently elevated from 09-2023 to 02-2024, QDM exhibits brief periods of elevated SSC throughout the year).

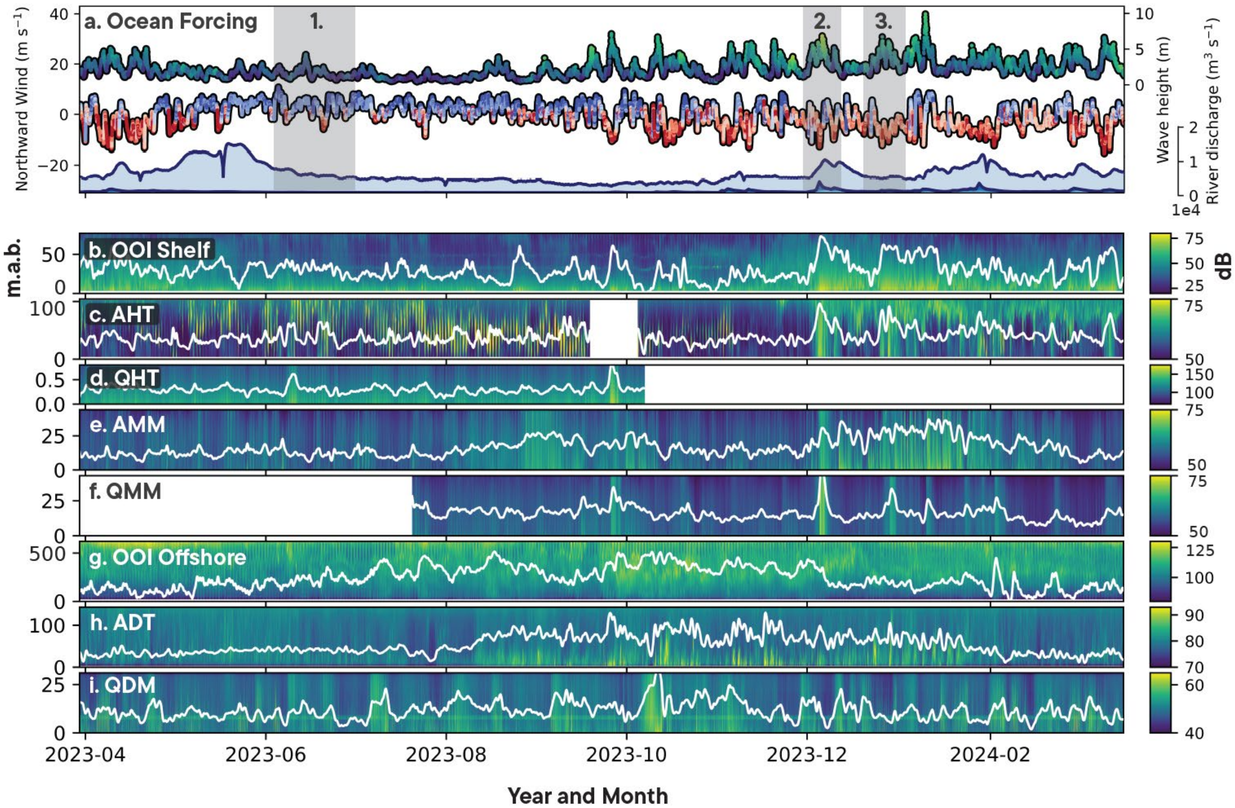

Figure 5.5. Acoustic backscatter in the lower water column. *Panel a shows ocean forcing during deployment (same visualization as in Fig. 5.2), and panels b–i show backscatter profiles plotted from height above bottom (mab). White line corresponds to the backscatter of the lowermost cell in each profile after 40-h low-pass filtering. Time periods associated with elevated SSC are highlighted in gray and labeled 1-3.*

A cumulative nearbed sediment transport proxy was computed from the product of nearbed velocity and relative acoustic backscatter anomaly (Fig. 5.6). Because backscatter is not calibrated to SSC, this metric has arbitrary units and represents a relative index of transport intensity rather than an absolute flux. Accordingly, it is used to compare the relative magnitude and timing of transport across sites. On the continental shelf, cumulative transport is dominated by winter wave events, during which elevated SSCs coincide with large current velocities. In contrast, canyon-head sites exhibit a more persistent downslope transport signal, punctuated by short-lived increases associated with enhanced suspended sediment concentrations. At these sites, the largest cumulative transport occurs during summer, when sustained nearbed flow is enhanced despite relatively low suspended sediment concentrations. Although winter conditions are associated with larger SSCs, lower current velocities limit the resulting transport. Mid- and deep-canyon sites exhibit comparatively weak and less directionally consistent cumulative transport, with minimal response to individual forcing events. Overall, this proxy indicates that sediment transport at shallow sites (the continental shelf and canyon heads) is substantially greater than at mid- and deep-canyon locations.

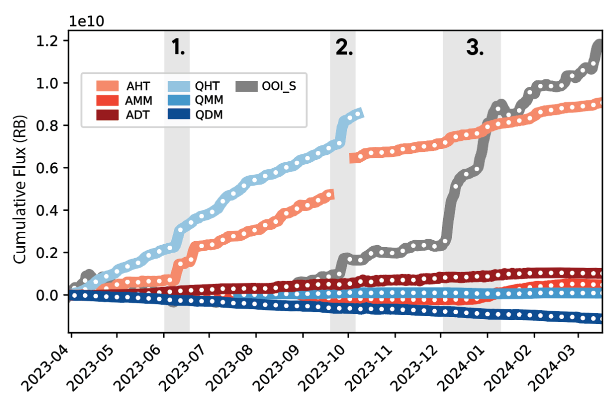

***Figure 5.6. Along-canyon (along-shelf) cumulative particulate flux**. Red tones denote Astoria Canyon sites and blue tones denote Quinault Canyon sites (grey line denotes flux along the continental shelf), white markers indicate one calendar week. Differences in slope reflect the temporal variability in inferred sediment-transport rates between sites. Highlighted time periods 1-3 correspond to periods of enhanced sediment transport.*

5.3.4 Along-Margin Synchroneity

Pearson correlation coefficients calculated for each ocean forcing parameter between observation sites at Astoria and Quinault canyons assess the linear similarity of ocean forcing between the observation sites at zero lag. The northward component of wind, significant wave height, and coastal water-level anomaly are strongly correlated at sites across the margin (r >0.85). River discharge is weakly correlated across the study area (r = 0.40) where the Columbia River enters the ocean to the south, and a set of small mountainous rivers enter the ocean to the north (Chehalis, Queets, Quinault, Hoh; Fig. 5.1). While both river types increase discharge in response to regional precipitation, the discharge from the much larger Columbia River Watershed is slower to increase and decrease, and also exhibits a summer, snowmelt-driven freshet not present on small mountainous rivers. Upper-ocean density stratification is moderately correlated (r = 0.56): while seasonal stratification is similar across sites, large residuals exist where AHT exhibits 2-10 day maxima in stratification contemporaneous with peak discharge on the Columbia River.

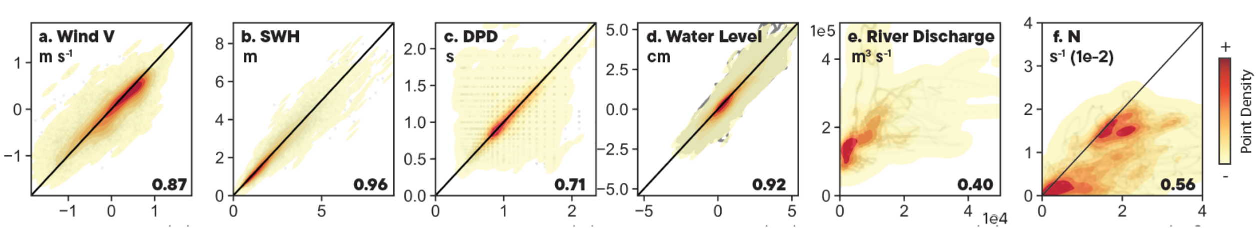

Figure 5.7. Synchroneity of forcing conditions across the Washington Margin*. Cross plots comparing contemporaneous observations from the northern and southern observational sites along the WA margin, data from USGS and NOAA. Panels (a-c)*

compare stations 46041 (x-axis) and 46029 (y-axis) for wind (V), significant wave height (SWH), and dominant period (DPD), respectively. (d) Water-level anomaly crossplots across all station pairs (i–v). (e) Total discharge from small mountainous rivers (x) versus the Columbia River (y). (f) Buoyancy frequency (N) at AHT (x-axis) versus QHT (y-axis). Pearson r displayed at bottom right.

Pearson correlation coefficients were also calculated for all inter-site pairings of nearbed backscatter, and principal-axis currents over each pairwise period of overlap. This metric quantifies zero-lag linear similarity in bottom boundary layer conditions along and across the margin. Principal-axis currents exhibit uniformly weak correlations across site pairs ($r < 0.2$ and not significant at $p < 0.05$), with the exception of shallow sites (AHT, QHT, OOI Shelf), where correlations reach a maximum of $r = 0.43$ (Figs. 5.7, 5.8a). Backscatter shows stronger coherence, with higher correlation coefficients and more statistically significant pairings, reaching a maximum of $r = 0.57$. The largest values occur between sites of similar depth (e.g., head and shelf pairs, r = 0.32–0.45; deep canyon and slope pairs, r = 0.25–0.57), but also between spatially proximal sites across depth gradients (e.g., QMM–QHT, $r = 0.56$). Sediment flux exhibits a similar pattern, with the highest correlations at shallow sites ($r = 0.61$ for QHT–OOI Shelf) and weaker correlations between site pairs separated by greater distance or depth.

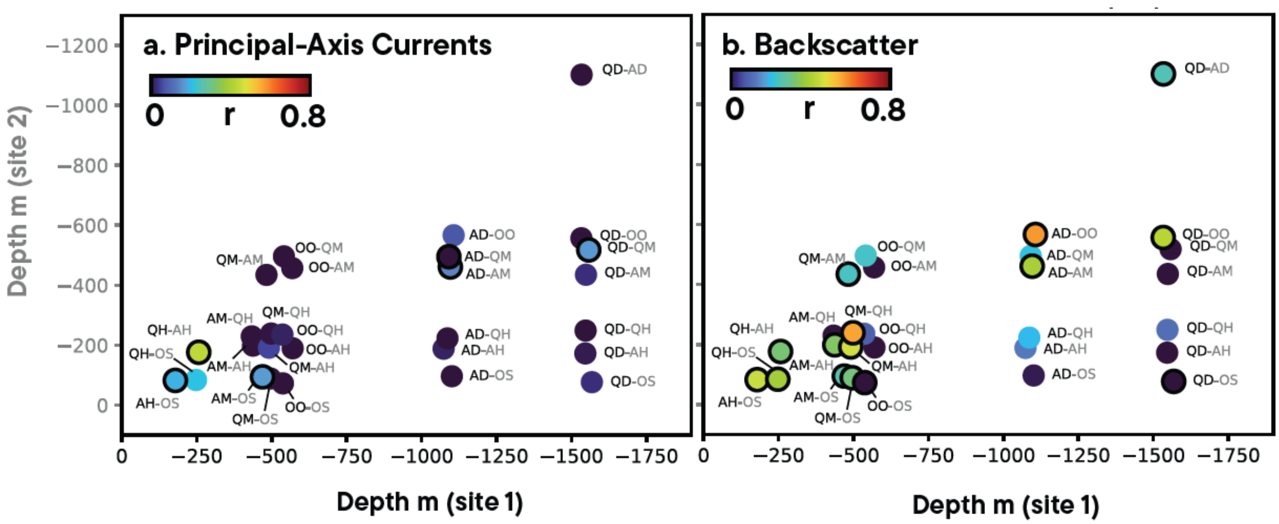

Figure 5.8. Linear similarity of near-seabed conditions among site pairs. *Points represent Pearson correlation coefficients for each site pair, plotted as a function of the depths of site 1 and site 2 and labeled by site pair. Color indicates the magnitude of the correlation coefficient (0–0.8), and a bold black outline marks correlations that are significant at $p < 0.05$.*

5.3.5 Excess Density and Bottom Boundary Layer Flow

The most temporally complete record of nearbed SSC was obtained at site AHT, where calibrated measurements at ~50 cmab document episodic increases associated with energetic forcing. Background SSC values are typically <50 mg l^{-1}, punctuated with increased SSC events lasting hours to days (Figs. 5.9, 5.10). The largest concentrations observed are during winter wave events, where SSC exceeds 1 g L^{-1} (Fig. 5.9), with elevated values persisting for 4-5 days following peak wave conditions and shear stress. Current profiles between 0 and 100 mab indicate that these events are bottom-intensified (Fig. 5.9), with greatest velocity near the seabed and decreasing or reversing higher in the water column. Lower-layer thicknesses are ~10–20 m above bottom (Fig.

5.9). The vertical extent of suspension varies with event magnitude, and no persistent, thin, high-intensity basal layer is observed. Comparable, synchronous vertical expansion of backscatter is not evident at deep canyon or open-slope sites, indicating that strong suspension events are largely confined to canyon heads and shallow shelf sites.

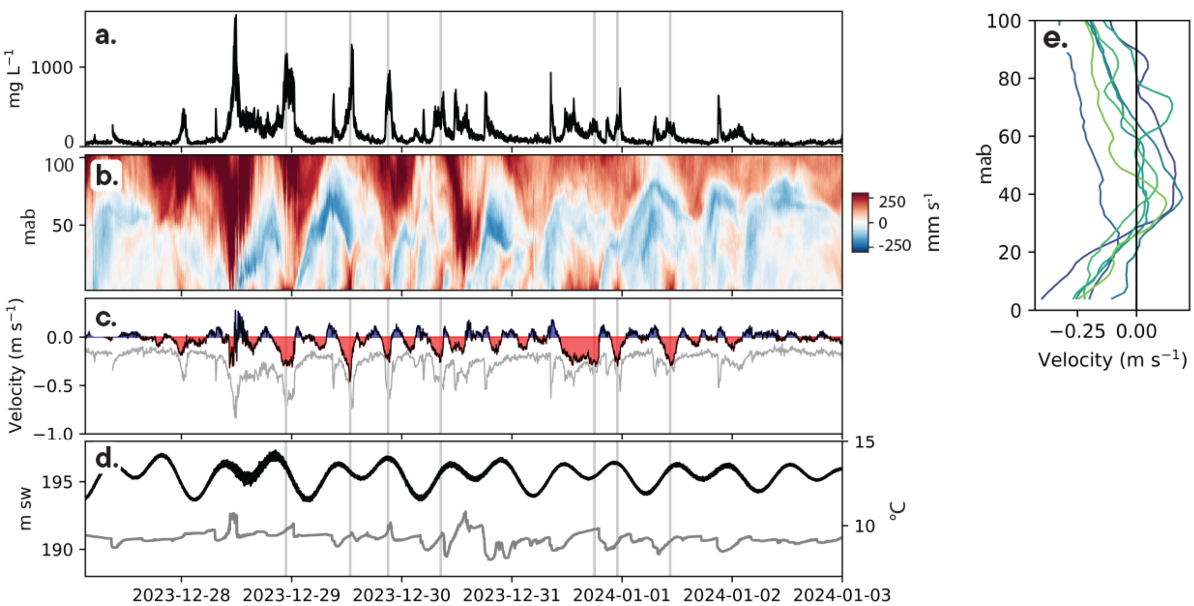

Figure 5.9. SSC and current structure during a winter wave event at site AHT. *For event timing, see Fig. 5.3. (a) SSC (mg l^{-1}). (b) Along-canyon ADCP velocity profiles (cm s^{-1}), with downslope flow in red and upslope flow in blue. (c) Nearbed velocity (m s^{-1}) timeseries, both observed at 5 mab and predicted by Chezy equation. (d) Bottom pressure (m sw) and temperature (°C). (e) Vertical profiles of along-canyon velocity (m s^{-1}) for large-SSC time periods as noted in gray lines on panels a-d.*

Moderate increases to SSC (200–400 mg l^{-1}) are also observed during summer upwelling–relaxation transitions. These events are typically preceded by strong northerly winds persistent over multiple days, and the onset of SSC and downslope flow begins after upwelling-favorable conditions weaken and eventually transition to downwelling-favorable wind state.

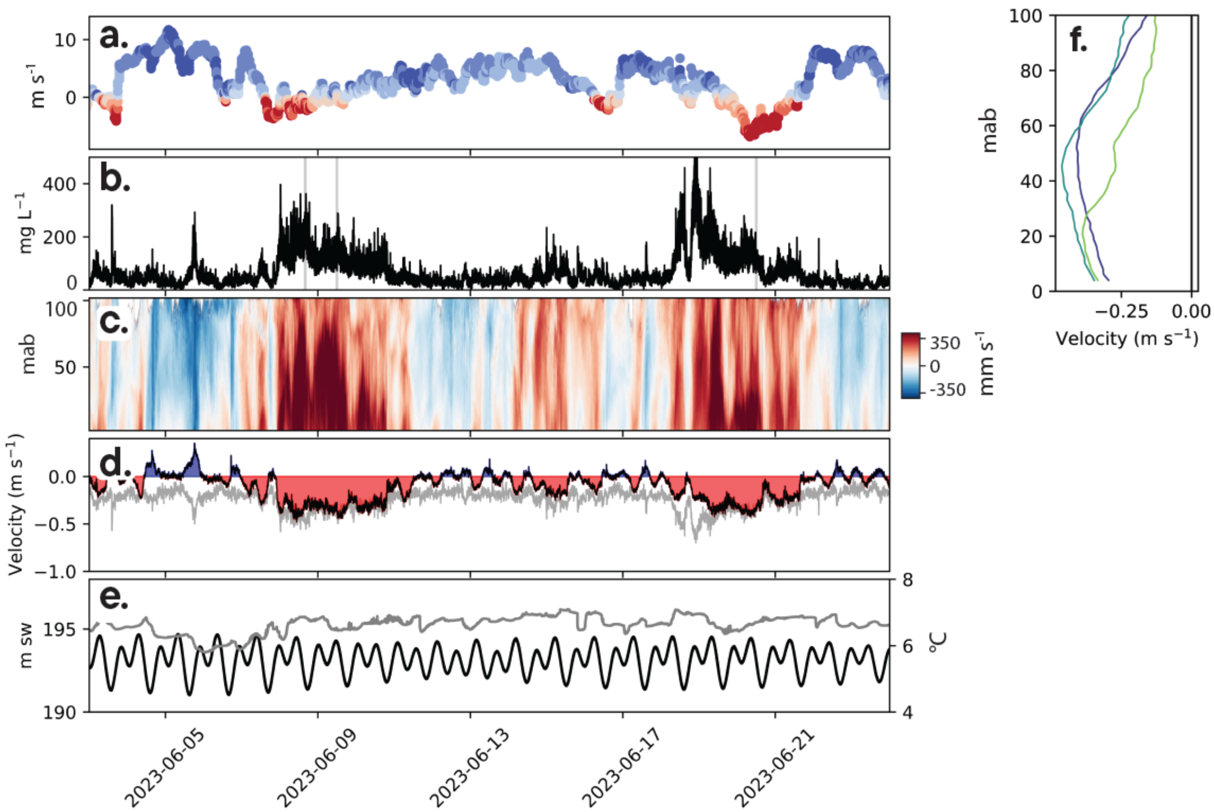

Figure 5.10. SSC and current structure during summer downwelling transitions at site AHT. *For event timing, see Fig. 5.3. (a) Northward component of wind speed, color also indicates direction, where blue is northerly. (b) SSC (mg l^{-1}). (c) Along-canyon ADCP velocity profiles (cm s^{-1}), with downslope flow in red and upslope flow in blue. (d) Nearbed velocity (m s^{-1}) timeseries, both observed at 5 mab and predicted by Chezy equation. (e) Bottom pressure (m sw) and temperature (°C). (f) Vertical profiles of along-canyon velocity (m s^{-1}) for large-SSC time periods as noted in gray lines on panels a-d.*

Periods of elevated SSC co-vary with enhanced downslope flow in the bottom boundary layer. Nearbed SSC (1 mab) increases are temporally aligned with stronger downslope velocities at ~5 mab, and during these events, downslope flow is observed throughout the lowermost ~10–20 m of the water column (Figs. 5.9, 5.10). Converting

SSC to bulk density yields corresponding increases in reduced gravity (g′), with peak values coincident with SSC maxima. Using these observations, parameterized estimates of density-driven flow speed based on a Chezy formulation (Eq. 2) indicate velocities of ~0.2-0.75 m s^{-1} for SSC values between 0.5–1.0 g L^{-1} and layer thicknesses of 1–10 m (Fig. 5.11), comparable and slightly greater in magnitude to observed downslope currents during peak events due to layer averaging. Despite these conditions, no evidence of fully developed sediment gravity flows—such as sustained high-velocity downslope motion, sharp velocity fronts, or propagation of events between canyon sites—is observed within the timeseries.

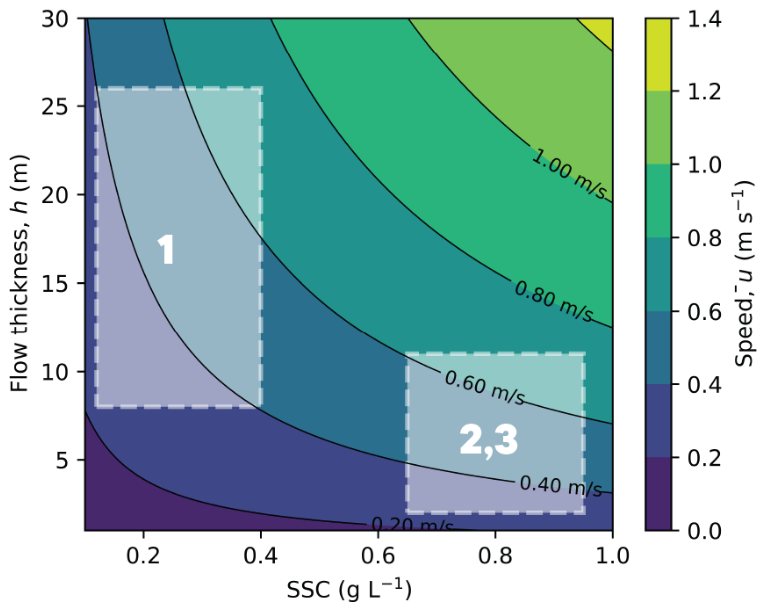

Figure 5.11. Predicted density-driven flow speed on a 2° slope. *Speed estimated as a function of SSC and flow thickness. Color shading and contour lines indicate depth-averaged velocity (m s^{-1}) calculated using the Chezy equation (Eq. 2). Contours are labeled in 0.2 m s^{-1} increments. The parameter space shown encompasses conditions observed during major resuspension events at canyon-head sites (1 = downwelling*

transitions, 2 and 3 = surface wave events), where nearbed SSC increases and downslope-oriented layers extend several meters above the seabed.

5.4. Discussion

5.4.1 Highstand Canyons Responsive to Ocean Forcing

This study is one of several recent studies reframing the highstand–dormant paradigm by demonstrating that submarine canyon heads remain dynamically active under modern conditions and reside within the zone of meteorologically driven sediment resuspension (Amaro et al., 2016; Heijnen et al., 2022; Puig et al., 2004). This interpretation is supported by in-situ estimates of wave–current shear stress that exceed critical thresholds for grain motion, and the direct observation of episodic increases in SSC within canyon heads. Together, these observations indicate that sediment mobilization in canyon heads is not anomalous, but instead represents the response to annually recurring ocean forcing. Beyond local resuspension, highstand canyon heads remain effective conduits drawing sediment from the continental shelf into deeper regions between 500 and 1000 m water depth (Carson et al., 1986; Gardner, 1989; Heijnen et al., 2022; Lahr et al., 2025; Ogston et al., 2008; Puig et al., 2013). Canyon sites at 500 m exhibit similar nearbed suspended sediment events to canyon heads, documenting that the signal of suspended sediment on the shelf can be extended to depth within the canyon, whereas the open-slope (OOI Offshore site, Fig. 5.1) does not share these events (Fig. 5.5, December events). Once suspended sediment reaches the canyon, whether delivered from shallow sources or resuspended directly from the canyon floor, it is advected along canyon axes both within the bottom boundary layer and intermediate nepheloid layers; in the bottom boundary layer, bathymetric steering produces a persistent downslope bias in nearbed flow. This directional asymmetry enhances export efficiency. As a result, canyon heads route shelf-derived sediment signals deeper onto the slope, rather than simply reflecting local hydrodynamic conditions on the adjacent slope environment.

5.4.2 Mechanisms of Synoptic Scale Sediment Transport

Canyon heads exhibit synchronous forcing between the shelf break and 500 m water depth as observed in the correlation of both long-term records and event-scale forcing (Figs. 5.5 and 5.8), however, sites located in greater water depth (>1000 m) do not exhibit similar event forcing. The drivers of sediment transport measured at the sea surface—wind and wave energy, water level anomaly and stratification—are strongly coherent at the 100-km scale, establishing the conditions required for synchronous transport. Sediment-transport events observed in both canyon heads remain coupled to these forcing conditions and exhibit synchronous transport, particularly during the times of greatest energetic forcing. Nearly all of the Shelf, Head and Mid-depth site pairs exhibit statistically significant SSC correlation, indicating a common underlying sediment supply and resuspension signal. By contrast, Shelf, Head and Mid-depth signals did not align with deep-canyon or OOI Slope sites. Current velocity is weakly correlated across canyon heads and the continental shelf, but deeper sites are not correlated, indicating that site-specific processes regulate or modify current structure (e.g., canyon geometry, incident flow) at depth in the canyons. Despite the differences in the timing of current speed between sites, flow in the bottom boundary layer at all sites is bathymetrically steered and oriented downslope at canyon heads, highlighting a general similarity in transport direction. Further, it is relevant to consider that these relationships are robust for Pearson r, which is a strict measure of linear, complete-timeseries similarity and does not reflect improved coherence during peak forcing, temporal lag, or nonlinear similarity.

In addition to complete-timeseries correlation, two event-scale drivers of synchronous sediment transport are identifiable in canyon-head timeseries: 1) surface wave events during winter, and 2) upwelling-relaxation events during summer. Surface wave events are known to be very energetic during winter storm conditions (Allan & Komar, 2000), and in this study, wave events drive the largest shear stresses observed over the annual record. Wave events are associated with prolonged resuspension on the shelf, but also in both canyon heads, including the Dec-Jan events exhibiting an increase in SSC of the shelf and also all four upper canyon sites (AHT, AMM, QHT, QMM; Figs. 5.5, 5.9). While shelf-to-canyon transport is known to generate intermediate nepheloid layers in canyons at the shelf break, we also observe the formation of dense, bottom-focused nepheloid layers during these events (Fig. 5.9; Gardner, 1989; Hickey et al., 1986; Puig & Palanques, 1998; Snyder & Carson, 1986; Wilson et al., 2015). Notably, this wave event is driven by the longest wave period and not the largest wave heights, as the depth of wave base becomes a critical factor in τ_w at sites >200 m water depth. Not only is the wave field a primary trigger of resuspension during the observational record, it is also nearly uniform at 100 km scale, confirming its possibility as a synchronous trigger. Upwelling–relaxation events occur in canyons during the transition in the surface wind from upwelling-favorable to downwelling-favorable conditions and are characterized by enhanced downslope current velocities (>40 cm s^{-1} at 5 mab, Fig. 5.9). This phenomenon has been observed and modeled in nearby canyons (Allen & Hickey, 2010; B. M. Hickey, 1997; Mirshak & Allen, 2005), and our results further demonstrate that this process can drive shear stresses exceeding the threshold of grain motion, affect multiple canyons along the margin, and drive increased SSC (e.g., Fig. 5.5). While the suspended sediment concentrations associated with this process are moderate (~300 mg l^{-1}), the high-velocity currents associated with these events can drive large downslope sediment fluxes. Notably, both resuspension event types identified here—wind-field transitions and major wave events—have a spatial coherence scale which can be much greater than the study site addressed here (Mass & Dotson, 2010; Tillotson & Komar, 1997; Warner et al., 2012).

Taken together, the coherence in the temporal structure of sediment transport indicates that adjacent canyon heads can respond as a network of coupled conduits forced by regional oceanic conditions on the shelf and not as isolated sedimentary systems. Over longer timescales, this tightly linked depositional environment appears to be reflected in the century-scale sediment accumulation rates observed in both canyons. In both Astoria and Quinault canyons, accumulation at the head sites (200-300 m) is minimal, increases to a maximum at approximately 500-800 m water depth, and decreases beyond this depth (Thorbjarnarson et al., 1986; Lahr et al., 2025; Lahr et al., in prep; Moore et al., in prep). This pattern aligns with our timeseries indicating ocean-forced sediment export from canyon heads, diminished transport events at mid-depth sites, and no clear shelf-connected events at the deeper canyon sites.

5.4.3 Excess Density and the Potential for Sediment-Gravity Flows

Once highstand-canyon resuspension processes have been confirmed, the third and final research objective is to address whether or not processes drive excess densities in the bottom boundary layer sufficient to initiate gravity-driven flows. Importantly, we do not observe examples of classic, autosuspending gravity-driven flow in this timeseries (e.g., Azpiroz-Zabala et al., 2017; Paull et al., 2018), nor do we see transport events "progressing" between sites down canyon axes. This absence is likely driven by two main controls on flow formation. First, the grain size of canyon axis sediment across northern Cascadia is very fine (modal grain size 10 µm, sand content <5 vol %), and the slow settling velocity associated with this size class promotes diffuse density anomalies and slows the formation of dense basal layers. Second, there are several competing turbulent processes which act to diffuse sediment upward, generating thick layer heights with a relatively small overall density anomaly. Despite a less obvious signal in timeseries data, this type of slow-moving, dilute flow is known to form in a wide range of depositional environments (Hage et al., 2019; Parsons et al., 2007). Ocean-driven resuspension in the studied canyons is thus considered to be at a near-threshold state for gravity flows, where suspended-sediment events commonly occur and excess density enhances downslope advection, but flow development is limited by turbulent diffusion and fine sediment dynamics (Fig. 5.10).

In the absence of high-density, autosuspending sediment gravity flow activity, this study quantifies the strength of gravity-driven forcing by measuring sediment mass concentrations and current structure in the bottom boundary layer to compute the buoyancy anomaly, layer height, and range of density-driven flow speeds. We observe that suspended sediment reaches a maximum concentration of >1 g L^{-1} during and several days after wave stresses exceed the threshold of grain motion in canyon heads, and this concentration is above the lower limit of conditions known to initiate dilute density-driven flow (Hage et al., 2019; Kineke et al., 2000; Liu et al., 2023; McCool & Parsons, 2004). Critically, the negative buoyancy anomaly associated with suspended sediment in the flow during major suspension events does demonstrate a clear relationship with observed downslope flow in the lowermost 10-20 m of the water column. Specifically, increased SSC (1 mab) following wave events covaries with the strength of downslope flow at 5 mab. Estimates of layer-averaged flow speed for concentrations between 0.5-1.0 g L^{-1} and layer height between 1-10 m are estimated to be 0.2-0.75 m s^{-1}, comparable to observed flow speeds during peak SSC events (Figs. 5.9, 5.10). The comparable timing and magnitude of predicted and observed downslope flow indicate that surface wave-driven resuspension events on the shelf and canyon head can increase SSC for several days, intermittently forming negative buoyancy anomalies near the seabed and enhancing downslope flow. The intermittency of this process is overprinted by internal tides and flow coupled to wind and incident circulation, making the signal of the gravity flow component difficult to highlight in timeseries observation. Oceanic processes may directly govern sediment gravity flow formation, as changing mean flow and turbulence may decrease shear stress or decrease the nearbed sediment concentrations of density instabilities formed by fine-grained, slow-settling particles. While gravity-driven flows may be short-lived and controlled by stronger water-column processes (e.g., internal waves, wind-driven circulation), this provides a consistent mechanism for downslope transport, and likely contributes to the net-downslope mean current orientations observed at most sites.

One key implication highlighted by these results is that the propagation of gravity flows in some highstand canyon heads is limited not only by resuspension triggers but also by the sediment properties of available seabed sediment. The fine-grained, low-settling-velocity sediment characteristic in this study favors diffuse, lofted suspensions and limits the formation of dense nearbed layers, effectively limiting the development of high-density, low-drag turbidity currents. While fine sediment can generate sediment gravity flows with much greater density, such flows are often observed on shelf or shallow-water settings with low gradients (0.5°) and with thinner, more defined lower layers, e.g., fluid muds (Kineke et al., 1996; Kineke & Sternberg, 1995). In contrast, access to coarse sediment supply—through flood events or failures of relict sediment—may promote stronger density contrasts and more coherent, self-sustaining gravity flows. This is supported by the grain size of turbidite event layers observed across the continental margin from both coseismic mass wasting (Goldfinger, 2012) and flood events (Lahr et al., 2025). In both cases, a significant portion of the deposited sediment was sand, which is not present in large quantities at the seabed. This reinforces that variability in sediment supply may exert a primary control on whether canyon systems operate in a diffuse flow regime or maintain fully developed turbidity current activity. As such, constraints on grain size and sediment availability may be critical for interpreting the origin and dynamics of turbidite deposits in modern submarine canyon systems.

5.4.4 Implications for the highstand-dormant paradigm

The results presented here challenge the conventional view that submarine canyons are largely inactive during sea-level highstand and instead demonstrate that canyon heads remain coupled to oceanographic forcing and transport sediment downslope multiple times each year. Wind stress and surface waves, which are often organized and uniform over spatial scales >100 km, act as the primary drivers of sediment mobilization in canyons and promote synchronous transport across the margin. Although these processes are known to drive sediment transport on the continental shelf, our observations indicate that upper canyon axes efficiently transmit this signal to intermediate depths on the continental margin, supporting the presence of a ^{210}Pb accumulation rate depocenter of 500 m water depth (Lahr et al., in prep; Moore et al., in prep). Further, the suspended sediment remobilized from the seabed in this environment does create excess density which is predicted to drive slow gravity-driven flows, although these flows appear secondary to other drivers of canyon flow (e.g., internal waves and tides) and limited by small buoyancy anomaly and tall, high-drag layer heights.

Importantly, the highstand-detached configuration represents the majority of canyons on Earth today, and the updated view of highstand canyons as partially active and linked to broad ocean forcing permits new assumptions and open questions for active transport and stratigraphic interpretation. In this framework, canyons are neither fully dormant nor persistently active, but instead operate as intermittently active systems responsive to and amplifying the forcing conditions on the shelf. Bathymetric morphology, sediment preconditioning, and water column processes all play a role in how each system is expressed, but adjacent canyon systems are often embedded within the same synoptic-scale forcing, and can therefore respond coherently over spatial scales exceeding individual canyon networks. This perspective has important implications for the interpretation of event stratigraphy in highstand canyon systems, including the seismoturbidite record along the Cascadia margin. Although no high-velocity, autosuspending sediment gravity flows were directly observed in this study, the forcing conditions responsible for sediment resuspension were shown to be synchronous over spatial scales larger than the canyon channels used in the confluence test. This raises the possibility that sufficiently energetic oceanographic events could initiate sediment gravity flows in multiple adjacent canyons simultaneously, complicating the attribution of synchronous turbidite deposits to seismic triggering alone. Finally, these results highlight the need to better constrain sediment budgets in highstand canyon systems. Downslope transport within shelf and coastal bottom boundary layers is known to generate substantial sediment fluxes (Geyer et al., 2004; Hage et al., 2019; Kineke et al., 2000), and this study further documents that this material can be moved efficiently through canyon heads. These findings demonstrate that regional oceanic forcing sustains recurring sediment export through highstand canyon systems, highlighting that important mechanisms of shelf-to-deep-sea sediment transfer operate coherently across spatial scales greater than those captured by single-canyon studies.

5.5 Conclusions

In this study, we show that highstand submarine canyon sediment transport along the Cascadia margin demonstrates a higher level of active sediment transport in the bottom boundary layer than traditionally assumed. Specifically, we find that sediment routing through upper canyon systems remains coupled to wind- and wave-driven forcing, with resuspension events generating excess density and density-enhanced downslope flow near the seabed. These transport events can be temporally synchronous across canyon systems separated by more than 100 km, reflecting the regional scale of meteorological forcing. Upper-canyon channels act as downslope-oriented conduits that efficiently transmit shelf- and head-derived sediment signals to intermediate depths (~500 m), but depths below this (>1000 m) are comparatively decoupled. Although fully developed autosuspending sediment gravity flows were not observed during this study period, canyon heads concentrate sediment and episodically generate excess density in the bottom boundary layer that enhances downslope transport. These observations indicate that highstand-canyon systems operate in a near-threshold regime, in which sediment transport occurs multiple times per year and density-modified flow is common but transient, often diffused into thick bottom boundary layers and overprinted by other energetic oceanic processes. Our findings also highlight two complexities in the assumptions underpinning the interpretation of turbidite stratigraphy in highstand canyons, i.e., synchronous sediment transport across canyons may not uniquely indicate seismic triggering, and the conditions for density-driven flows remain partially active during the Holocene. More broadly, these results demonstrate that the highstand-dormant paradigm presents an overly simplified view of modern sediment routing for relatively inactive canyons, representing a majority of canyons on Earth today, and there is a need to establish a mechanistic understanding of downslope flow and constrain geochemical budgets in light of these findings.

Chapter 6. SUMMARY AND SYNTHESIS

Submarine canyons are among the most important conduits for sediment transport on continental margins, yet as demonstrated in this dissertation, the processes governing sediment transport during sea-level highstand do not cleanly align with broad conceptual models of canyon activity. Highstand canyon systems are commonly interpreted as dormant environments where sediment gravity flows are infrequent, primarily earthquake-triggered, and sourced from major slope failures. These assumptions underpin interpretations of highstand canyon stratigraphy globally and form a central basis for paleoseismic reconstructions along active margins such as Cascadia. The studies presented in this dissertation demonstrate that highstand submarine canyons remain partially active sediment-routing systems that are influenced by a broad range of oceanic, fluvial, and tectonic processes. Taken together, these studies provide a more complete framework for understanding sediment transport and gravity flow behavior in modern canyon systems by integrating sediment stratigraphy and hydrodynamic observations.

The first two studies provide well-constrained evidence of active sediment transport processes and oceanic turbidity current activity related to fluvial events within a highstand-detached submarine canyon. Sedimentological observations, radioisotope geochronology, grain size measurements, and organic matter geochemistry demonstrated that Astoria Canyon contains modern flood-associated turbidites linked to the 1894 and 1948 Columbia River floods. This finding demonstrates how multiple nonseismic sediment gravity flows can occur in Cascadia over a single interseismic period of 300-500 y. These deposits were characterized by graded and laminated sedimentary structures, low excess ^{210}Pb activity, and terrestrial organic matter signatures. The deposits indicate rapid transfer of terrestrial sediment and organic matter from the Columbia River to the canyon floor, with minimal storage in intermediate environments on the continental shelf. These findings provide the first direct evidence of modern nonseismic sediment gravity flow deposition within a northern Cascadia canyon and demonstrate that fluvial forcing remains capable of generating turbidity currents during sea-level highstand. More broadly, these results show that highstand canyons remain partially coupled to coastal sediment supply and that event-driven transport may contribute substantially to sediment and organic carbon burial.

The third study builds upon the first two by comparing flood-generated and earthquake-generated event beds within the canyon and also by characterizing how a canyon head redistributes sediment during a major subduction zone earthquake. Astoria Canyon provides a rare opportunity to evaluate contrasting event deposits because the canyon preserves stratigraphy associated with both historical Columbia River floods and the 1700 Cascadia megathrust earthquake, which produced two fundamentally different deposit types. Flood-derived deposits were thin, laminated turbidites with strong terrestrial organic matter signatures and depositional ages synchronous with major river floods. In contrast, earthquake-related deposits consisted of thick, compositionally heterogeneous mass transport deposits characterized by sheared mud, debris-flow fabrics, and marine-derived organic matter. These observations demonstrate that organic matter can provide a reliable method for distinguishing between seismic and nonseismic event deposits, whereas in this location, density structure is variable and evolves significantly over short spatial scales. The study further demonstrated that earthquake-triggered sediment gravity flows in canyon heads do not necessarily flush sediment directly into abyssal environments but instead may partially infill canyon channels with cohesive debris-flow deposits over multiple seismic cycles. These findings update several assumptions of the seismoturbidite conceptual model, including the assumptions that highstand canyon systems are inactive between earthquakes, that event-bed density structure is laterally correlatable, and that earthquake-driven slope failures are efficiently "flushed", or routed into the deep sea.

The fourth study evaluates whether sediment resuspension within highstand submarine canyons reflects regional, synoptic-scale forcing and triggers synchronous sediment transport across canyon systems separated by more than 100 km. Year-long hydrodynamic observations from Astoria and Quinault Canyons demonstrate that the atmospheric and oceanographic conditions forcing sediment transport—waves, wind, water-level anomalies, and stratification—were coherent across the Washington margin. Nearbed sediment resuspension occurred in both canyon systems during energetic conditions, and events were partially synchronous between canyon systems, primarily within canyon heads. This indicates that transport magnitude and timing can be linked to forcing on the shelf and coast on spatial scales relevant to the interpretation of Cascadia turbidite records. Specifically, regional synchroneity of sediment transport may not uniquely indicate earthquake triggering. More broadly, these findings emphasize that adjacent submarine canyon channels act as a responsive and coherent set of conduits that export shelf and riverine sediment to depth.

These four studies provide new insight into the sediment dynamics of highstand inactive canyons and highlight common themes on the triggers for active sediment transport within highstand canyons and the limitations of margin-scale assumptions. This work also demonstrates that sea-level highstand does not fully suppress sediment gravity flow activity, but instead modifies the pathways, triggers, and preservation of sediment transport within canyon systems. Collectively, these findings indicate that highstand submarine canyons are neither fully dormant nor uniformly active but instead operate as dynamic and spatially heterogeneous sediment-routing systems that intermittently couple tectonic, fluvial and oceanic processes on the continental shelf to initiate transport to the deep ocean. This revised framework has important implications for the development and interpretation of canyon stratigraphy, particularly in paleoseismic studies where assumptions of synchroneity, earthquake exclusivity, and direct canyon flushing are commonly invoked.

BIBLIOGRAPHY

Adams, J. (1990). Paleoseismicity of the Cascadia Subduction Zone: Evidence from turbidites off the Oregon-Washington Margin. Tectonics, 9(4), 569–583.

Alford, M. H., Mickett, J. B., Zhang, S., MacCready, P., Zhao, Z., & Newton, J. (2012). Internal waves on the Washington continental shelf. Oceanography, 25(2), 66–79.

Allan, J., & Komar, P. (2000). Are ocean wave heights increasing in the eastern North Pacific? Eos, Transactions American Geophysical Union, 81(47), 561–567.

Allan, J. C., & Komar, P. D. (2002). Extreme storms on the Pacific Northwest Coast during the 1997-98 El Niño and 1998-99 La Niña. Journal of Coastal Research, 18(1), 175–193.

Allan, J. C., & Komar, P. D. (2006). Climate controls on US west coast erosion processes. Journal of Coastal Research, 22(3), 511–529.

Allen, S. E., & Hickey, B. M. (2010). Dynamics of advection-driven upwelling over a shelf break submarine canyon. Journal of Geophysical Research: Oceans, 115(C8).

Amaro, T., Huvenne, V. A. I., Allcock, A. L., Aslam, T., Davies, J. S., Danovaro, R., et al. (2016). The Whittard Canyon – A case study of submarine canyon processes. Progress in Oceanography, 146, 38–57.

Atwater, B. F., & Yamaguchi, D. K. (1991). Sudden, probably coseismic submergence of Holocene trees and grass in coastal Washington State. Geology, 19(7), 706–709.

Atwater, B. F., Musumi-Rokkaku, S., Satake, K., Tsuji, Y., Ueda, K., & Yamaguchi, D. K.

(2016). The orphan tsunami of 1700: Japanese clues to a parent earthquake in North America. University of Washington Press.

Ayranci, K., Lintern, D. G., Hill, P. R., & Dashtgard, S. E. (2012). Tide-supported gravity flows on the upper delta front, Fraser River delta, Canada. Marine Geology, 326–328, 166–170.

Azpiroz-Zabala, M., Cartigny, M. J. B., Talling, P. J., Parsons, D. R., Sumner, E. J., Clare, M. A., et al. (2017). Newly recognized turbidity current structure can explain prolonged flushing of submarine canyons. Science Advances, 3(10), e1700200.

Bailey, L. P., Clare, M. A., Rosenberger, K. J., Cartigny, M. J. B., Talling, P. J., Paull, C. K., et al. (2021). Preconditioning by sediment accumulation can produce powerful turbidity currents without major external triggers. Earth and Planetary Science Letters, 562, 116845.

Baker, E. T., & Hickey, B. M. (1986). Contemporary sedimentation processes in and around an active West Coast submarine canyon. Marine Geology, 71(1), 15–34.

Barnard, W. D. (1978). The Washington continental slope: Quaternary tectonics and sedimentation. Marine Geology, 27(1), 79–114.

Bentley, S. J., & Nittrouer, C. A. (2003). Emplacement, modification, and preservation of event strata on a flood-dominated continental shelf: Eel shelf, Northern California. Continental Shelf Research, 23(16), 1465–1493.

Bernhardt, A., & Schwanghart, W. (2021). Where and why do submarine canyons remain connected to the shore during sea-level rise? Insights from global topographic analysis and Bayesian regression. Geophysical Research Letters, 48(10), e2020GL092234.

Biscara, L., Mulder, T., Martinez, P., Baudin, F., Etcheber, H., Jouanneau, J.-M., & Garlan, T. (2011). Transport of terrestrial organic matter in the Ogooué deep sea turbidite system (Gabon). Marine and Petroleum Geology, 28(5), 1061–1072.

Boegman, L., & Stastna, M. (2019). Sediment resuspension and transport by internal solitary waves. Annual Review of Fluid Mechanics, 51, 129–154.

Bosley, K. L., Lavelle, J. W., Brodeur, R. D., Wakefield, W. W., Emmett, R. L., Baker, E. T., & Rehmke, K. M. (2004). Biological and physical processes in and around Astoria Submarine Canyon, Oregon, USA. Journal of Marine Systems, 50(1), 21–37.

Bouma, A. H. (1962). Sedimentology of some Flysch deposits: A graphic approach to facies interpretation. Ann Arbor, MI: University Microfilms International.

Bourget, J., Zaragosi, S., Mulder, T., Schneider, J.-L., Garlan, T., Van Toer, A., et al. (2010). Hyperpycnal-fed turbidite lobe architecture and recent sedimentary processes: A case study from the Al Batha turbidite system, Oman margin. Sedimentary Geology, 229(3), 144–159.

Bruel, R., & Sabatier, P. (2020). serac: An R package for ShortlivEd RAdionuclide chronology of recent sediment cores. Journal of Environmental Radioactivity, 225, 106449.

Burnett, W. C., Bidorn, B., & Wang, Y. (2023). Can 210Pb be used as a paleo-storm proxy? Quaternary Science Reviews, 315, 108242.

Canals, M., Puig, P., de Madron, X. D., Heussner, S., Palanques, A., & Fabres, J. (2006). Flushing submarine canyons. Nature, 444(7117), 354–357.

Carlson, P. R. (1968). Marine geology of Astoria Submarine Canyon (Ph.D.). Oregon State University.

Carpenter, R., Bennett, J. T., & Peterson, M. L. (1981). 210Pb activities in and fluxes to sediments of the Washington continental slope and shelf. Geochimica et Cosmochimica Acta, 45(7), 1155–1172.

Carson, B., Baker, E. T., Hickey, B. M., Nittrouer, C. A., DeMaster, D. J., Thorbjarnarson, K. W., & Snyder, G. W. (1986). Modern sediment dispersal and accumulation in Quinault submarine canyon — A summary. Marine Geology, 71(1), 1–13.

Carter, G. S., & Gregg, M. C. (2002). Intense, variable mixing near the head of Monterey Submarine Canyon. Journal of Physical Oceanography, 32(11), 3145–3165.

Center for Operational Oceanographic Products and Services. (2024). Water-level observations for stations 9437540, 9440581, 9440910, 9441102, and 9442396. National Oceanic and Atmospheric Administration.

Clare, M. A., Hughes Clarke, J. E., Talling, P. J., Cartigny, M. J. B., & Pratomo, D. G. (2016). Preconditioning and triggering of offshore slope failures and turbidity currents revealed by most detailed monitoring yet at a fjord-head delta. Earth and Planetary Science Letters, 450, 208–220.

Covault, J. A., & Graham, S. A. (2010). Submarine fans at all sea-level stands: Tectono-morphologic and climatic controls on terrigenous sediment delivery to the deep sea. Geology, 38(10), 939–942.

Crisóstomo-Figueroa, A., McArthur, A. D., Dorrell, R. M., Amy, L., & McCaffrey, W. D. (2020). A new modelling approach to sediment bypass prediction applied to the

East Coast Basin, New Zealand. GSA Bulletin, 133(7–8), 1734–1748.

Curray, J. R., Emmel, F. J., & Moore, D. G. (2002). The Bengal Fan: Morphology, geometry, stratigraphy, history and processes. Marine and Petroleum Geology, 19(10), 1191–1223.

Cutshall, N. H., Larsen, I. L., Olsen, C. R., Nittrouer, C. A., & DeMaster, D. J. (1986). Columbia River sediment in Quinault Canyon, Washington — Evidence from artificial radionuclides. Marine Geology, 71(1), 125–136.

Dyer, K. R., & Manning, A. J. (1999). Observation of the size, settling velocity and effective density of flocs, and their fractal dimensions. Journal of Sea Research, 41(1), 87–95.

Feng, X., Benitez-Nelson, B. C., Montluçon, D. B., Prahl, F. G., McNichol, A. P., Xu, L., et al. (2013). 14C and 13C characteristics of higher plant biomarkers in Washington margin surface sediments. Geochimica et Cosmochimica Acta, 105, 14–30.

Flores, R. P., Rijnsburger, S., Meirelles, S., Horner-Devine, A. R., Souza, A. J., Pietrzak, J. D., et al. (2018). Wave generation of gravity-driven sediment flows on a predominantly sandy seabed. Geophysical Research Letters, 45(15), 7634–7645.

Fox, J. M., Hill, P. S., Milligan, T. G., Ogston, A. S., & Boldrin, A. (2004). Floc fraction in the waters of the Po River prodelta. Continental Shelf Research, 24(15), 1699–1715.

Galy, V., France-Lanord, C., Beyssac, O., Faure, P., Kudrass, H., & Palhol, F. (2007). Efficient organic carbon burial in the Bengal fan sustained by the Himalayan erosional system. Nature, 450(7168), 407–410.

Gardner, W. D. (1989). Periodic resuspension in Baltimore canyon by focusing of internal waves. Journal of Geophysical Research: Oceans, 94(C12), 18185–18194.

Geyer, W. R., Hill, P. S., & Kineke, G. C. (2004). The transport, transformation and dispersal of sediment by buoyant coastal flows. Continental Shelf Research, 24(7), 927–949.

Goldfinger, C., Morey, A. E., Black, B., Beeson, J., Nelson, C. H., & Patton, J. (2013). Spatially limited mud turbidites on the Cascadia margin: Segmented earthquake ruptures? Natural Hazards and Earth System Sciences, 13(8), 2109–2146.

Goldfinger, C., Morey, A. E., Nelson, C. H., Gutiérrez-Pastor, J., Johnson, J. E., Karabanov, E., et al. (2007). Rupture lengths and temporal history of significant earthquakes on the offshore and north coast segments of the Northern San Andreas Fault based on turbidite stratigraphy. Earth and Planetary Science Letters, 254(1), 9–27.

Goldfinger, C., Nelson, C. H., Morey, A. E., Johnson, J. E., Patton, J. R., Karabanov, E. B., et al. (2012). Turbidite event history—Methods and implications for Holocene paleoseismicity of the Cascadia subduction zone (No. 1661-F). U.S. Geological Survey.

Goldfinger, C., Galer, S., Beeson, J., Hamilton, T., Black, B., Romsos, C., et al. (2017). The importance of site selection, sediment supply, and hydrodynamics: A case study of submarine paleoseismology on the northern Cascadia margin, Washington USA. Marine Geology, 384, 4–46.

Goñi, M. A., & Montgomery, S. (2000). Alkaline CuO oxidation with a microwave digestion system: Lignin analyses of geochemical samples. Analytical Chemistry, 72(14), 3116–3121.

Grant, W. D., & Madsen, O. S. (1979). Combined wave and current interaction with a rough bottom. Journal of Geophysical Research: Oceans, 84(C4), 1797–1808.

Guo, J. (2020). Empirical model for Shields diagram and its applications. Journal of Hydraulic Engineering, 146(6), 04020038.

Gust, G., & Müller, V. (1997). Interfacial hydrodynamics and entrainment functions of currently used erosion devices. In N. Burt, R. Parker, & J. Watts (Eds.), Cohesive sediments (pp. 149–174). John Wiley & Sons.

Guyard, H., Chapron, E., St-Onge, G., Anselmetti, F. S., Arnaud, F., Magand, O., et al. (2007). High-altitude varve records of abrupt environmental changes and mining activity over the last 4000 years in the Western French Alps (Lake Bramant, Grandes Rousses Massif). Quaternary Science Reviews, 26(19), 2644–2660.

Hage, S., Cartigny, M. J. B., Sumner, E. J., Clare, M. A., Hughes Clarke, J. E., Talling, P. J., et al. (2019). Direct monitoring reveals initiation of turbidity currents from extremely dilute river plumes. Geophysical Research Letters, 46(20), 11310–11320.

Harris, P. T., & Whiteway, T. (2011). Global distribution of large submarine canyons: Geomorphic differences between active and passive continental margins. Marine Geology, 285(1), 69–86.

Hatten, J. A., Goñi, M. A., & Wheatcroft, R. A. (2012). Chemical characteristics of particulate organic matter from a small, mountainous river system in the Oregon

Coast Range, USA. Biogeochemistry, 107(1), 43–66.

Hedges, J. I., & Mann, D. C. (1979a). The characterization of plant tissues by their lignin oxidation products. Geochimica et Cosmochimica Acta, 43(11), 1803–1807.

Hedges, J. I., & Mann, D. C. (1979b). The lignin geochemistry of marine sediments from the southern Washington coast. Geochimica et Cosmochimica Acta, 43(11), 1809–1818.

Heijnen, M. S., Mienis, F., Gates, A. R., Bett, B. J., Hall, R. A., Hunt, J., et al. (2022). Challenging the highstand-dormant paradigm for land-detached submarine canyons. Nature Communications, 13(1), 3448.

Hickey, B., Baker, E., & Kachel, N. (1986). Suspended particle movement in and around Quinault submarine canyon. Marine Geology, 71(1), 35–83.

Hickey, B., Geier, S., Kachel, N., & MacFadyen, A. (2005). A bi-directional river plume: The Columbia in summer. Continental Shelf Research, 25(14), 1631–1656.

Hickey, B. M., Pietrafesa, L. J., Jay, D. A., & Boicourt, W. C. (1998). The Columbia River Plume Study: Subtidal variability in the velocity and salinity fields. Journal of Geophysical Research: Oceans, 103(C5), 10339–10368.

Hickey, B. M. (1979). The California current system—hypotheses and facts. Progress in Oceanography, 8(4), 191–279.

Hickey, B. M. (1997). The response of a steep-sided, narrow canyon to time-variable wind forcing. Journal of Physical Oceanography, 27(5), 697–726.

Hill, J. C., Watt, J. T., Brothers, D. S., & Kluesner, J. W. (2020). Submarine canyons, slope failures and mass transport processes in southern Cascadia. Geological Society, London, Special Publications, 500(1), 453–475.

Hill, J. C., Watt, J. T., & Brothers, D. S. (2022). Mass wasting along the Cascadia subduction zone: Implications for abyssal turbidite sources and the earthquake record. Earth and Planetary Science Letters, 597, 117797.

Hill, J. C., Watt, J. T., Paull, C. K., Caress, D. W., Brothers, D. S., Arizmendi, K., et al. (2026). Widespread abyssal turbidites record megathrust earthquake-triggered landslides and coseismic deformation in the Cascadia subduction zone. Science Advances, 12(3).

Hilton, R. G., & West, A. J. (2020). Mountains, erosion and the carbon cycle. Nature Reviews Earth & Environment, 1(6), 284–299.

Hizzett, J. L., Hughes Clarke, J. E., Sumner, E. J., Cartigny, M. J. B., Talling, P. J., & Clare, M. A. (2018). Which triggers produce the most erosive, frequent, and longest runout turbidity currents on deltas? Geophysical Research Letters, 45(2), 855–863.

Howarth, J. D., Orpin, A. R., Kaneko, Y., Strachan, L. J., Nodder, S. D., Mountjoy, J. J., et al. (2021). Calibrating the marine turbidite palaeoseismometer using the 2016 Kaikōura earthquake. Nature Geoscience, 14(3), 161–167.

Jacobs, G. A., D'Addezio, J. M., Bartels, B., & Spence, P. L. (2021). Constrained scales in ocean forecasting. Advances in Space Research, 68(2), 746–761.

Kammerer, J. C. (1990). Largest rivers in the United States. U.S. Geological Survey Open-File Report 87-242.

Kao, S.-J., Hilton, R. G., Selvaraj, K., Dai, M., Zehetner, F., Huang, J.-C., et al. (2014). Preservation of terrestrial organic carbon in marine sediments offshore Taiwan: Mountain building and atmospheric carbon dioxide sequestration. Earth Surface Dynamics, 2(1), 127–139.

Keil, R. G., Dickens, A. F., Arnarson, T., Nunn, B. L., & Devol, A. H. (2004). What is the oxygen exposure time of laterally transported organic matter along the Washington margin? Marine Chemistry, 92(1), 157–165.

Kenney, W. F., Shields, M. R., Bianchi, T. S., Kolker, A. S., & Mohrig, D. (2022). Excess 210Pb as an indicator of flood-stage sediments in prograding Wax Lake Delta, USA. Marine Geology, 453, 106914.

Khripounoff, A., Crassous, P., Lo Bue, N., Dennielou, B., & Silva Jacinto, R. (2012). Different types of sediment gravity flows detected in the Var submarine canyon (northwestern Mediterranean Sea). Progress in Oceanography, 106, 138–153.

Kilcher, L. F., & Nash, J. D. (2010). Structure and dynamics of the Columbia River tidal plume front. Journal of Geophysical Research: Oceans, 115(5).

Kineke, G. C., & Sternberg, R. W. (1995). Distribution of fluid muds on the Amazon continental shelf. Marine Geology, 125(3), 193–233.

Kineke, G. C., Sternberg, R. W., Trowbridge, J. H., & Geyer, W. R. (1996). Fluid-mud processes on the Amazon continental shelf. Continental Shelf Research, 16(5), 667–696.

Kineke, G. C., Woolfe, K. J., Kuehl, S. A., Milliman, J. D., Dellapenna, T. M., & Purdon, R. G. (2000). Sediment export from the Sepik River, Papua New Guinea: Evidence for a divergent sediment plume. Continental Shelf Research, 20(16), 2239–2266.

Knudson, K. P., & Hendy, I. L. (2009). Climatic influences on sediment deposition and turbidite frequency in the Nitinat Fan, British Columbia. Marine Geology, 262(1), 29–38.

Kuhn, A. M., Dutkiewicz, S., Jahn, O., Clayton, S., Rynearson, T. A., Mazloff, M. R., & Barton, A. D. (2019). Temporal and spatial scales of correlation in marine phytoplankton communities. Journal of Geophysical Research: Oceans, 124(12), 9417–9438.

Kunze, E., Rosenfeld, L. K., Carter, G. S., & Gregg, M. C. (2002). Internal waves in Monterey Submarine Canyon. Journal of Physical Oceanography, 32(6), 1890–1913.

Lahr, E. J., Ogston, A. S., Hill, J. C., Glover, H. E., & Rosenberger, K. J. (2025). Submarine canyon sediment transport and accumulation during sea level highstand: Interactive seasonal regimes in the head of Astoria Canyon, WA. Marine Geology, 484, 107516.

Lamb, M. P., & Mohrig, D. (2009). Do hyperpycnal-flow deposits record river-flood dynamics? Geology, 37(12), 1067–1070.

Lamb, M. P., Parsons, J. D., Mullenbach, B. L., Finlayson, D. P., Orange, D. L., & Nittrouer, C. A. (2008). Evidence for superelevation, channel incision, and formation of cyclic steps by turbidity currents in Eel Canyon, California. GSA Bulletin, 120(3–4), 463–475.

Leithold, E. L., & Hope, R. S. (1999). Deposition and modification of a flood layer on the northern California shelf: Lessons from and about the fate of terrestrial particulate organic carbon. Marine Geology, 154(1), 183–195.

Liu, J. T., Wang, Y.-H., Yang, R. J., Hsu, R. T., Kao, S.-J., Lin, H.-L., & Kuo, F. H. (2012). Cyclone-induced hyperpycnal turbidity currents in a submarine canyon. Journal of Geophysical Research: Oceans, 117(C4).

Liu, M., Wang, Z., Yu, K., & Xu, J. (2023). Two distinct types of turbidity currents observed in the Manila Trench, South China Sea. Communications Earth & Environment, 4(1), 108.

Ma, Y., Wright, L. D., & Friedrichs, C. T. (2008). Observations of sediment transport on the continental shelf off the mouth of the Waiapu River, New Zealand: Evidence for current-supported gravity flows. Continental Shelf Research, 28(4), 516–532.

MacCready, P., McCabe, R. M., Siedlecki, S. A., Lorenz, M., Giddings, S. N., Bos, J., et al. (2021). Estuarine circulation, mixing, and residence times in the Salish Sea. Journal of Geophysical Research: Oceans, 126(2), e2020JC016738.

Madsen, O. S. (1994). Spectral wave-current bottom boundary layer flows. Proceedings of the 24th International Conference on Coastal Engineering, 384–398.

Maier, K. L., Gales, J. A., Paull, C. K., Rosenberger, K., Talling, P. J., Simmons, S. M., et al. (2019). Linking direct measurements of turbidity currents to submarine canyon-floor deposits. Frontiers in Earth Science, 7.

Maier, K. L., Nodder, S. D., Deppeler, S., Gerring, P., Frontin-Rollet, G., Hale, R., et al. (2024). Dynamic near-seafloor sediment transport in Kaikōura Canyon following a large canyon-flushing event. Journal of Sedimentary Research, 94(3), 283–301.

Mass, C., & Dotson, B. (2010). Major extratropical cyclones of the northwest United States: Historical review, climatology, and synoptic environment. Monthly Weather Review, 138(7), 2499–2527.

McCool, W. W., & Parsons, J. D. (2004). Sedimentation from buoyant fine-grained suspensions. Continental Shelf Research, 24(10), 1129–1142.

Meiburg, E., & Kneller, B. (2010). Turbidity currents and their deposits. Annual Review of Fluid Mechanics, 42, 135–156.

Mikkelsen, O. A., & Pejrup, M. (2000). In situ particle size spectra and density of particle aggregates in a dredging plume. Marine Geology, 170(3), 443–459.

Mirshak, R., & Allen, S. E. (2005). Spin-up and the effects of a submarine canyon: Applications to upwelling in Astoria Canyon. Journal of Geophysical Research: Oceans, 110(C2).

Moum, J. N., Klymak, J. M., Nash, J. D., Perlin, A., & Smyth, W. D. (2007). Energy transport by nonlinear internal waves. Journal of Physical Oceanography, 37(7), 1968–1988.

Mountjoy, J. J., Howarth, J. D., Orpin, A. R., Barnes, P. M., Bowden, D. A., Rowden, A. A., et al. (2018). Earthquakes drive large-scale submarine canyon development and sediment supply to deep-ocean basins. Science Advances, 4(3).

Mulder, T., Migeon, S., Savoye, B., & Faugères, J.-C. (2001a). Inversely graded turbidite sequences in the deep Mediterranean: A record of deposits from flood-generated turbidity currents? Geo-Marine Letters, 21(2), 86–93.

Mulder, T., Migeon, S., Savoye, B., & Jouanneau, J.-M. (2001b). Twentieth century floods recorded in the deep Mediterranean sediments. Geology, 29(11), 1011–1014.

Mulder, T., & Alexander, J. (2001). The physical character of subaqueous sedimentary density flows and their deposits. Sedimentology, 48(2), 269–299.

Mulder, T., & Chapron, E. (2012). Flood deposits in continental and marine environments: Character and significance. In R. M. Slatt & C. Zavala (Eds.), Sediment Transfer from Shelf to Deep Water—Revisiting the Delivery System (Vol. 61). American Association of Petroleum Geologists.

Mulder, T., & Syvitski, J. P. M. (1995). Turbidity currents generated at river mouths during exceptional discharges to the world oceans. The Journal of Geology, 103(3), 285–299.

Mulder, T., Syvitski, J. P. M., Migeon, S., Faugères, J.-C., & Savoye, B. (2003). Marine hyperpycnal flows: Initiation, behavior and related deposits. A review. Marine and Petroleum Geology, 20(6), 861–882.

Mullenbach, B. L., & Nittrouer, C. A. (2006). Decadal record of sediment export to the deep sea via Eel Canyon. Continental Shelf Research, 26(17), 2157–2177.

Mullenbach, B. L., Nittrouer, C. A., Puig, P., & Orange, D. L. (2004). Sediment deposition in a modern submarine canyon: Eel Canyon, northern California. Marine Geology, 211(1), 101–119.

Naik, P. K., & Jay, D. A. (2011). Distinguishing human and climate influences on the Columbia River: Changes in mean flow and sediment transport. Journal of Hydrology, 404(3), 259–277.

Nakajima, T., & Kanai, Y. (2000). Sedimentary features of seismoturbidites triggered by the 1983 and older historical earthquakes in the eastern margin of the Japan Sea. Sedimentary Geology, 135(1), 1–19.

Nakajima, T. (2006). Hyperpycnites deposited 700 km away from river mouths in the central Japan Sea. Journal of Sedimentary Research, 76(1), 60–73.

Nash, J. D., & Moum, J. N. (2005). River plumes as a source of large-amplitude internal waves in the coastal ocean. Nature, 437(7057), 400–403.

National Data Buoy Center. (2019, 2024). Historical meteorological data for stations 46029 and 46041. National Oceanic and Atmospheric Administration.

National Science Foundation Ocean Observatories Initiative. (2024). Washington Coastal Endurance Array.

Nelson, C. H. (1968). Marine geology of Astoria Deep-Sea Fan (Ph.D.). Oregon State University.

Nelson, C. H., Carlson, P. R., Byrne, J. V., & Alpha, T. R. (1970). Development of the Astoria Canyon-Fan physiography and comparison with similar systems. Marine Geology, 8(3), 259–291.

Nelson, C. H., Goldfinger, C., Johnson, J. E., & Dunhill, G. (2000). Variation of modern turbidite systems along the subduction zone margin of Cascadia basin and implications for turbidite reservoir beds. In P. Weimer (Ed.), Deep-Water Reservoirs of the World (Vol. 20). SEPM Society for Sedimentary Geology.

Nelson, C. H. (1976). Late Pleistocene and Holocene depositional trends, processes, and history of Astoria deep-sea fan, Northeast Pacific. Marine Geology, 20(2), 129–

173.

Nieminski, N. M., Sylvester, Z., Covault, J. A., Gomberg, J., Staisch, L., & McBrearty, I. W. (2024). Turbidite correlation for paleoseismology. GSA Bulletin, 137(1–2), 29–40.

Nittrouer, C. A., & Sternberg, R. W. (1981). The formation of sedimentary strata in an allochthonous shelf environment: The Washington Continental Shelf. In Sedimentary Dynamics of Continental Shelves (Vol. 32, pp. 201–232). Elsevier.

Nittrouer, C. A., Sternberg, R. W., Carpenter, R., & Bennett, J. T. (1979). The use of Pb-210 geochronology as a sedimentological tool: Application to the Washington continental shelf. Marine Geology, 31(3), 297–316.

Normandeau, A., Bourgault, D., Neumeier, U., Lajeunesse, P., St-Onge, G., Gostiaux, L., & Chavanne, C. (2020). Storm-induced turbidity currents on a sediment-starved shelf: Insight from direct monitoring and repeat seabed mapping of upslope migrating bedforms. Sedimentology, 67(2), 1045–1068.

Normark, W. R., & Reid, J. A. (2003). Extensive deposits on the Pacific Plate from Late Pleistocene North American glacial lake outbursts. The Journal of Geology, 111(6), 617–637.

Nowacki, D. J., Horner-Devine, A. R., Nash, J. D., & Jay, D. A. (2012). Rapid sediment removal from the Columbia River plume near field. Continental Shelf Research, 35, 16–28.

O'Connor, J. E., Baker, V. R., Waitt, R. B., Smith, L. N., Cannon, C. M., George, D. L., & Denlinger, R. P. (2020). The Missoula and Bonneville floods—A review of ice-age megafloods in the Columbia River basin. Earth-Science Reviews, 208, 103181.

Ogston, A. S., Cacchione, D. A., Sternberg, R. W., & Kineke, G. C. (2000). Observations of storm and river flood-driven sediment transport on the northern California continental shelf. Continental Shelf Research, 20(16), 2141–2162.

Ogston, A. S., Drexler, T. M., & Puig, P. (2008). Sediment delivery, resuspension, and transport in two contrasting canyon environments in the southwest Gulf of Lions. Continental Shelf Research, 28(15), 2000–2016.

Okutsu, N., Ashi, J., Yamaguchi, A., Irino, T., Ikehara, K., Kanamatsu, T., et al. (2019). Evidence for surface sediment remobilization by earthquakes in the Nankai forearc region from sedimentary records. Geological Society, London, Special Publications, 477(1), 37–45.

Parsons, J. D., Bush, J. W. M., & Syvitski, J. P. M. (2001). Hyperpycnal plume formation from riverine outflows with small sediment concentrations. Sedimentology, 48(2), 465–478.

Parsons, J. D., Friedrichs, C. T., Traykovski, P. A., Mohrig, D., Imran, J., Syvitski, J. P. M., et al. (2007). The mechanics of marine sediment gravity flows. In Continental Margin Sedimentation (pp. 275–337). John Wiley & Sons, Ltd.

Paull, C. K., McGann, M., Sumner, E. J., Barnes, P. M., Lundsten, E. M., Anderson, K., et al. (2014). Sub-decadal turbidite frequency during the early Holocene: Eel Fan, offshore northern California. Geology, 42(10), 855–858.

Paull, C. K., Talling, P. J., Maier, K. L., Parsons, D., Xu, J., Caress, D. W., et al. (2018). Powerful turbidity currents driven by dense basal layers. Nature Communications, 9(1), 4114.

Pike, J., & Kemp, A. E. S. (1996). Preparation and analysis techniques for studies of laminated sediments. Geological Society, London, Special Publications, 116(1), 37–48.

Piper, D. J. W., & Normark, W. R. (2009). Processes that initiate turbidity currents and their influence on turbidites: A marine geology perspective. Journal of Sedimentary Research, 79(6), 347–362.

Piper, D. J. W., Cochonat, P., & Morrison, M. L. (1999). The sequence of events around the epicentre of the 1929 Grand Banks earthquake: Initiation of debris flows and turbidity current inferred from sidescan sonar. Sedimentology, 46(1), 79–97.

Pohl, F., Eggenhuisen, J. T., Cartigny, M. J. B., Tilston, M. C., de Leeuw, J., & Hermidas, N. (2020). The influence of a slope break on turbidite deposits: An experimental investigation. Marine Geology, 424, 106160.

Prahl, F. G., Ertel, J. R., Goñi, M. A., Sparrow, M. A., & Eversmeyer, B. (1994). Terrestrial organic carbon contributions to sediments on the Washington margin. Geochimica et Cosmochimica Acta, 58(14), 3035–3048.

Puig, P., Ogston, A. S., Mullenbach, B. L., Nittrouer, C. A., Parsons, J. D., & Sternberg, R. W. (2004). Storm-induced sediment gravity flows at the head of the Eel submarine canyon, northern California margin. Journal of Geophysical Research: Oceans, 109(C3).

Puig, P., & Palanques, A. (1998). Nepheloid structure and hydrographic control on the Barcelona continental margin, northwestern Mediterranean. Marine Geology, 149(1), 39–54.

Puig, P., Greenan, B. J. W., Li, M. Z., Prescott, R. H., & Piper, D. J. W. (2013). Sediment transport processes at the head of Halibut Canyon, eastern Canada margin: An interplay between internal tides and dense shelf-water cascading. Marine Geology, 341, 14–28.

Puig, P., Palanques, A., & Martín, J. (2014). Contemporary sediment-transport processes in submarine canyons. Annual Review of Marine Science, 6, 53–77.

Quaresma, L. S., Vitorino, J., Oliveira, A., & da Silva, J. (2007). Evidence of sediment resuspension by nonlinear internal waves on the western Portuguese mid-shelf. Marine Geology, 246(2), 123–143.

Rabouille, C., Dennielou, B., Baudin, F., Raimonet, M., Droz, L., Khripounoff, A., et al. (2019). Carbon and silica megasink in deep-sea sediments of the Congo terminal lobes. Quaternary Science Reviews, 222, 105854.

Rantz, S. E., & Riggs, H. C. (1949). Floods of May-June 1948 in Columbia River basin, with a section on magnitude and frequency of floods. USGPO.

Reynolds, N. D., O'Connor, J. E., Pringle, P. T., Bourdeau, A. C., & Schuster, R. L. (2022). Age of the late Holocene Bonneville landslide and submerged forest of the Columbia River Gorge, Oregon and Washington, USA, by radiocarbon dating. Quaternary Research, 109, 65–82.

Ribó, M., Mountjoy, J. J., Mitchell, N., Watson, S. J., Hoffmann, J. J. L., & Woelz, S. (2024). New insights on gravity flow dynamics during submarine canyon flushing events. Geology, 53(1), 34–39.

Ruggiero, P., Komar, P. D., & Allan, J. C. (2010). Increasing wave heights and extreme value projections: The wave climate of the U.S. Pacific Northwest. Coastal Engineering, 57(5), 539–552.

Satake, K., Wang, K., & Atwater, B. F. (2003). Fault slip and seismic moment of the 1700 Cascadia earthquake inferred from Japanese tsunami descriptions. Journal of Geophysical Research: Solid Earth, 108(B11).

Schlacher, T. A., & Connolly, R. M. (2014). Effects of acid treatment on carbon and nitrogen stable isotope ratios in ecological samples: A review and synthesis. Methods in Ecology and Evolution, 5(6), 541–550.

Shanmugam, G., & Moiola, R. J. (1982). Eustatic control of turbidites and winnowed turbidites. Geology, 10(5), 231–235.

Shanmugam, G., & Moiola, R. J. (1988). Submarine fans: Characteristics, models, classification, and reservoir potential. Earth-Science Reviews, 24(6), 383–428.

Shanmugam, G., Moiola, R. J., & Damuth, J. E. (1985). Eustatic control of submarine fan development. In A. H. Bouma, W. R. Normark, & N. E. Barnes (Eds.), Submarine Fans and Related Turbidite Systems (pp. 23–28). New York, NY: Springer.

Sherwood, C. R., & Creager, J. S. (1990). Sedimentary geology of the Columbia River Estuary. Progress in Oceanography, 25(1), 15–79.

Shields, A. (1936). Application of similarity principles and turbulence research to bed-load movement.

Snyder, G. W., & Carson, B. (1986). Bottom and suspended particle sizes: Implications for modern sediment transport in Quinault submarine canyon. Marine Geology, 71(1), 85–105.

Sommerfield, C. K. (1997). Modern sedimentation and diagenetic processes on the Eel River shelf and slope, northern California continental margin (Ph.D.). State University of New York at Stony Brook.

Spahn, E. Y., Horner-Devine, A. R., Nash, J. D., Jay, D. A., & Kilcher, L. (2009). Particle resuspension in the Columbia River plume near field. Journal of Geophysical Research: Oceans, 114(C2).

Sternberg, R. W. (1986). Transport and accumulation of river-derived sediment on the Washington continental shelf, USA. Journal of the Geological Society, 143(6), 945–956.

Stevenson, C. J., Jackson, C. A.-L., Hodgson, D. M., Hubbard, S. M., & Eggenhuisen, J. T. (2015). Deep-water sediment bypass. Journal of Sedimentary Research, 85(9), 1058–1081.

St-Onge, G., Mulder, T., Piper, D. J. W., Hillaire-Marcel, C., & Stoner, J. S. (2004). Earthquake and flood-induced turbidites in the Saguenay Fjord (Québec): A Holocene paleoseismicity record. Quaternary Science Reviews, 23(3), 283–294.

Sumner, E. J., Talling, P. J., Amy, L. A., Wynn, R. B., Stevenson, C. J., & Frenz, M. (2012). Facies architecture of individual basin-plain turbidites: Comparison with existing models and implications for flow processes. Sedimentology, 59(6), 1850–1887.

Talling, P. J., Hage, S., Baker, M. L., Bianchi, T. S., Hilton, R. G., & Maier, K. L. (2024). The global turbidity current pump and its implications for organic carbon cycling. Annual Review of Marine Science, 16, 105–133.

Talwani, P., & Cox, J. (1985). Paleoseismic evidence for recurrence of earthquakes near

Charleston, South Carolina. Science, 229(4711), 379–381.

Thomsen, L., Aguzzi, J., Costa, C., De Leo, F., Ogston, A., & Purser, A. (2017). The oceanic biological pump: Rapid carbon transfer to depth at continental margins during winter. Scientific Reports, 7(1), 10763.

Thorbjarnarson, K. W., Nittrouer, C. A., & DeMaster, D. J. (1986). Accumulation of modern sediment in Quinault submarine canyon. Marine Geology, 71(1), 107–124.

Tillotson, K., & Komar, P. D. (1997). The wave climate of the Pacific Northwest (Oregon and Washington): A comparison of data sources. Journal of Coastal Research, 13(2), 440–452.

Traykovski, P., Wiberg, P. L., & Geyer, W. R. (2007). Observations and modeling of wave-supported sediment gravity flows on the Po prodelta and comparison to prior observations from the Eel shelf. Continental Shelf Research, 27(3), 375–399.

Tripsanas, E. K., Piper, D. J. W., Jenner, K. A., & Bryant, W. R. (2008). Submarine mass-transport facies: New perspectives on flow processes from cores on the eastern North American margin. Sedimentology, 55(1), 97–136.

U.S. Geological Survey. (2023a, 2024). National water information system data available on the world wide web (USGS Water Data for the Nation). U.S. Geological Survey.

U.S. Geological Survey. (2023b). USGS earthquake catalog. U.S. Geological Survey.

Vandekerkhove, E., Van Daele, M., Praet, N., Cnudde, V., Haeussler, P. J., & De Batist, M.

(2020). Flood-triggered versus earthquake-triggered turbidites: A sedimentological study in clastic lake sediments (Eklutna Lake, Alaska). Sedimentology, 67(1), 364–389.

Warner, M. D., Mass, C. F., & Salathé, E. P. (2012). Wintertime extreme precipitation events along the Pacific Northwest coast: Climatology and synoptic evolution. Monthly Weather Review, 140(7), 2021–2043.

Warrick, J. A., Xu, J., Noble, M. A., & Lee, H. J. (2008). Rapid formation of hyperpycnal sediment gravity currents offshore of a semi-arid California river. Continental Shelf Research, 28(8), 991–1009.

Wheatcroft, R. A., & Borgeld, J. C. (2000). Oceanic flood deposits on the northern California shelf: Large-scale distribution and small-scale physical properties. Continental Shelf Research, 20(16), 2163–2190.

Wheatcroft, R. A., Borgeld, J. C., Born, R. S., Drake, D. E., Leithold, E. L., Nittrouer, C. A., & Sommerfield, C. K. (1996). The anatomy of an oceanic flood deposit. Oceanography, 9(3), 158–162.

Wiberg, P. L., & Sherwood, C. R. (2008). Calculating wave-generated bottom orbital velocities from surface-wave parameters. Computers & Geosciences, 34(10), 1243–1262.

Wilson, A. M., Raine, R., Mohn, C., & White, M. (2015). Nepheloid layer distribution in the Whittard Canyon, NE Atlantic Margin. Marine Geology, 367, 130–142.

Wright, L. D., & Nittrouer, C. A. (1995). Dispersal of river sediments in coastal seas: Six contrasting cases. Estuaries, 18(3), 494–508.

Wright, L. D., Friedrichs, C. T., Kim, S. C., & Scully, M. E. (2001). Effects of ambient currents and waves on gravity-driven sediment transport on continental shelves. Marine Geology, 175(1), 25–45.

Xu, J. P., Barry, J. P., & Paull, C. K. (2013). Small-scale turbidity currents in a big submarine canyon. Geology, 41(2), 143–146.

Yamaguchi, D. K., Atwater, B. F., Bunker, D. E., Benson, B. E., & Reid, M. S. (1997). Tree-ring dating the 1700 Cascadia earthquake. Nature, 389(6654), 922–923.

Zavala, C. (2020). Hyperpycnal (over density) flows and deposits. Journal of Palaeogeography, 9(1), 17.

Zavala, C., & Arcuri, M. (2016). Intrabasinal and extrabasinal turbidites: Origin and distinctive characteristics. Sedimentary Geology, 337, 36–54.

Zavala, C., & Pan, S. X. (2018). Hyperpycnal flows and hyperpycnites: Origin and distinctive characteristics. Lithologic Reservoirs, 30(1), 1–27.

Zhang, S., Alford, M. H., & Mickett, J. B. (2015). Characteristics, generation and mass transport of nonlinear internal waves on the Washington continental shelf. Journal of Geophysical Research: Oceans, 120(2), 741–758.

Zulberti, A., Jones, N. L., & Ivey, G. N. (2020). Observations of enhanced sediment transport by nonlinear internal waves. Geophysical Research Letters, 47(19), e2020GL088499.

Appendix

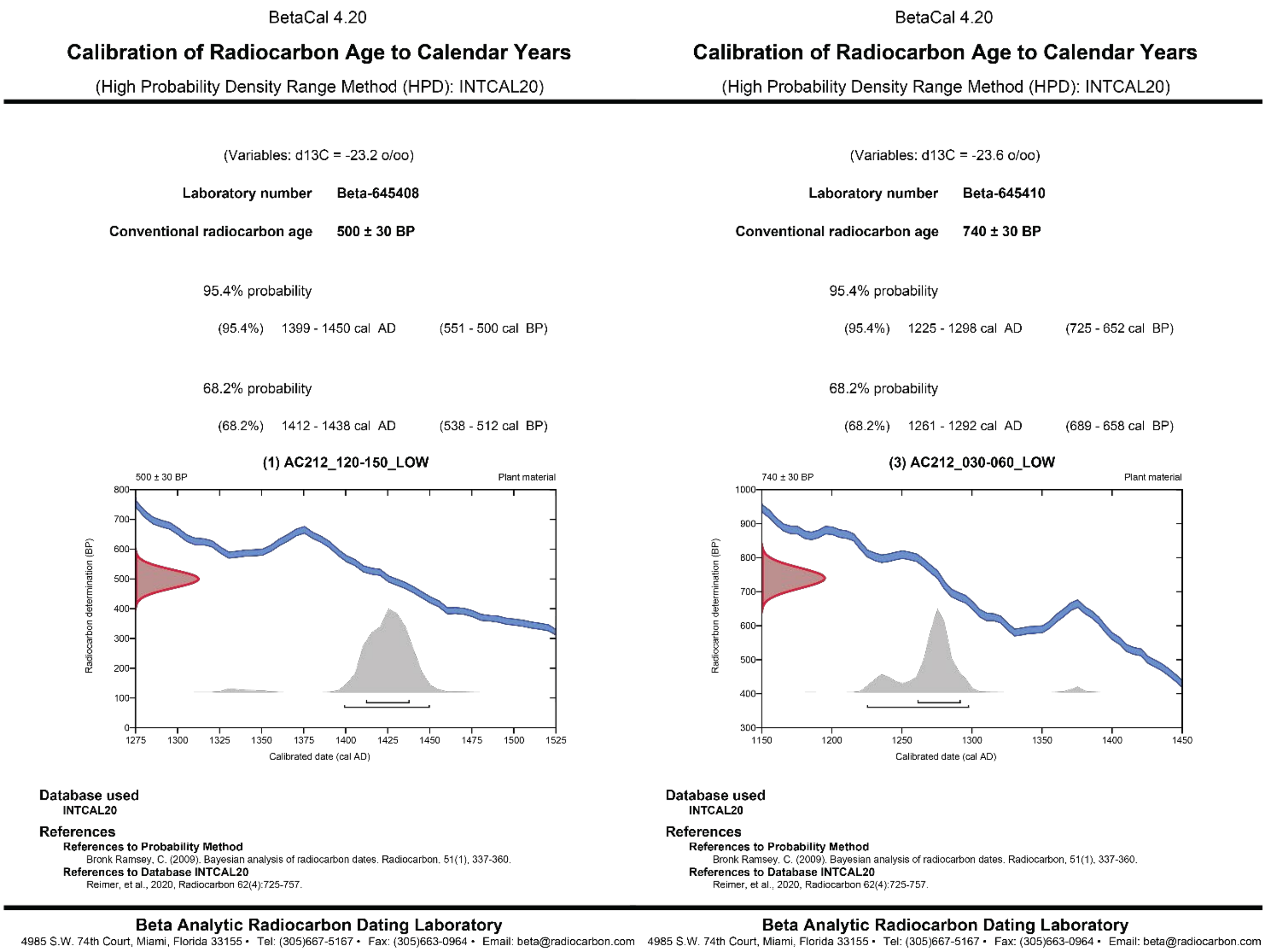

BetaCal 4.20

Calibration of Radiocarbon Age to Calendar Years

(High Probability Density Range Method (HPD): INTCAL20)

(Variables: d13C = -23.2 o/oo)

Laboratory number **Beta-645408**

Conventional radiocarbon age **500 ± 30 BP**

95.4% probability

(95.4%) 1399 - 1450 cal AD (551 - 500 cal BP)

68.2% probability

(68.2%) 1412 - 1438 cal AD (538 - 512 cal BP)

Database used
INTCAL20

References
References to Probability Method
Bronk Ramsey, C. (2009). Bayesian analysis of radiocarbon dates. Radiocarbon, 51(1), 337-360.
References to Database INTCAL20
Reimer, et al., 2020, Radiocarbon 62(4):725-757.

Beta Analytic Radiocarbon Dating Laboratory
4985 S.W. 74th Court, Miami, Florida 33155 • Tel: (305)667-5167 • Fax: (305)663-0964 • Email: beta@radiocarbon.com
Page 4 of 5

BetaCal 4.20

Calibration of Radiocarbon Age to Calendar Years

(High Probability Density Range Method (HPD): INTCAL20)

(Variables: d13C = -23.6 o/oo)

Laboratory number **Beta-645410**

Conventional radiocarbon age **740 ± 30 BP**

95.4% probability

(95.4%) 1225 - 1298 cal AD (725 - 652 cal BP)

68.2% probability

(68.2%) 1261 - 1292 cal AD (689 - 658 cal BP)

Database used
INTCAL20

References
References to Probability Method
Bronk Ramsey, C. (2009). Bayesian analysis of radiocarbon dates. Radiocarbon, 51(1), 337-360.
References to Database INTCAL20
Reimer, et al., 2020, Radiocarbon 62(4):725-757.

Beta Analytic Radiocarbon Dating Laboratory
4985 S.W. 74th Court, Miami, Florida 33155 • Tel: (305)667-5167 • Fax: (305)663-0964 • Email: beta@radiocarbon.com
Page 5 of 5

Figure S1. Radiocarbon analyses from terrestrial organic matter isolated from event layers E1 and E2, reported by Beta Analytic.

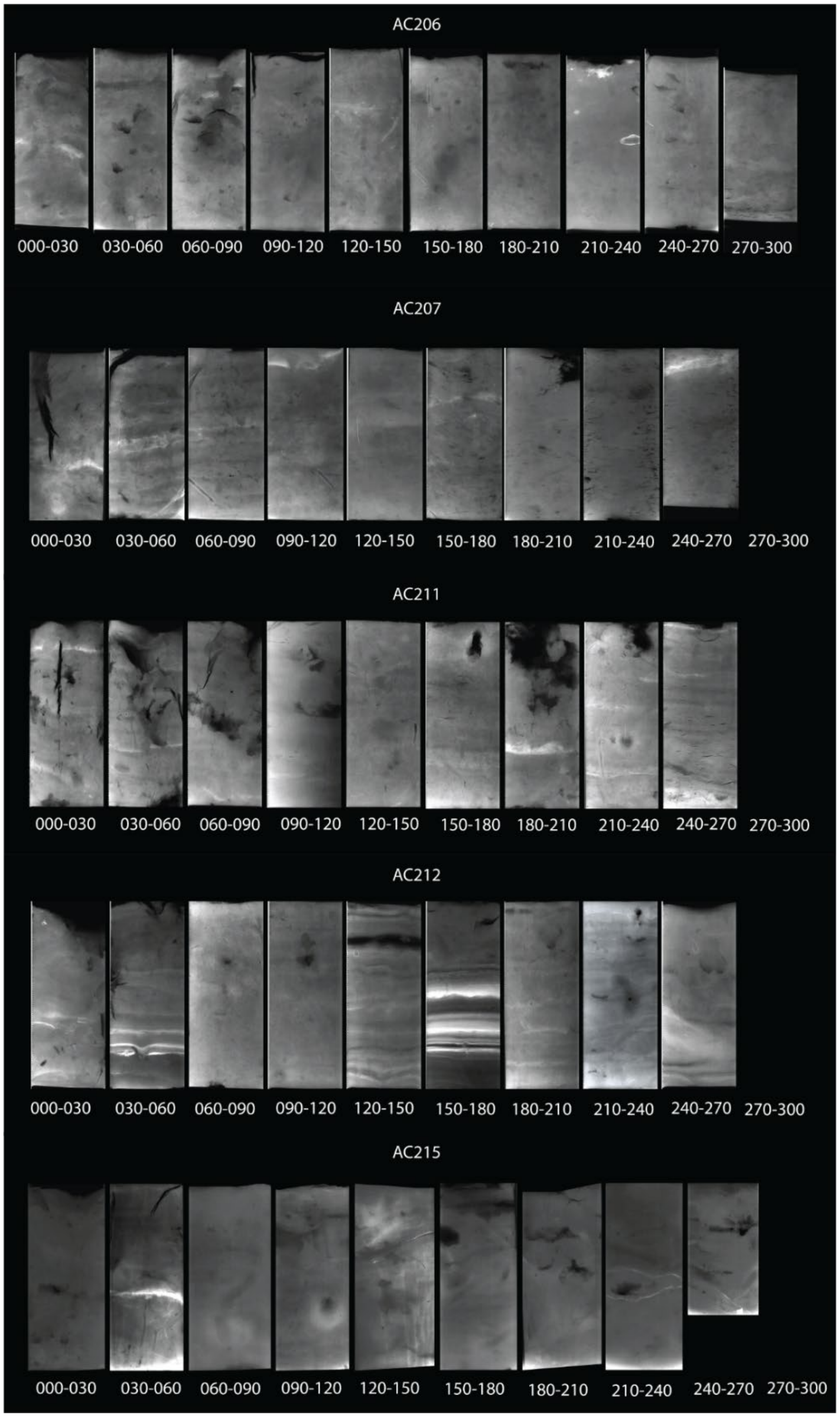

Figure S2. X-radiographs of kasten cores collected from within Astoria Canyon, dark shades representing low relative density, light shades representing high relative density. Cores were scanned in 30 cm sections which are arranged from top of core (left) to bottom of core (right).

Section intervals are listed numerically below each core section, e.g., 000-030 represents the interval from 0 cm below seafloor to 30 cm below seafloor.

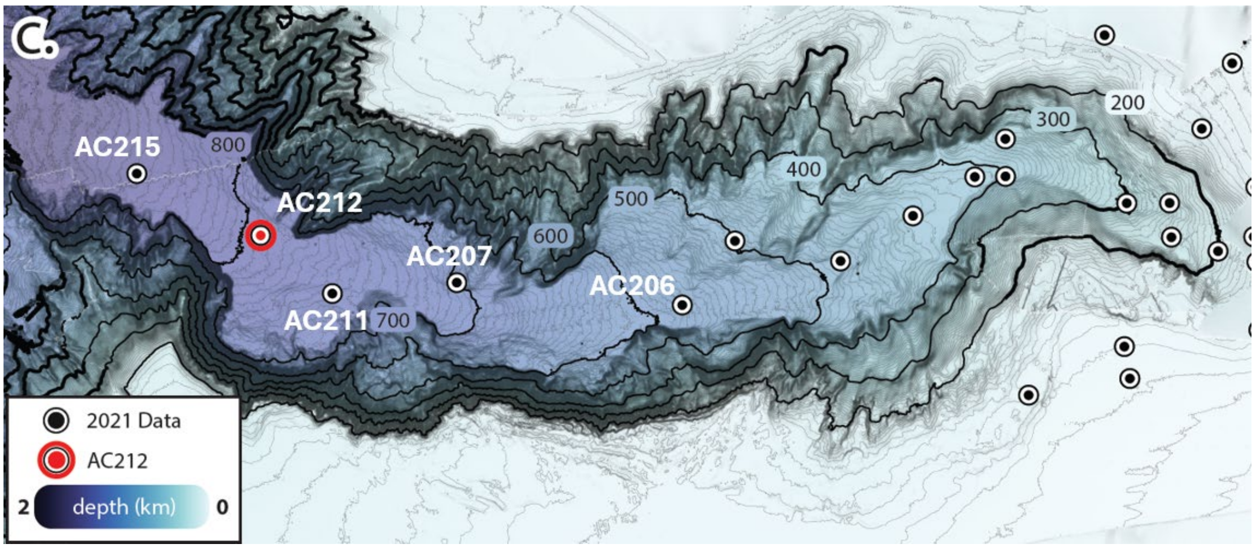

Figure S3. Core locations and site names corresponding to Fig. S2.

Figure S4. Co-located imagery from core deposit E2. Left: x-ray density scan (same color map as in Fig. S2), density scale as in Fig. S2. Right: photographic scan of deposit.

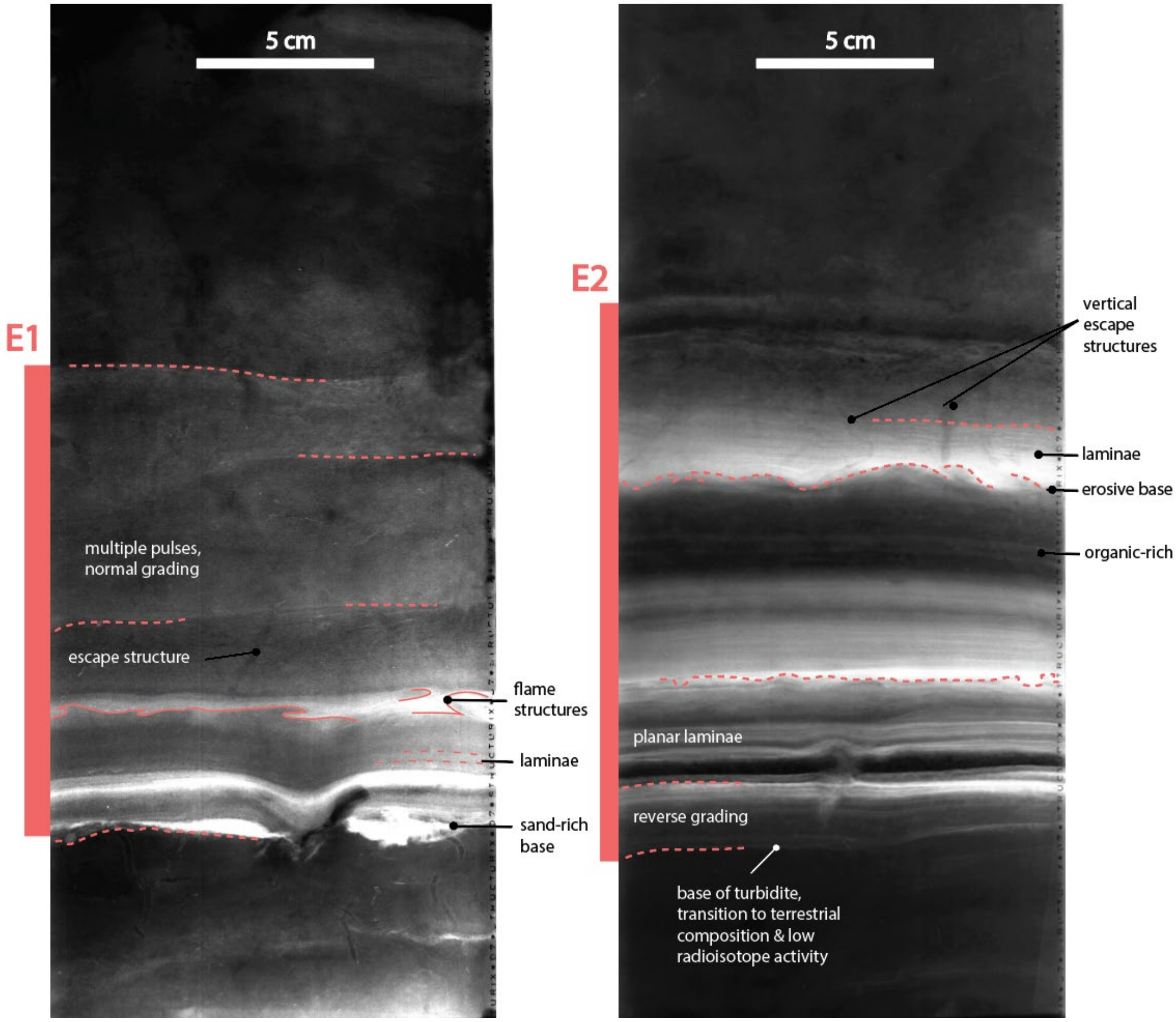

Figure S5. Illustrated sedimentological interpretation of event layers E1 and E2 (same color map as in Fig. S2).

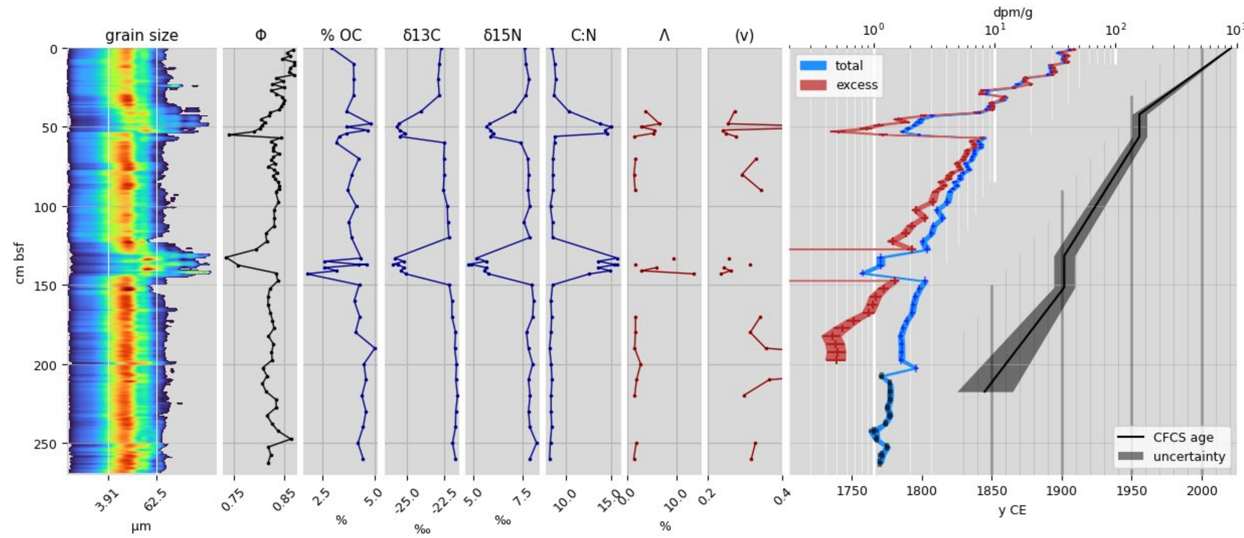

Figure S6. Complete down-core geochemical parameters for core AC212. Parameters include grain size distribution, porosity (Φ), % organic carbon, $\delta^{13}C_{org}$, $\delta^{15}N_{org}$, atomic C/N ratio, lignin concentration, vanillin acid:aldehyde ratio, ^{210}Pb activity, and modeled ^{210}Pb age.